INFRARED PHOTOMETRY OF GALAXIES

by

MICHAEL JAMES DOW

PRESENTED FOR THE DEGREE OF DOCTOR OF PHILOSOPHY
THE UNIVERSITY OF EDINBURGH
1976

This Thesis consists entirely of my own work.

Michael Dow

LIST OF CONTENTS

ABSTRACT

The design and construction of a Lead Sulphide Infrared Photometer is described along with the instrumentation and techniques of signal acquisition and data handling.

The detection mechanism of the Lead Sulphide detector is considered and the various sources of noise are described. The concept of The Noise Equivalent Power is introduced and discussed in the light of Astronomical applications. The need for an experimental approach to the optimisation of the operational parameters is underlined and described for two Lead Sulphide detectors. The resultant performance being somewhat enhanced.

Intermediate band infrared photometry of external galaxies and the galactic centre is reviewed.

Broad band H, K and L photometry of the central regions of galaxies is presented. The primary standard for the calibration of the photometry is α Lyr and is assigned magnitudes of 0.02, 0.02 and -0.02 in H, K and L respectively. The broad band photometry confirms the very large K-L colour of some galaxies. The H-K and K-L colours of the galaxies indicate a significant contribution of late-type giants.

In conjunction with the broad band photometry observations with a system of narrow band filters, used to define the CO index, are presented. The results indicate that for NGC 224 at least a population of late-type giants is

necessary to account for the CO index. A coarse radiation model based on the broad and narrow band photometry predicts a population of 1.39×10^5 such stars.

A prediction of the stellar population in the central 22 arc sec of the galactic centre based on broad band photometry and the similarity of the galactic centre with NGC 224 assigns 1.6×10^3 late-type giants to this region.

These results are presented to describe the stellar population - the near infrared background - in which other sources of longer and shorter infrared radiation may be found. This, in particular, seems to be the case for the galactic centre.

CHAPTER I

THE DESIGN CONSIDERATIONS AND A REVIEW OF THE INSTRUMENTATION OF PbS INFRA-RED PHOTOMETRY

1.1 THE PHOTOMETER

The use to which a photometric system is to be put determines to a considerable extent the procedures of measurement and reduction as well as the spectral regions and the width of the spectral bands that are to be employed. Furthermore, significant restrictions on the choice of the spectral regions and the width of the bands are imposed by the limitations of available detectors. While the Lead Sulphide detector cooled to liquid nitrogen temperatures - $77^{o}K$ - has a continuous response in the region 1μ to 4μ the transmission of the atmosphere allows observations in this region to be made through four windows 1·1μ to 1·4μ, 1·4μ to 1·8μ, 2·0μ to 2·4μ and 2·8μ to 4·2μ. These windows define to a more-or-less extent the J,H,K and L intermediate band filters. It should be pointed out that in the L band the transmission of the atmosphere is severely affected by water vapour and carbon dioxide bands from 2·8μ to 3·4μ (figure 1.1). The system of photometric bands in this region has now been well defined (Johnson 1965a, Low & Rieke 1974). These bands are analogous to the U,B and V bands used in photoelectric photometry and the observed fluxes are reduced to a magnitude scale in a similar way to the well established practice in photo-electric photometry. A difference of one magnitude corresponds to a ratio of $10^{0\cdot4} \equiv 2\cdot51$.

Intermediate band photometry of galaxies was first carried out by Johnson (1966a) from which mean colours for spiral and eliptical galaxies were obtained. Since then

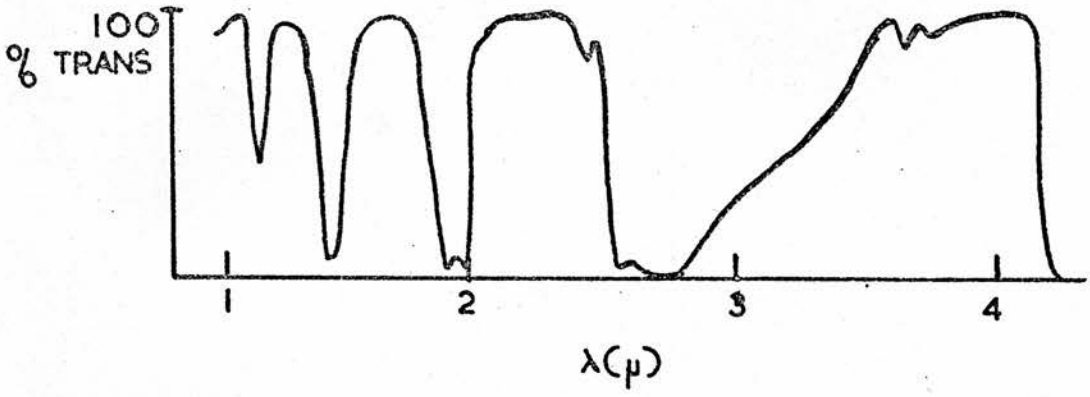

Figure(1.1)

other work has, in general, been confined to Seyfert galaxies e.g. Pacholczyk & Weymann (1968), Rieke & Low (1971) and Penston et al. (1974) with the exception of Glass (1973b), where J,H,K and L photometry of 27 Southern Galaxies of which only two were Seyferts was attempted, and the nucleus of our own galaxy (Becklin & Neugebauer 1968, 1969 and Rieke & Low 1973).

Infrared photometry of galaxies presents its own brand of problems not the least of these being their visual faintness. Finding and guiding on an infrared object visually very faint requires special techniques which, though they have now become standard practice (Becklin & Neugebauer 1968, Glass 1973b and Low & Rieke 1974), require special consideration in the design and construction of an Infrared Photometer.

The Photometer described below, was designed and constructed to be used on the 60 inch Infrared Flux Collector at Izaña, Tenerife and to incorporate the special features available, especially a highly accurate off-setting capability. The photometer was used at the f|12·8 Cassegrain focus of the telescope figure (1.2). The general layout of the photometer figure (1.3a) is similar to photometers described by Glass (1973b) and Rieke & Low (1974) and incorporates such features as focal plane chopping and an off-set guiding facility.

The mounting flange of the photometer was designed to allow rotation of the photometer on the mounting flange of the telescope. This meant that sky chopping could be

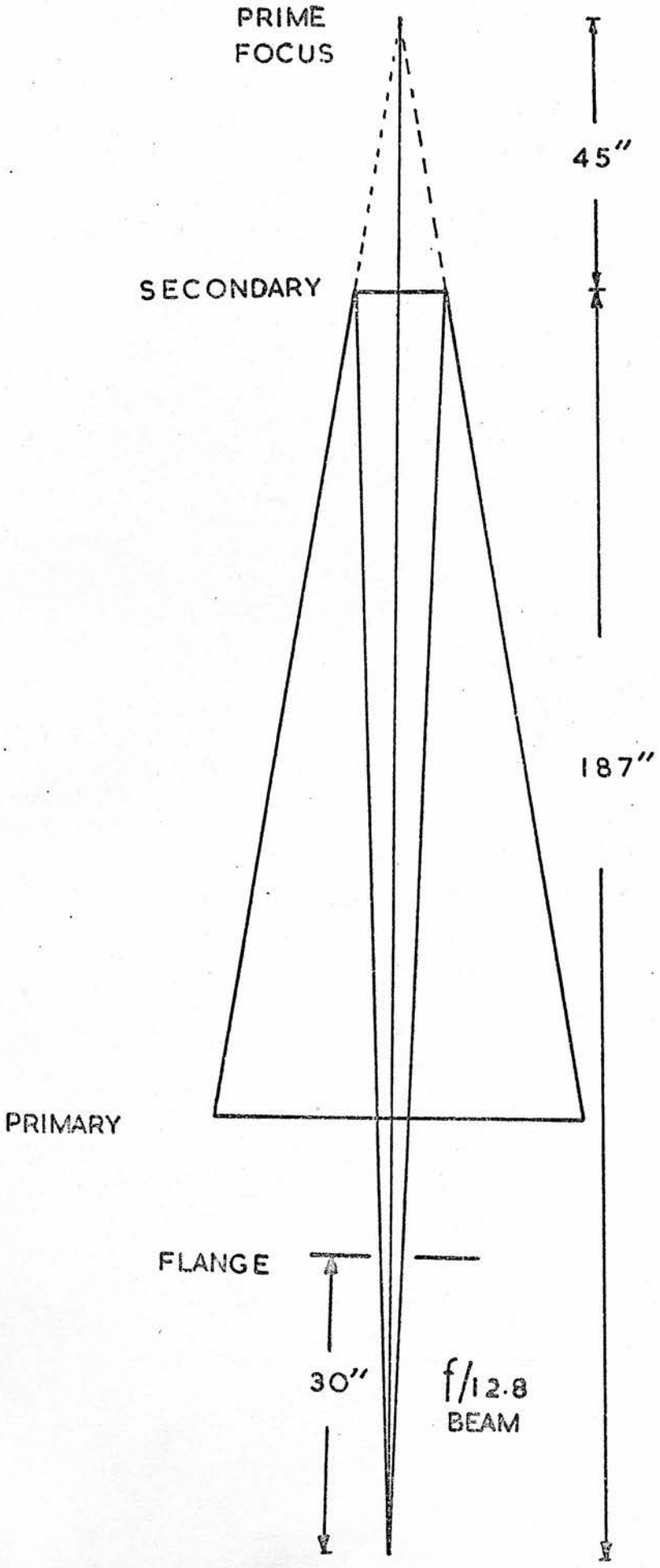

Figure(1.2)

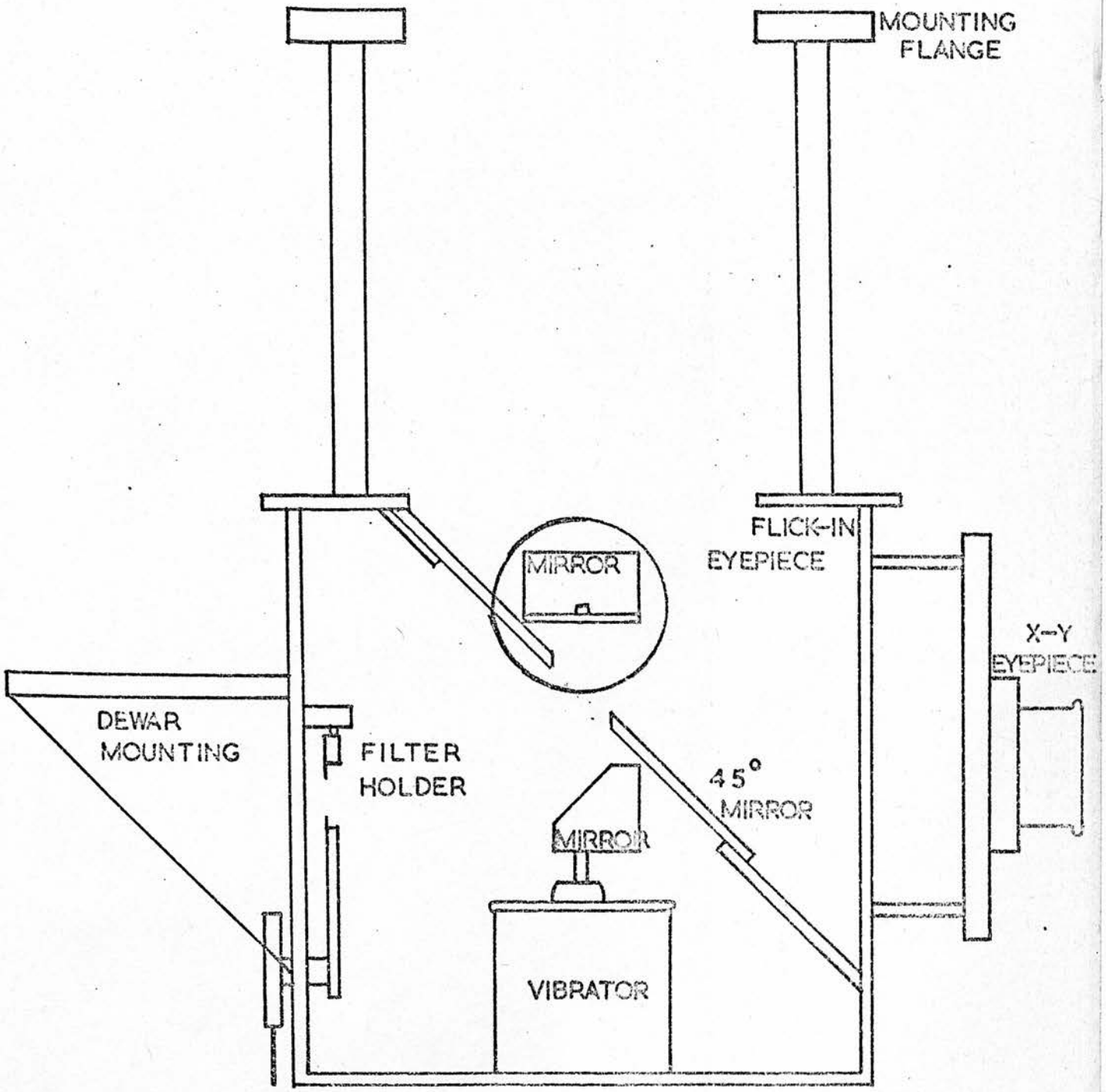
MOUNTING
FLANGE
FLICK-IN
EYEPIECE
MIRROR
X-Y
EYEPIECE
DEWAR
MOUNTING
FILTER
HOLDER
45°
MIRROR
MIRROR
VIBRATOR

Figure(1.3a)

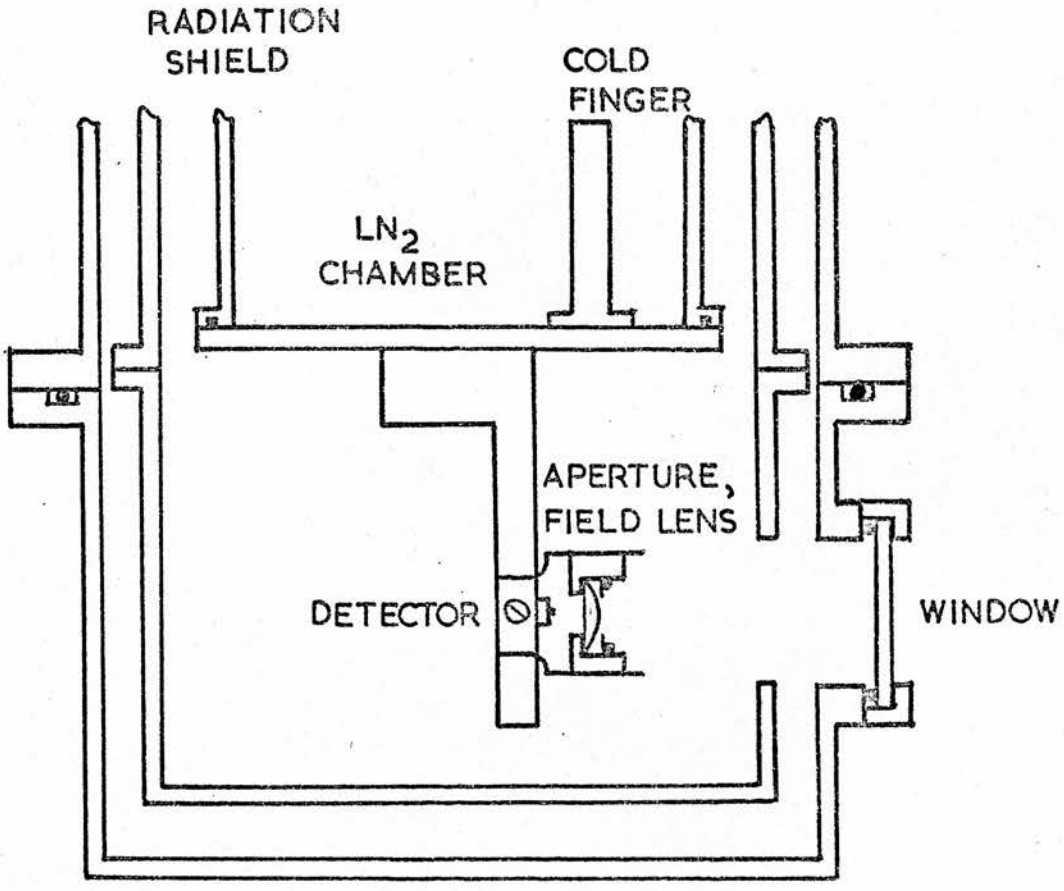
RADIATION
SHIELD
COLD
FINGER
LN_2
CHAMBER
APERTURE,
FIELD LENS
DETECTOR
WINDOW

Figure (1.3b)

done in right ascension or declination.

The main body of the photometer is a box containing the focal plane chopper, the filter holder, a large 45^{o} mirror and mountings for two eyepieces. The main body of the photometer also gives structured rigidity to the dewar mounting.

The detector is mounted in a dewar obtained from Thor Cryogenics, Oxford. The mounting arrangement allows adjustment of the orientation of the dewar in the final aligning procedure (Appendix 1). The optical tail of the dewar was designed to take a set of filters and apertures at some future date as part of the development of this programme of research.

The layout of the optical arrangement used is given in figure (1.4) and the filter transmission curves are given in figure (1.5).

It is well known that the infrared radiation coming from a celestial source must be modulated in order to discriminate it from the atmospheric background. The main body of the photometer contains a focal plane chopper as a means of star-sky modulation. Modulation is achieved by square oscillation of an optical flat set at 45^{o} to the optical axis of the telescope. The flat then deflects the image in and out of the focal plane aperture so that the detector sees an image of the primary mirror filled with light by the star and sky alternatively with an image of the primary mirror filled with light from the sky only.

This method and the other, more commonly used method

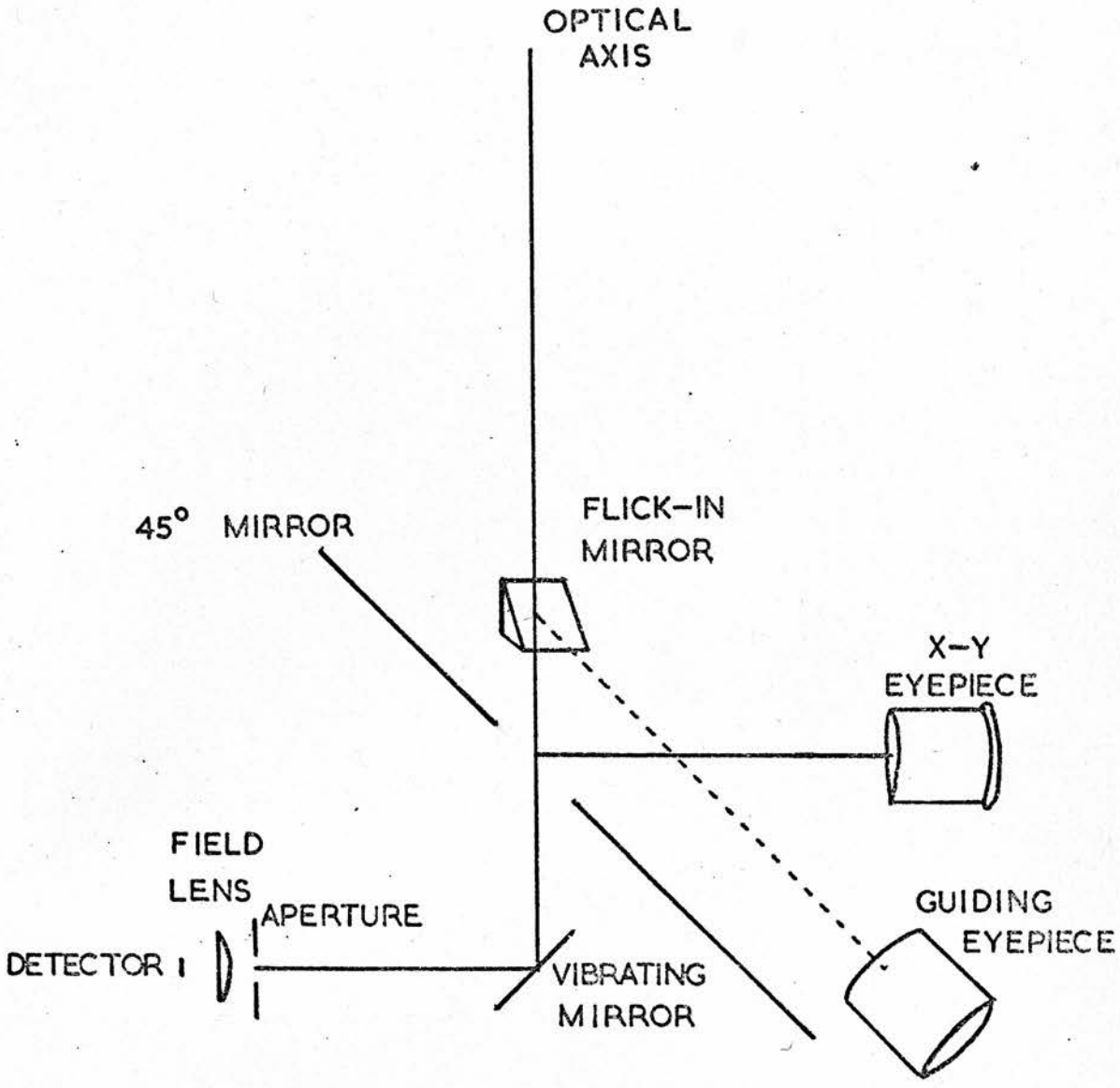
OPTICAL
AXIS
45° MIRROR
FLICK-IN
MIRROR
X-Y
EYEPIECE
FIELD
LENS
APERTURE
DETECTOR
GUIDING
EYEPIECE
VIBRATING
MIRROR

Figure(1.4)

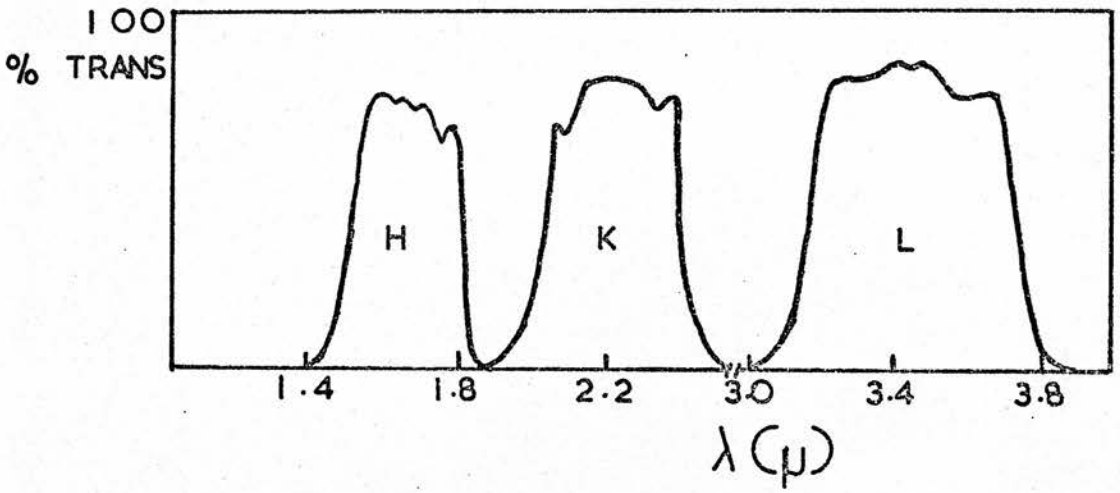

Figure (1.5)

- a two level mirror (Becklin et al. 1969 and Glass 1973b) - involve defocussing of the beam. The diameter of the defocussed beam at the aperture is given by

$$d/F/no \quad \ldots (1.1)$$

where d is the chopper throw, and F/no the focal ratio of the telescope. It can be seen then that this defocussing becomes important for large amplitudes of chopper throw and usually manifests itself as assymetry in scans of an object parallel to the chopping direction (Low & Aumann 1970). However, for small amplitudes of throw the amount of defocussing is small. The focal plane chopper was normally operated with a throw of 2mm which in conjunction with a 2mm aperture and f|12·8 telescope resulted in defocussing of the order of 8%.

These two methods of chopping have their advantages and disadvantages. The advantage of the rotating chopper is that large beam separation can be obtained at high modulation frequencies, while it may be difficult to adjust the two mirrors so that the two beams are equivalent and the mirrors must be large to simulate true square wave modulation.

The stepped chopper can achieve a better balance between the two beams and when adjusted to eliminate edge effects, produces the lowest amount of offset. However, true square wave modulation can only be achieved for a small amplitude and a limited range of chopping frequencies.

A lens placed at or behind the focal plane of the telescope which images the primary mirror onto the detector is called a field-lens. It is used to perform a number of

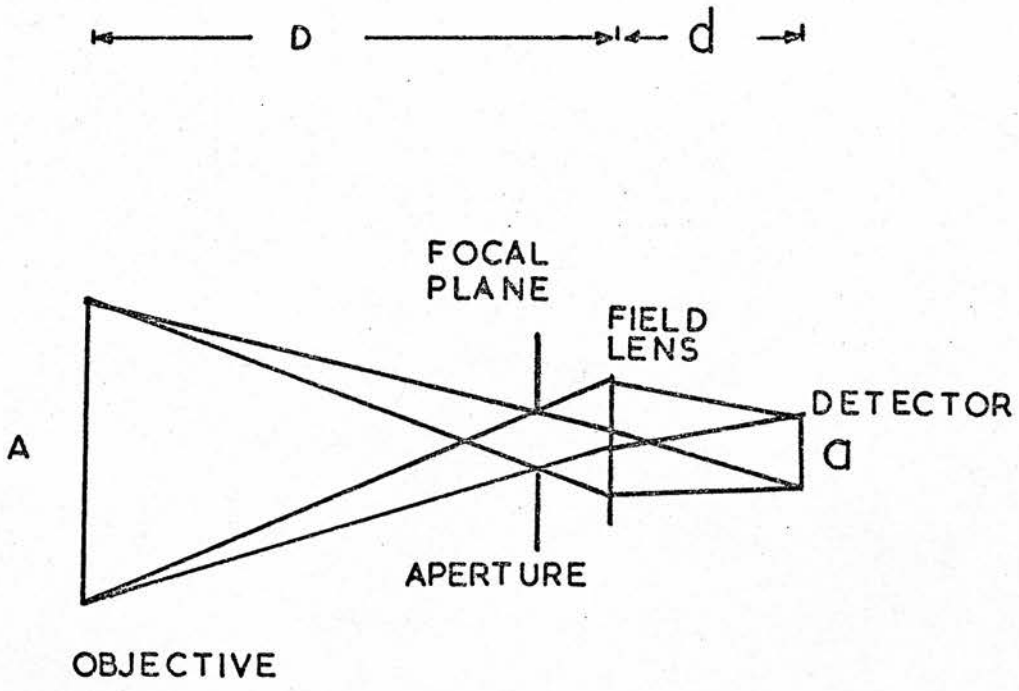

Figure(1.6)

important functions. Since it will distribute the energy from any point within a focal plane aperture over the entire detector it can overcome problems associated with the non-uniform response exhibited by the sensitive areas of infrared detectors. A field-lens aperture combination restricts the field of view of the detector and therefore reduces the background radiation incident on it. The use of a field-lens permits the use of a dector smaller than the field aperture. The principle of the field-lens is shown in figure (1.6).

The objective forms an image in the focal plane beyond which the rays diverge. The field-lens causes the rays of light at the edge of the field to be bent towards the axis so that they fall on the detector. When a field-lens is designed the power and position of the lens are selected so that the objective aperture imaged on the detector is the same size as the detector.

From figure (1.6)

$$A/a = D/d$$

$$\frac{1}{f} = \frac{1}{-D} + \frac{1}{d}$$

then combining, the focal length of the field-lens is

$$f = \frac{Da}{(-a+A)} \qquad \ldots (1.2)$$

If the field-lens is placed in the focal plane then $D = f_0$ so, the focal length f, is given by

$$f = \frac{f_0}{(-a+A)} \cdot a \qquad \ldots (1.3)$$

and if a A then

$$f = \frac{f_0}{A} \cdot a \qquad \ldots (1.4)$$

This then shows that the focal length of the field-lens to be used is given by the product of the telescope F/no and the detector diameter.

The optimum position for the field-lens is at the focal plane. Practical considerations of interference with the aperture enforce a compromise position. The illumination at the detector under these conditions is now identical to that at the aperture of the objective. If there is no vignetting a point image may be moved all over the field of view without affecting the energy distribution or the illumination at the detector.

Usually the objective aperture is circular and the detector is square. If the detector's signal/noise ratio varies inversely with the square root of its area then the detector can be reduced in size until its square is inscribed in the illumination circle with a loss of only 10% in signal/noise ratio (Smith 1965).

The field-lens is designed to minimize aberrations and place the maximum amount of energy on the detector. The technique is to consider the field-lens as an image forming device in itself and to evaluate the quality of the image of the objective aperture which it forms.

The lens used is made of Al_2O_3 which has a refractive index of 1·67 in the 1μ to 3μ range.

Let $C_1 = 1/R_1$ and $C_2 = 1/R_2$ where R_1 and R_2 are the

radii of curvature for the lens surfaces.

Let $K = C_1/(C_1-C_2)$ be the shape factor. Then when $C_2 = 0$, $K = +1$.

The angular blur due to spherical aberration for a lens of this shape factor - plano convex - and refractive index is given by $\beta = 0{\cdot}36y^3\phi^3$ (Smith 1965) where y = half diameter of the lens and $\phi = 1/f$. The lens used has $y = 3{\cdot}5$mm and f = 6mm so the angular blur β is given by

$$\beta = 0{\cdot}059 \text{ radians} \qquad .07$$

and the geometrical image size is given by $6{\cdot}F/no$ mm = 0·469 mm. The total image size is given by the sum of these viz. the sum of the geometrical image and the blur due to spherical aberration.

Although refractive optics are used to perform these functions in relatively narrow bands $\Delta\lambda < 0{\cdot}5\mu$ and at intermediate wavelengths they are not used at longer wavelengths and very broad passbands since dispersion in the refractive material results in unsatisfactory performance. The alternative is an off-axis mirror to perform the functions of the field-lens.

The filters used were a set of H, K and L filters sponsored by J.A. Frogel, Harvard. The filters were used uncooled and their room temperature transmission is given in figure (1.5). These filters were obtained from Optical Coating Laboratories Inc. (OCLI) and are fully blocked on either side of the pass band. The characteristics of the infrared filters are summarized in table (1.1). These compare favourably with the filters used by Johnson (1965),

TABLE 1.1 - CHARACTERISTICS OF INFRARED FILTERS

NAME	λ_0 (μ)	$\Delta\lambda$ (μ)
H	1·65	0·3
K	2·2	0·4
L	3·5	0·8

Glass (1973b) and Low & Rieke (1974). Transmission up to 70% is obtained in the passband and attenuation of $>10^3$ is obtained in the stop band.

The Dewar window material is Sapphire (Al_2O_3) and its transmission curve is given in figure (1.7). The field-lens is made from the same material. The window used has a transmission of 70% in the region 1μ to 5μ. The transmission drops sharply to zero around 6μ.

Cooling the detector, its associated field optics and the filters is essential if the best possible performance is to be achieved. The degree of cooling depends entirely upon the requirement of the detector and the wavelength region. While it is essential for work at wavelengths longer than 4μ, cooling of the filters for work in the 1μ to 4μ region does not result in substantial increase in performance. It will be shown later that the performance of the system compares favourably with others where cooling of the filters is standard practice.

The cooling requirements of the Lead Sulphide detector are met by using liquid nitrogen as a coolant. Figure (1.3b) shows a cross-sectional view of the Dewar. The liquid nitrogen is protected by a vacuum, which is maintained for long periods by an activated Carbon sorption pump to deal with any outgassing which might occur. Radiation losses are reduced by wrapping the cold parts with many layers of aluminised Mylar foil. The general pumping requirements were met by the pumping system provided at the telescope namely an oil diffusion rotary pump combination.

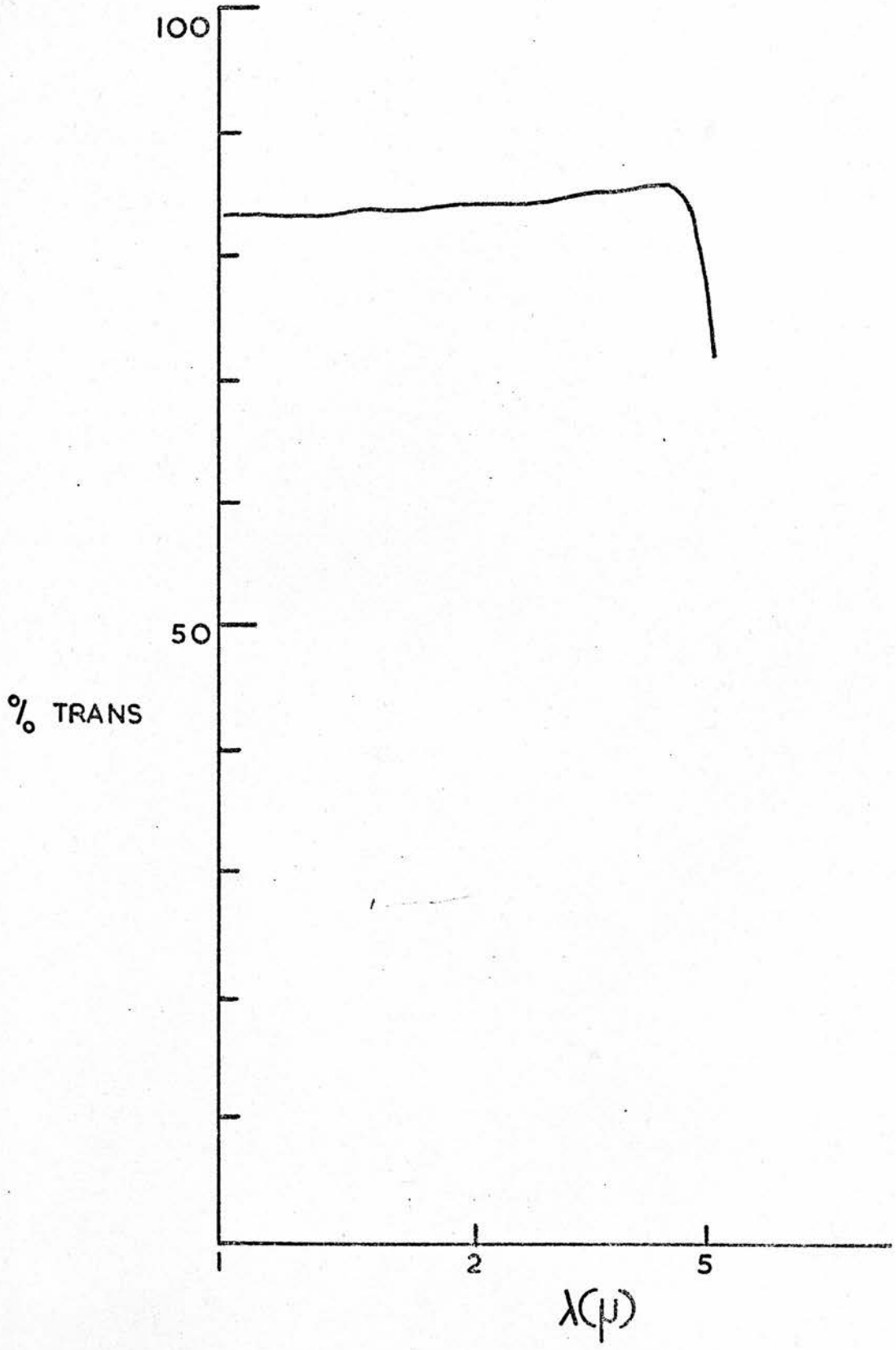

Figure (1.7)

The requirement for cooling intrinsic photoconductive infrared detectors to obtain maximum performance is well known. The observed fact is that the longer the wavelength response the lower the cooling temperature required. It has been shown (Beyen & Pagel, 1966) that the upper limit for cooling a lead sulphide detector is 240^{o}K and they suggest that detectors operating at temperatures near this point are within a factor of 10 or less of the ultimate performance.

The other parts of the body of the photometer are the centering eyepiece, the large 45^{o} mirror and a mounting for an off-set guiding eyepiece. The centering eyepiece views the central part of the telescope beam when an adjustable optical flat is moved into place above the large 45^{o} mirror. The optical flat is adjustable so that sets of cross-wires may be made to correspond with the position of the focal plane apertures. The off-set guiding eyepiece, a 2 inch diameter Erfle eyepiece is mounted on a carriage designed by Mr. R.J. Beetles, Royal Observatory, Edinburgh, and can be accurately and rapidly positioned. The eyepiece, when unlocked, is free running for coarse positioning and when locked uses a small amount of lead-screw for accurate positioning. The off-set guiding eyepiece receives the outer parts of the beam from the telescope reflected by the large pierced 45^{o} mirror.

1.2 ELECTRONICS

The special problems of infrared photometry are not solved by the design and construction of a photometer along

the lines of the one described. They remain as an important consideration in the design and construction of signal recovery and data acquisition systems. The signal to be recovered is an alternating one. The whole point of the modulation system is to code the signal to be recovered so that the signal recovery system can be designed for that specific code. The requirement then is that the signal recovery system and any amplifiers used must be a.c. coupled.

The block diagram shown in figure (1.8) illustrates the entire electronic system. The development of the Phase Sensitive Detector (P.S.D) and the Lock In Amplifier (L.I.A) has made the recovery of a modulated signal from a high background of noise a process of relative simplicity.

Briefly the signal is a.c. coupled, phase sensitively detected, the d.c. deflections are recorded on a chart recorder, digitized, integrated and recorded on printer output. This system is similar to the system developed by Johnson (1962) and the system described by Low & Rieke (1974).

The heart of the signal recovery is the PSD. This and the principles of phase sensitive detection will be described in a later chapter.

Figure (1.9) shows the circuit used to extract the signal from the detector. The detector can be considered as a resistor such that

$$R_D = R_0 + \delta R$$

where δR is the change in resistance due to incident radiation.

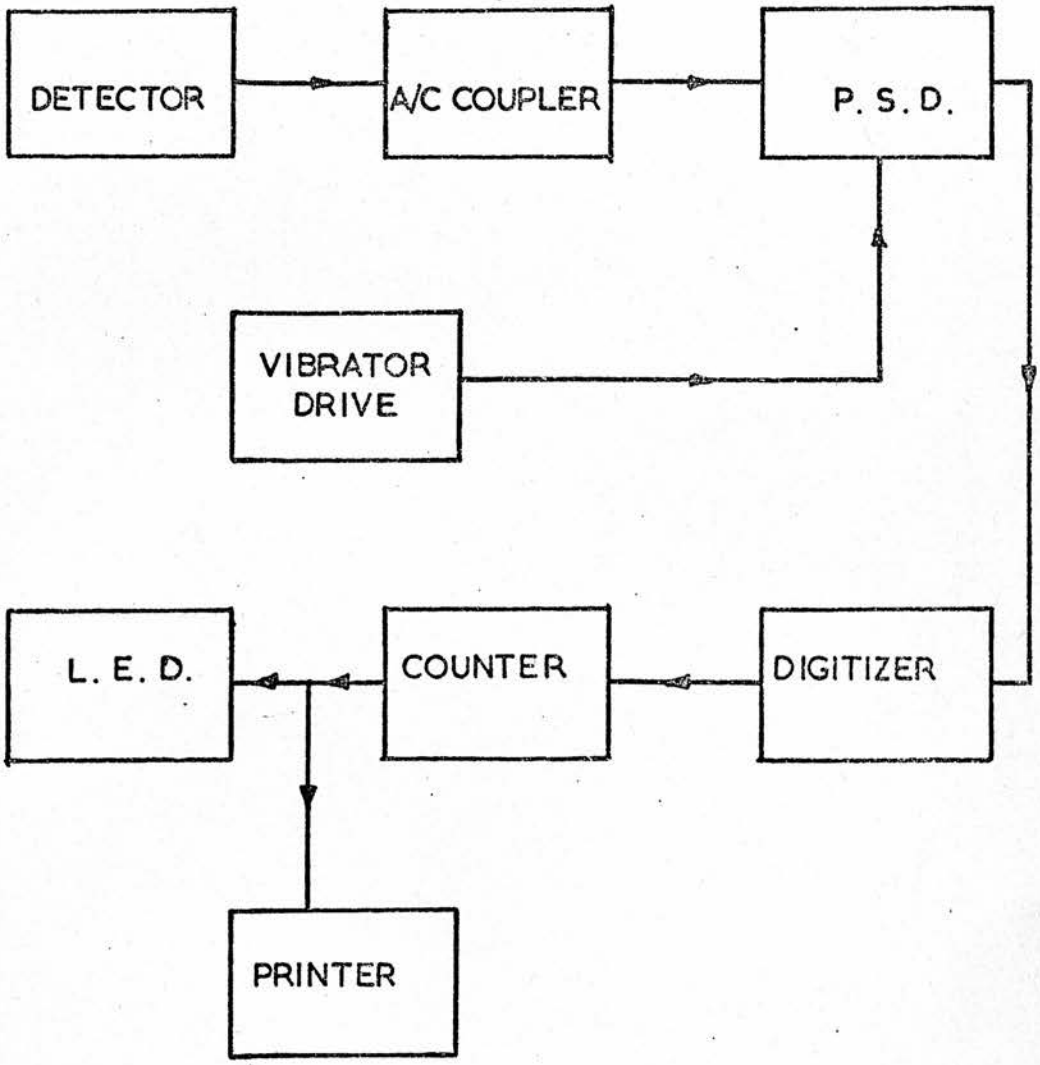
DETECTOR
A/C COUPLER
P. S. D.
VIBRATOR DRIVE
L. E. D.
COUNTER
DIGITIZER
PRINTER

Figure (1.8)

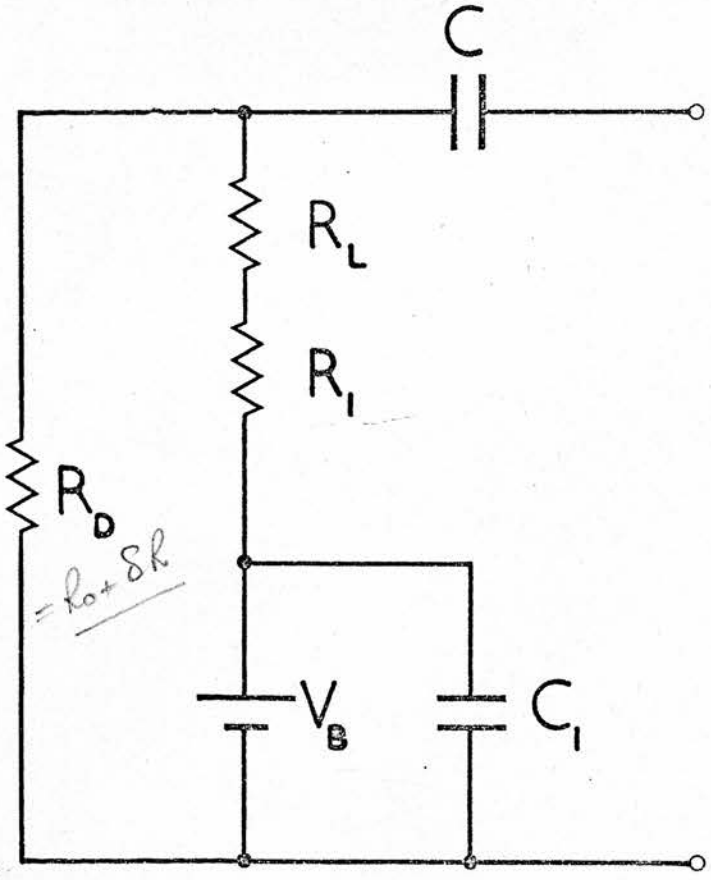

Figure (1.9)

From the circuit (figure 1.9)

$$V_0 = i_0(R_0 + R_L)$$

is a d.c. voltage where i_0 is due to the voltage V_0 through R_D. Then the effect of δR is that

$$\delta V = i_0 \delta R$$

or

$$V^\omega = i_0 R^\omega \qquad \ldots (1.5)$$

then the a.c. voltage is given by

$$V^\omega = i^\omega \left[R_0 + \frac{1}{\frac{1}{R_L} + \frac{1}{\sqrt{R_z^2 + \frac{i^2}{w^2 c^2}}}} \right] \qquad \ldots (1.6)$$

and if $R_z \gg R_L$ and

$$V^\omega = i^\omega (R_0 + R_L) \qquad \ldots (1.7)$$

then V^ω across R_L is given by $R_z \gg C^2/\omega^2$

$$V^\omega - i^\omega R_0 = i^\omega R_L$$

and on substitution for i^ω from equation (1.7)

$$V^\omega \text{ across } R_L = \frac{V^\omega R_L}{R_0 + R_L}$$

and on substitution for V^ω from equation (1.5)

$$V^\omega_{\text{load}} = i_0 R^\omega \frac{R_L}{R_0 + R_L}$$

and

$$V^\omega_{\text{load}} = V_0 R^\omega \frac{R_L}{(R_0 + R_L)^2} \qquad \ldots (1.8)$$

which is a maximum if $R_0 = R_L$ i.e. if the load resistance is equal to the dark resistance of the detector.

The use of this circuit imposes the following constraints; for a maximum in V^{ω}_{load}, $R_L = R_D$ dark resistance; the amplifier input impedance $R_z \gg R_L$ and $R_z \gg C^2/\omega^2$, and the capacitor C will pass only frequencies greater than those given by

$$\omega = 1/R_z C \qquad \ldots (1.9)$$

This means that only the modulated signal can pass through to the Low Noise Amplifier (LNA) since for frequencies above that given by equation (1.9), C is negligible.

The LNA used is, in fact, the signal input channel of the Brookdeal Model 401A Lock-in-Amplifier. The LNA operates over a frequency range of 1Hz to 50KHz and will accept in-phase signals up to 100mVs p-p and noise voltages up to 3V p-p. It has a sensitivity range for full scale deflections of 1μV to 100mV in 1, 3, 10 steps. It has short circuit noise figures at frequencies greater than 100Hz of less than $10nVHz^{-\frac{1}{2}}$. Details of the performance of the LNA and the LIA used are given in a later chapter dealing with the principles of phase sensitive detection.

The d.c. output of the PSD is then digitized (figure (1.10)) using a board designed and built by Mr. D.H. Beattie, Royal Observatory, Edinburgh. The main component on this board is a Teledyne Philbrick 4701 Voltage-to-Frequency converter which provides linear conversion of analog data to a digital pulse train with output compatibility with standard or high-noise-immunity T^2L logic. The V-to-F converter has a full scale range of 0Vdc to 10Vdc and the

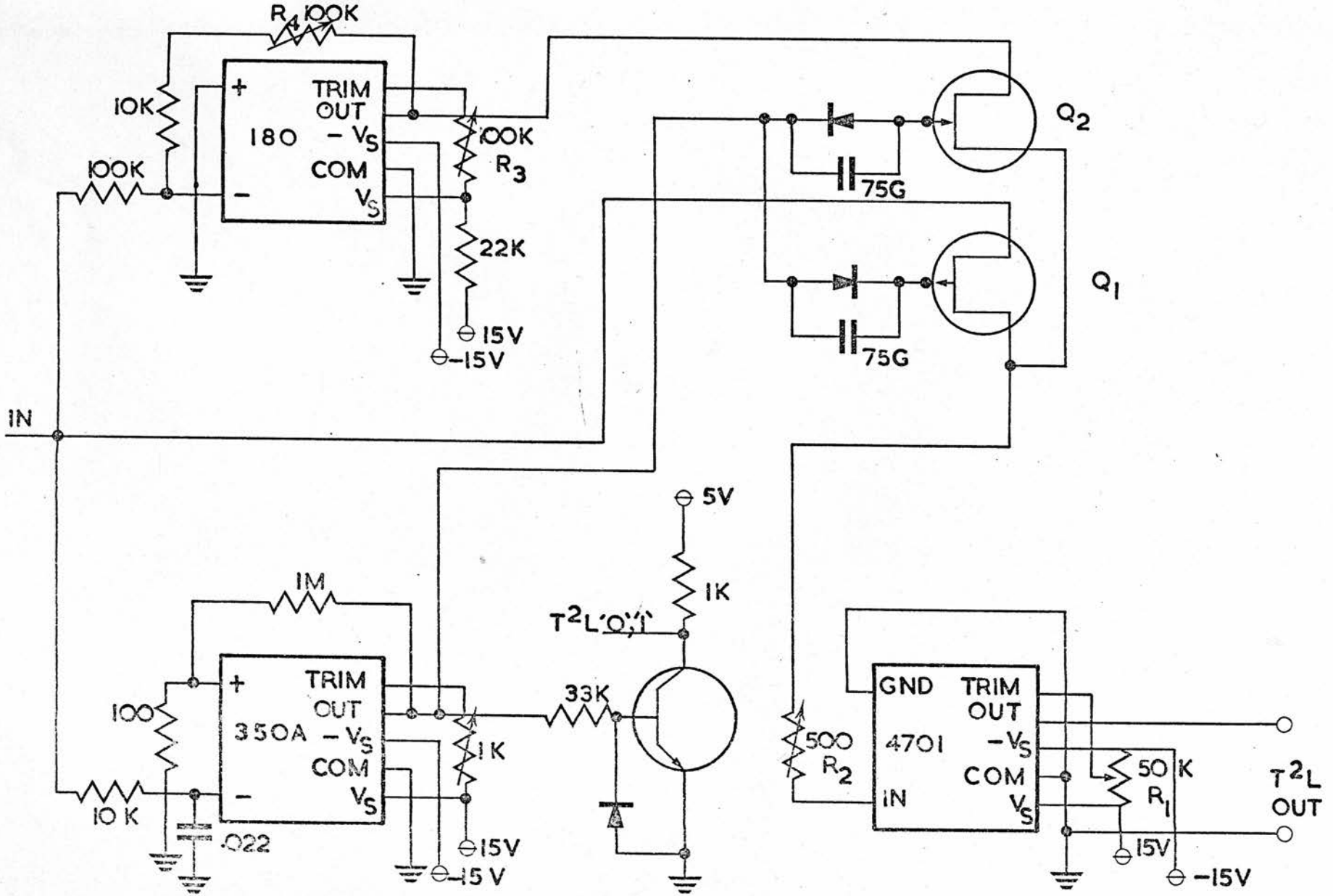
R1 100K
10K
100K
180
TRIM
OUT
-VS
COM
VS
100K
R3
22K
15V
-15V
Q2
75G
Q1
75G
IN
5V
1K
T2L 0,1
1M
100
10 K
350A
.022
1K
33K
500
R2
GND
TRIM
OUT
4701
-VS
IN
COM
VS
50 K
R1
15V
-15V
T2L
OUT

Figure 1.10

output frequency is given by

$$f_{out} = 10KHz \frac{V_{in}}{10V} \quad \ldots (1.10)$$

What becomes immediately apparent is that the V-to-F converter is unipolar and will only accept positive d.c. voltages. As will be shown later the d.c. output from the PSD will be either positive or negative depending upon the phase difference of the signal and reference waveforms. When working on a bright object the output of the PSD should be large with little noise. While when working on a faint source the output will very probably be small and relatively noisy. Therefore, in order that the V-to-F converter will accept the output of the PSD whether it is a large positive or negative signal or a small signal with fluctuations about zero a switching circuit is used in conjunction with an operational amplifier to maintain a positive input voltage at the V-to-F converter.

The polarity of the input signal is measured by the Model 350A Comparator module. It is adjusted in such a way that when the signal is greater than + 1·5mV the output is -15V and when the signal is greater (more negative) than -1·5mV the output is + 15V. This output is then fed to the switching circuit and also made T^2L compatible. The T^2L compatible output is used to steer the count direction on the counter board.

The switching circuit works in the following way. When the output of the 350A is + 15V Q1 is on and Q2 is off thus the output of the 180H operational amplifier which in

this circuit acts as a one-to-one inverter is allowed to reach the V-to-F converter. Conversely, when the 350A output is -15V Q1 is off and Q2 is on thus the input goes direct to the V-to-F converter without inversion.

The adjustment of this board is carried out by applying +100mV to the input terminals and adjusting R_1 for an output frequency of 100Hz. A voltage of +10V is then applied and R_2 is adjusted for an output frequency of 10KHz. The T^2L output should be a logical '0' (less than 0·1V). The 180 should now be adjusted for an initial zero off-set. The positive and negative inputs should be shorted to ground and R_3 adjusted for zero output. A voltage of -10V is then applied to the input terminal and R_4 adjusted to give an output frequency of 10KHz at the V-to-F converter. The T^2L compatible output of the 350A should be a logical '1' (greater than 2·4V).

This board, when properly adjusted will give a string of T^2L compatible pluses whose frequency is given by equation (1.10) for voltages in the region 1·5mV to 10V and -1·5mV to -10V and a T^2L compatible output capable of steering the counter logic.

The counter board figure (1.11) consists of six SN74190 Binary Coded Decimal (BCD) synchronous up/down counters with down/up mode control. The outputs of the four master slave flip-flops are triggered by a low to high transition of the clock input if the count enable control input is low. A high at the enable input inhibits counting and level changes at the enable input should be made when the

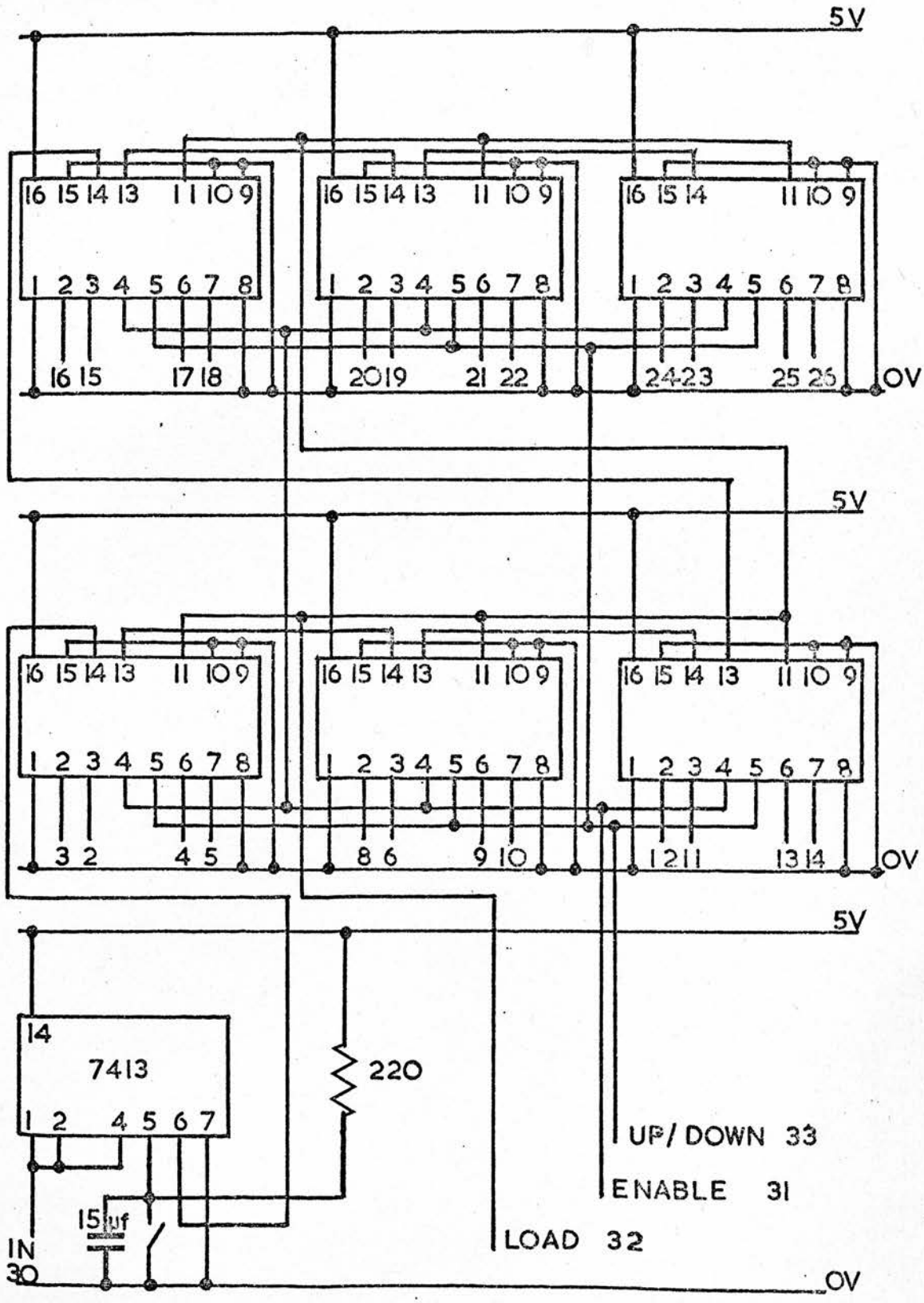
5V
16 15 14 13 11 10 9
1 2 3 4 5 6 7 8
16 15 17 18
16 15 14 13 11 10 9
1 2 3 4 5 6 7 8
20 19 21 22
16 15 14 11 10 9
1 2 3 4 5 6 7 8
24 23 25 26
OV
5V
16 15 14 13 11 10 9
1 2 3 4 5 6 7 8
3 2 4 5
16 15 14 13 11 10 9
1 2 3 4 5 6 7 8
8 6 9 10
16 15 14 13 11 10 9
1 2 3 4 5 6 7 8
12 11 13 14
OV
5V
14
7413
1 2 4 5 6 7
220
15 uf
IN
30
UP/ DOWN 33
ENABLE 31
LOAD 32
OV

Figure(1.11)

clock input is high. The direction of the count is determined by the state of the down/up input. When low, the counter counts up and when high, it counts down. These counters are fully programmable; that is the outputs may be preset to any state by placing a low on the load input and entering the desired data at the data inputs. The output will change to agree with the data inputs independently of the state of the clock input. This facility is used to zero the counters after each integration period. Outputs are available to perform cascading. The ripple clock output produces a low level output pulse equal in width to the low level portion of the clock input when an overflow or underflow condition exists. This facility is used to provide the clock input for each successive counter.

This board accepts the output from the V-to-F converter and the T^2L polarity signal and uses them to count up if the input signal from the PSD is greater than 1·5mV and down if the signal is more negative than -1·5mV. The six SN74190 provide a capability of six figure representation of the V-to-F converter output. Also on this board is a switch to allow interruption of the count at any time and an inverter for the polarity signal since the down/up requirements for the SN74190 are the reverse of the T^2L compatible polarity output of the voltage-to-frequency conversion board.

The SN74190 have an enable function which is used to define an accurate and repeatable integration time. A G.E.C Quartz Crystal Oscillator type QC 1233 made by Salford Electrical Instruments with a 1Hz output is used in conjunction with the clock circuit figure (1.12) to define an integration

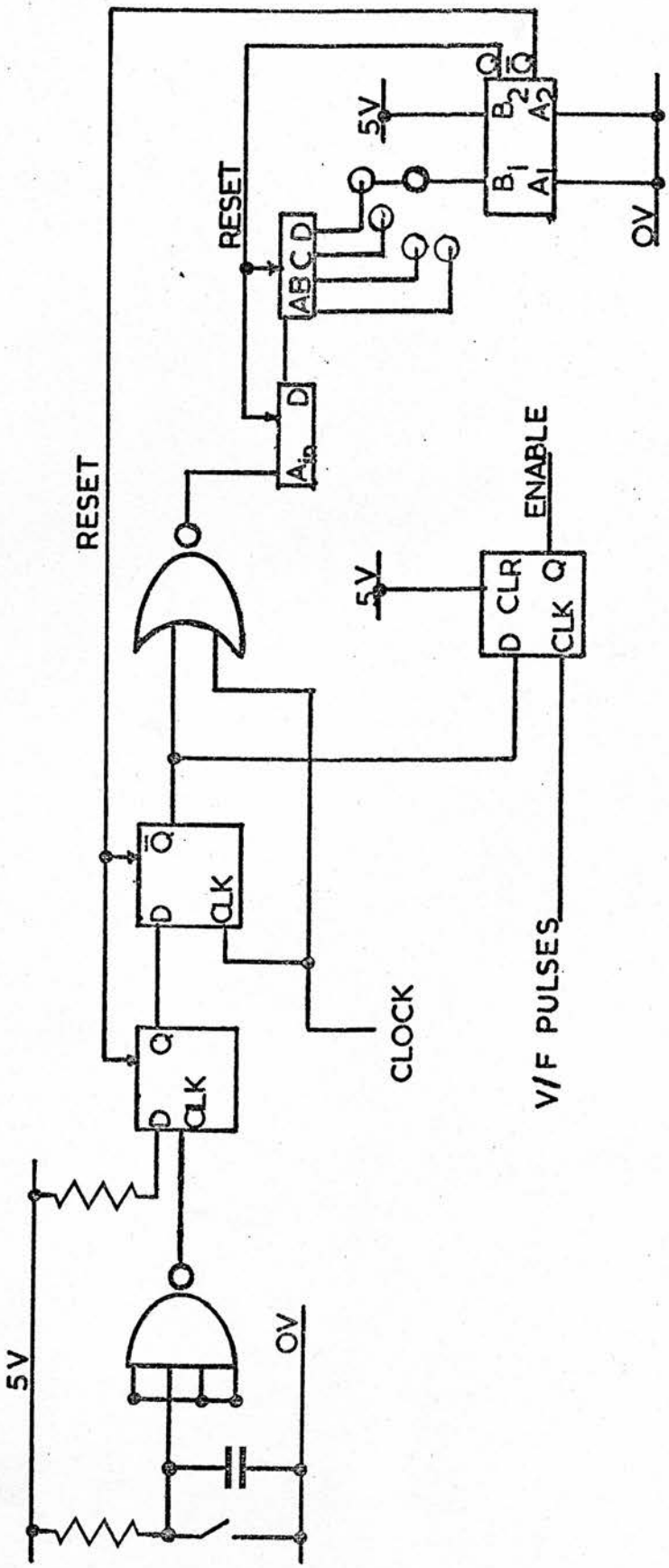
RESET
5V
0V
ABCD
D
A_{in}
RESET
ENABLE
5V
CLR
D
CLK
Q
CLOCK
V/F PULSES
5V
0V

Figure(1.12)

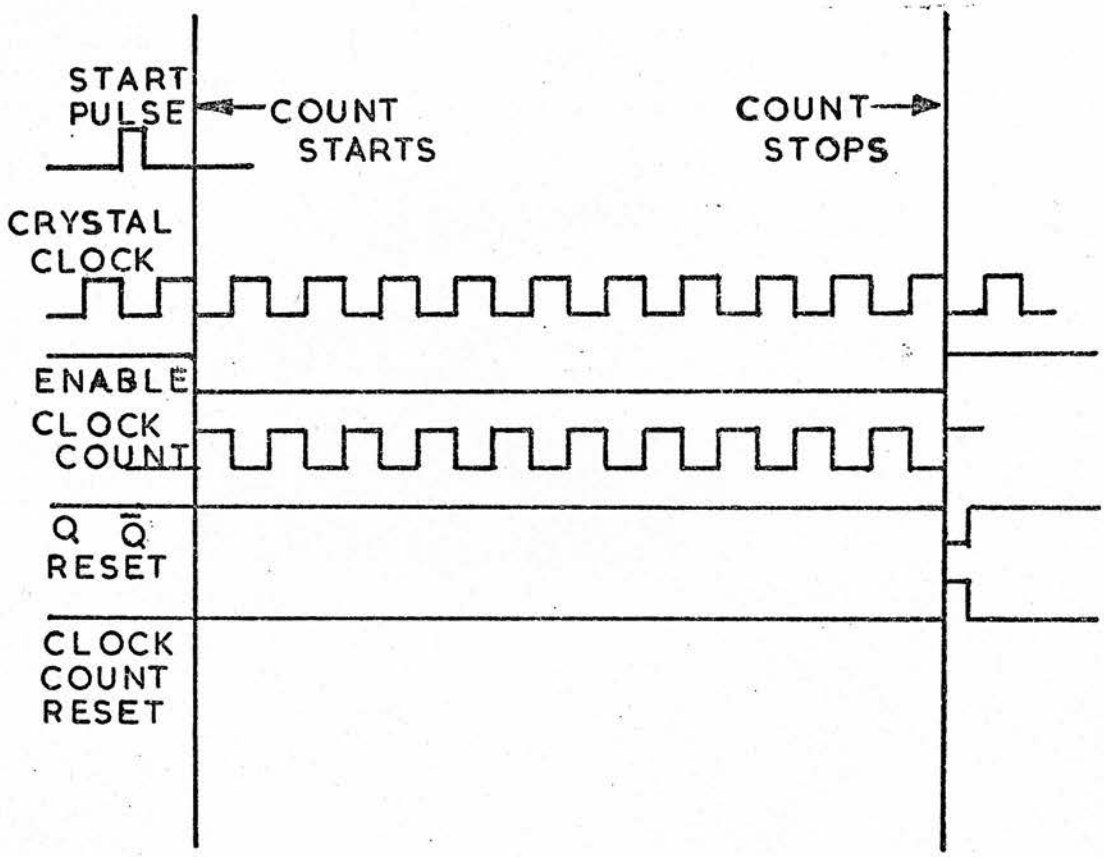
START
PULSE
COUNT
STARTS
COUNT
STOPS
CRYSTAL
CLOCK
ENABLE
CLOCK
COUNT
Q Q̄
RESET
CLOCK
COUNT
RESET

Figure (1.13)

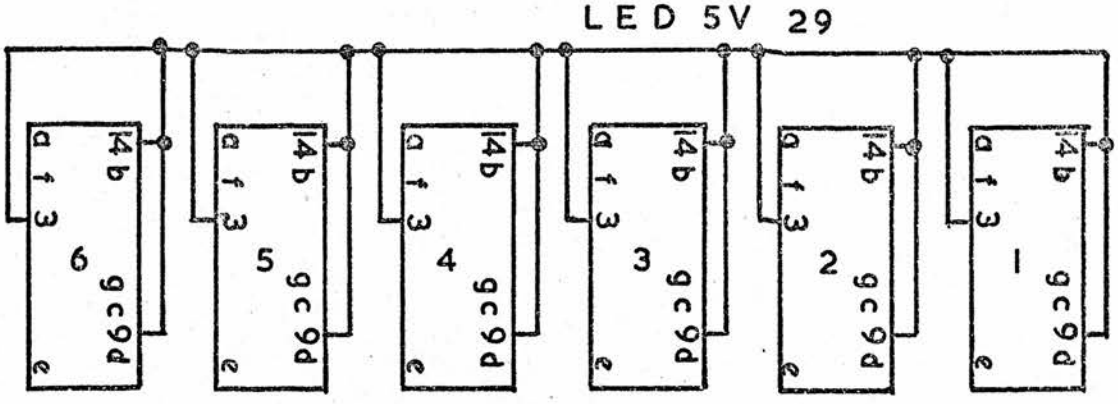
LED 5V 29
a f 3 14b g c 9d e
6
5
4
3
2
1

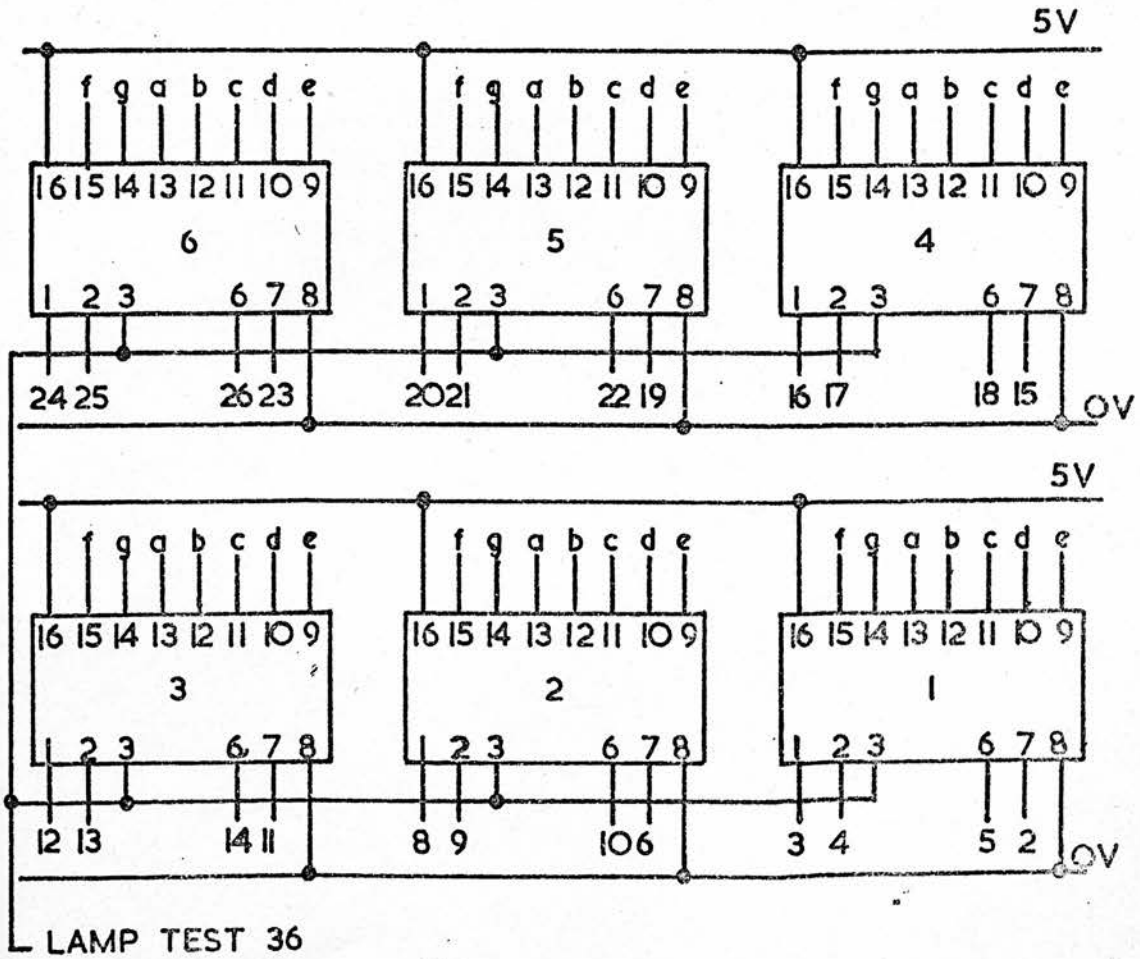
5V
f g a b c d e
16 15 14 13 12 11 10 9
6
5
4
1 2 3 6 7 8
24 25 26 23
20 21 22 19
16 17 18 15
0V
3
2
1
12 13 14 11
8 9 10 6
3 4 5 2
LAMP TEST 36

Figure(1.14)

period of 10, 20, 40 or 80 seconds. There is also a facility for continuous counting. The pulse train analysis figure (1.13) shows an example of a ten second count. A start pulse is generated by the push switch and an SN7413 Dual 4 Input Nand Schmitt trigger. The front edge of this pulse is used to latch an SN7474 Dual D-Type Flip-Flop. The Q output of this and the Crystal clock output latch a D-Type Flip-Flop whose $\bar{Q}$ output is taken as the enable signal. It can be seen from figure (1.13) that the SN7474 operates of a low-to-high transition and after the start pulse is generated waits for the next available low-to-high transition from the crystal clock to start the count. A five way switch in conjunction with two SN7490 Decade Counters feeds the tenth or twentieth or fortieth or eightieth clock pulse after the start of the count to an SN74123 Dual Monostable Multivibrator. The Q and $\bar{Q}$ outputs of the SN74123 reset the decade counter and the D-Type Flip-Flops respectively. This reset signal when applied to the SN7474 clear input sets the $\bar{Q}$ output to high and so inhibits the SN74190's. In order to change the state of the enable of the SN74190's only when the clock input is high, the $\bar{Q}$ output of the SN7474 and the V-to-F pulses are used to latch an SN7474 and the Q output of this is taken as the enable signal.

The parallel BCD outputs from the up/down counter board figure (1.11) are fed to SN7447 BCD to Seven Segment Decoder/Drivers which in turn drive TIL302 solid state visible display modules figure (1.14). A lamp test facility

is used to test the SN7447 and a dim control is incorporated in the TIL302 circuit. This is a very necessary feature for work in a darkened dome.

At this point, the result of any single observation - a six figure number - can either be recorded manually or electronically. For some time these numbers were transcribed manually which resulted in a loss of time. As part of the long term aims of this project a printer was introduced into the data handling system. An Anadex Instruments Inc. Digital Printer Model DP-SO/CK-51 is used. This provides nine data channels and Month, Day and Time in the 24-hour notation in hours and minutes. There is also a red/black option on the printout. The printer is adequately described in the manufacturer's data and a detailed description is not required here. However the way in which the printer is driven from the counter logic requires some explanation.

At the end of each count cycle the SN74123 outputs Q and $\bar{Q}$ pulses of 40nS nominal duration which are used to reset the clock logic. The printer has, as well as a push button print command, an external print command input. The positive going edge of an external print command initiates the print cycle. Paper is always automatically advanced one line to the next print position at the end of each print cycle. The minimum pulse length for this command is 10mS. The maximum width of this command is limited only by the fact that this line must be low for a minimum of 10mS before going positive again to initiate a subsequent print command.

The SN74123 is designed to provide complete flexibility in controlling the output pulse width. By triggering the input before the output pulse is terminated, the output pulse may be extended. By using an external capacitor and resister C_{ext} and R_{ext} respectively the output pulse width t_w defined as

$$t_w = 0{\cdot}25\ R_{ext}\ C_{ext}\ (1 + \frac{0{\cdot}7}{R_{ext}}) \qquad \ldots\ (1.11)$$

where R_{ext} is in KΩ, C_{ext} is in pF, and t_w is in ns. In this way the Q output is lengthened to 20ms and used as the print command. The $\bar{Q}$ output is also lengthened by this timing circuit. This modification has no effect on the reset function of the Q and $\bar{Q}$ outputs in the clock logic.

1.3 CHOPPING MIRROR DRIVE

The focal plane chopper is electronically driven by a square wave derived from an oscillator with a frequency range of 1Hz - 20KHz. The oscillator used is part of a Ling Dynamics Amplifier Model TP020. The moving mirror is mounted on a Ling dynamics Model 200 Vibrator. These components are fully compatible the amplifier, being designed to drive the vibrator. The two, amplifier and vibrator, were originally used as a unit with an external square wave being used to drive the amplifier. Unfortunately the external input to the amplifier was smoothed in such a way that high frequencies were removed from the square wave which was degraded to a sine wave. The internal oscillator

in the amplifier can only generate a sine wave so that either some external wave form generator had to be used or the internal oscillator output could be squared. Both of these solutions were tried.

Figure (1.15) shows the circuit diagram of one of the solutions tried. This circuit was designed and constructed by Mr. R.W. Parker, Royal Observatory, Edinburgh and Dr. P.W.L. Brand, Department of Astronomy, Edinburgh University. It was externally driven usually by a Farnell Sine/Square Oscillator and has an output matched to the vibrator characteristics. The external input drives a N5307 high performance Operational Amplifier used in a voltage-follower mode. The output of the N5307 drives two transisters which in turn drive two output power transisters. This circuit gave good square wave modulation for frequencies below 20Hz. Degradation of the waveform to a sinusoidal waveform occurred in increasing amounts above this frequency. The maximum displacement available was 3·68mm. The circuit operated well for short periods but operation for long periods resulted in a loss of performance. Since square wave modulation was desirable at frequencies above 25Hz and this set up required an external wave form generator and voltage supply another drive system was designed along the lines of the system described by Fahrbach et al. (1974).

The voltage transformer, the oscillator and the body of the Ling Amplifier were used as the basis of the drive system. Figure (1.16) shows the way in which the drive

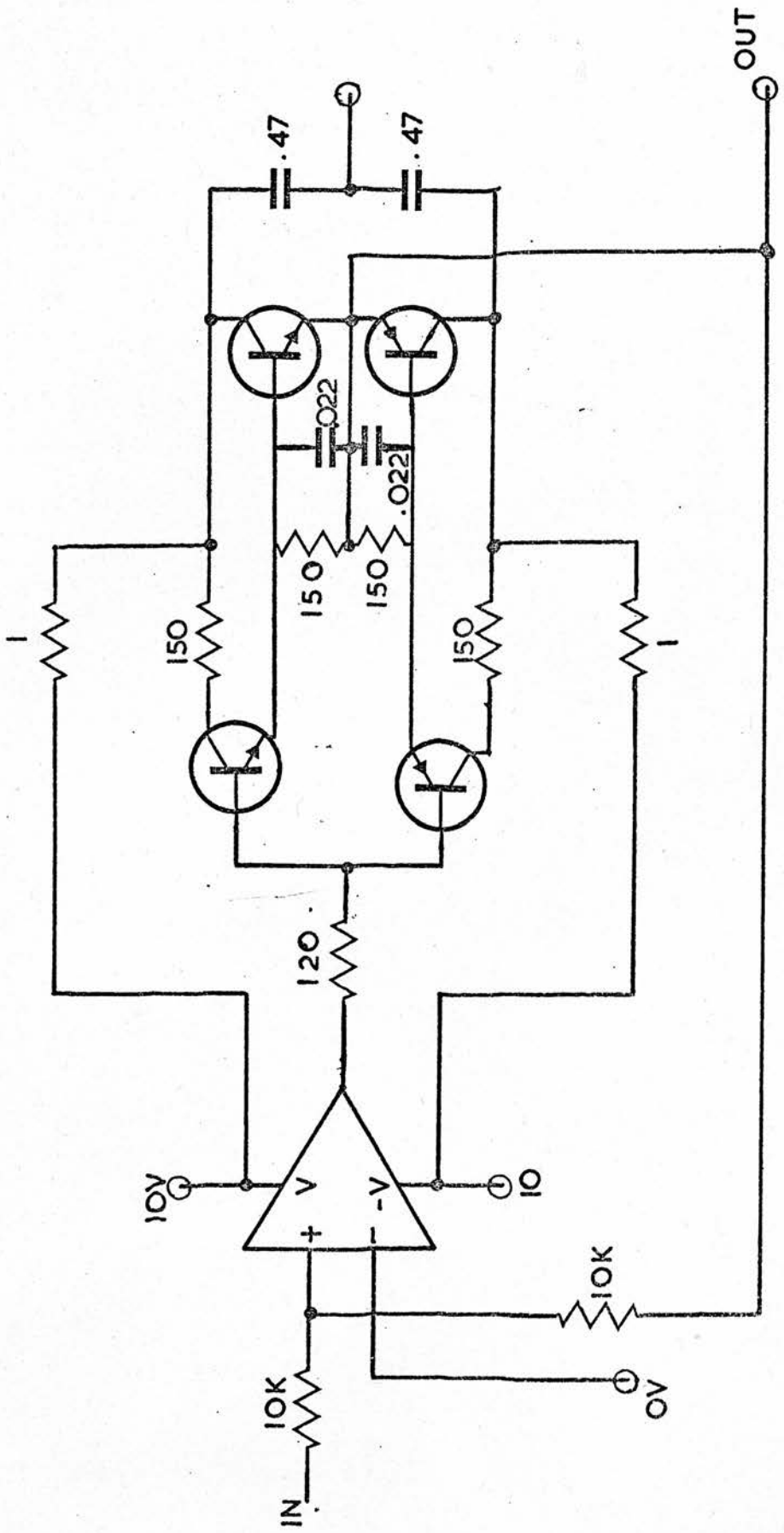

Figure (1.15)

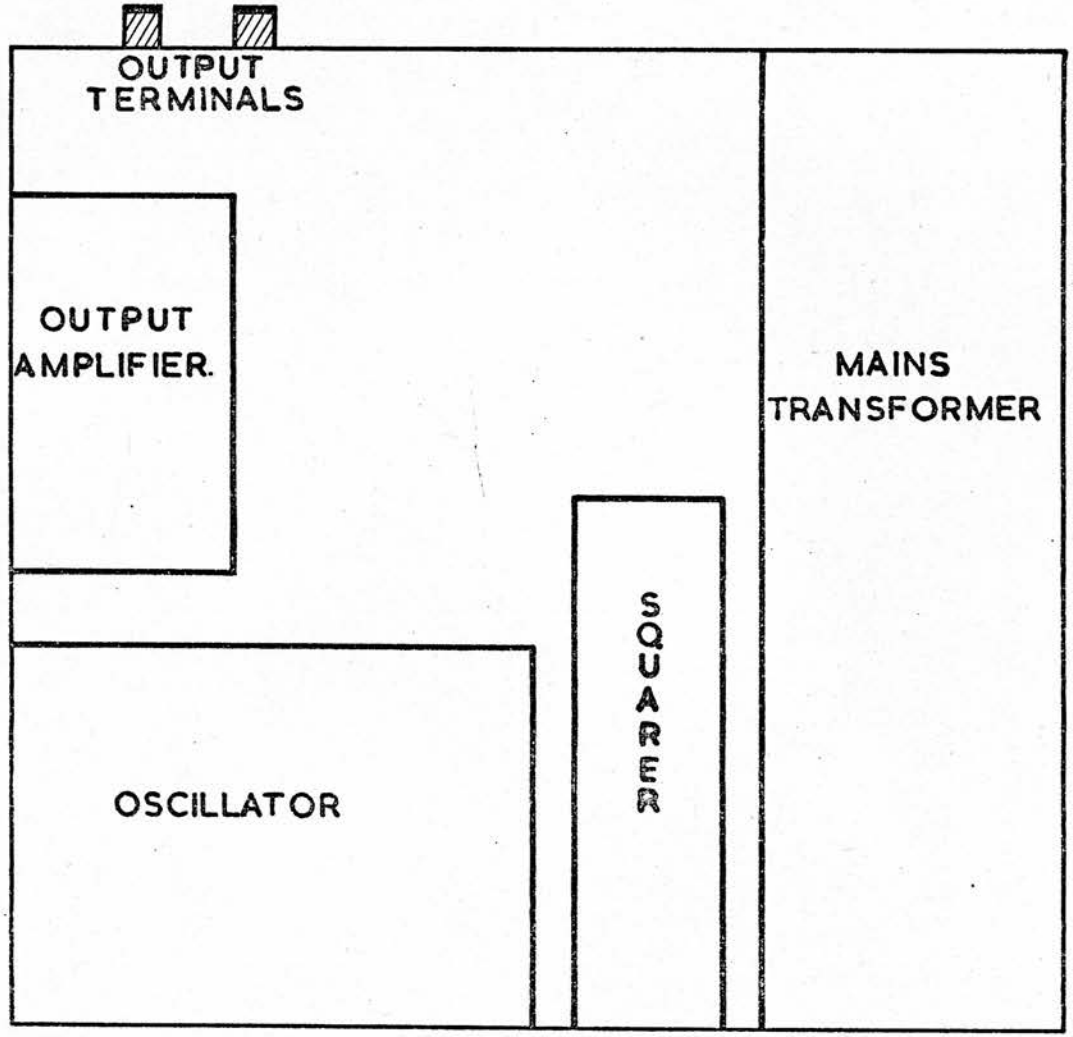
OUTPUT
TERMINALS
OUTPUT
AMPLIFIER.
MAINS
TRANSFORMER
SQUARER
OSCILLATOR

Figure C1.16)

waveform for the vibrating mirror was derived.

The oscillator output is squared by the board marked squarer (figure (1.17)) in figure (1.16). Here an SN72307 is overdriven in the voltage-follower mode to either side of a voltage drop defined by the two diodes D_1 and D_2. These Zener diodes ensure a well defined voltage drop relative to zero volts that is independent of the current being drawn. The resulting square wave is then power amplified using the circuit shown in figure (1.18).

The basis of this circuit is an RCA - HC2000H multi purpose operational amplifier which can deliver 100 watts r.m.s. to a 4Ω load at a maximum peak current of 7 amps. It is operated from a split (±34V) power supply. The d.c. resistance of the vibrator armature is 1·5Ω nominal. The waveform from the amplifier is fed to the armature in series with a 5Ω resistance. This limits the output power of the RCA HC2000H to 80 watts for frequencies below 20Hz.

The low frequency response of the HC200H is dependent upon the input network. In this application the non-inverting input is used and the feedback waveform is shaped. The output network incorporates a 22Ω resistance and an eight micro Henry choke as external phase compensation. This produces a zero phase shift up to frequencies of around 10Hz. In some circumstances, despite the phase shift compensation, some loads and methods of external wiring can produce extraneous feedback signals that cause the amplifier to oscillate. This can be corrected by the introduction of bypass capicators from the supply lines and the output

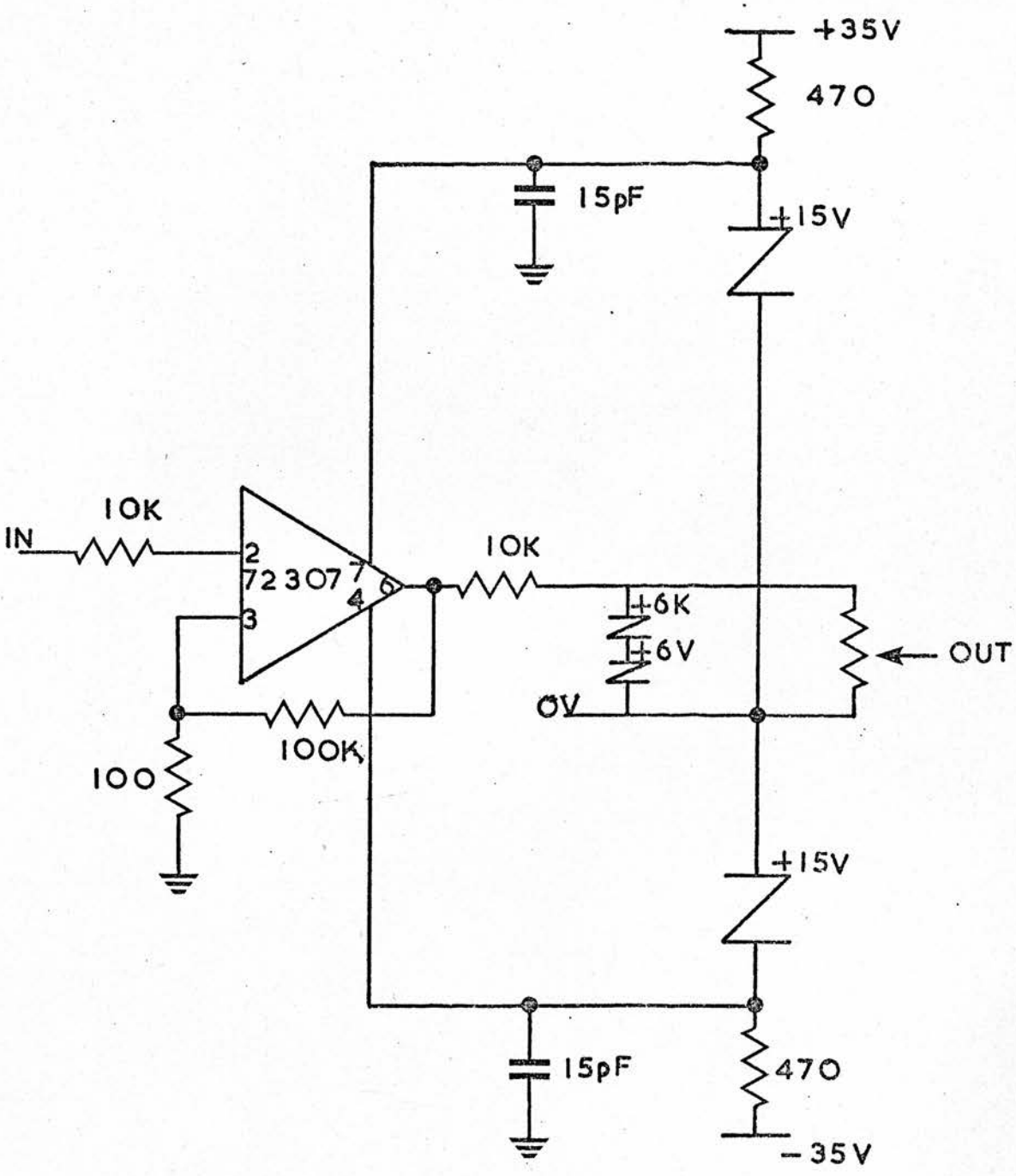
+35V
470
15pF
+15V
IN
10K
2
72307
7
4
6
3
10K
+6K
+6V
OUT
0V
100K
100
+15V
15pF
470
-35V

Figure (1.17)

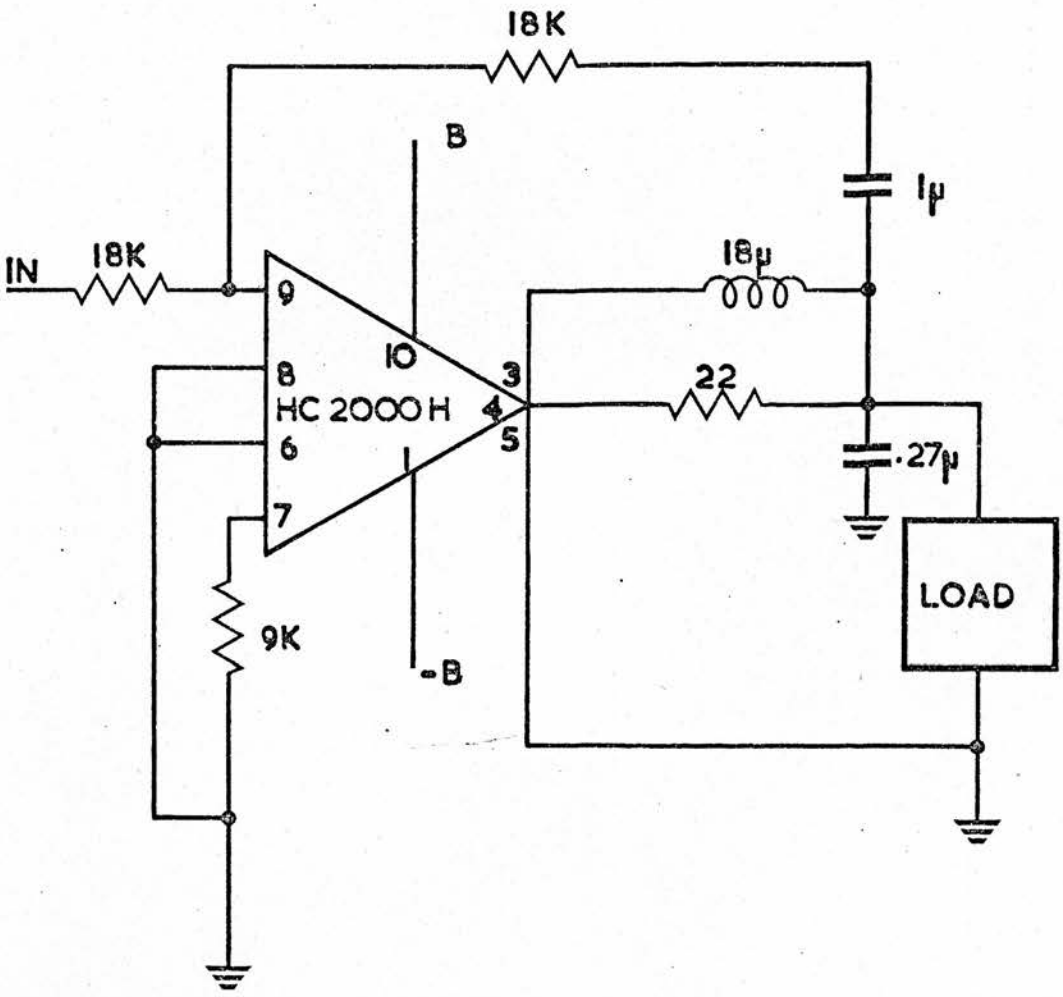

Figure (1.18)

terminal to ground.

The off-set voltage of the HC200H is typically ±30mVs and in most high power applications can be neglected. In typical operation conditions driving the armature with the adjustable mirror mounted on it the overall power required is small. However accelerating the arm from one end of the travel to the other requires about 40 watts at 4 amps. A trace of the mirror movement is shown in figure (1.19a).

This system was designed to operate at frequencies of less than 20Hz and it is interesting to note that the rise time of the waveform is typically 5ms in this frequency range. It remains the same at higher frequencies which suggests that the system is power limited by the maximum current of around 4 amps being drawn. Since the current waveform figure (1.19b) is related to the acceleration of the armature any extension to higher frequencies will require greater accelerating and hence more amps. So degradation from a square waveform to a sinusoidal one is rapid at frequencies above 25Hz. It is true to say that this process is complete at 30Hz.

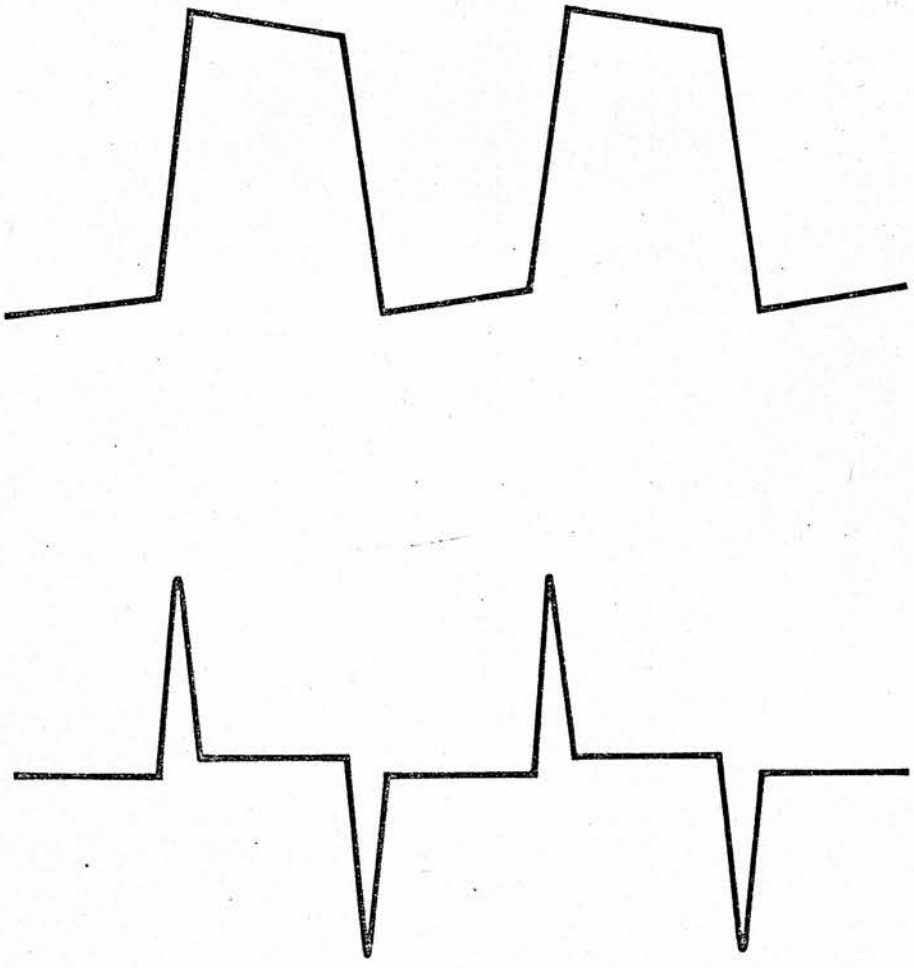

Figure (1.19a,b)

CHAPTER II

THE LEAD SULPHIDE DETECTOR AND PHASE-SENSITIVE DETECTION

2.1 DETECTION MECHANISM

Any measurement involving infrared radiation clearly needs some means for its detection. The quantities of energy to be detected are usually very small because the source is at a considerable distance and subtends a small solid angle as in astrophysical applications. All modern detectors convert an incident radiation signal into an electrical output. This output will be made up of two parts, the response of the detector to the incident radiation (called the signal) and random fluctuations known as 'noise'. Some of this 'noise' is present because of thermodynamic reasons and cannot be eliminated although it may be reduced in a number of ways.

In all infrared detectors the change in some property of the material on which the radiation is incident is measured. This change may either be measured directly, or more usually the incident radiation beam may be varied periodically or 'chopped'. The alternating signal so produced is then amplified and measured. This alternating method of detection possesses a number of advantages over the direct method. The most important of these is the rejection of unwanted radiation from the equipment. Further advantages are that:

1) a.c. signals are much easier to amplify electrically than d.c. ones,
2) any drift with time of the zero will automatically be rejected,
3) for certain types of detector, noise may be reduced by working at selected chopping frequencies.

The lead sulphide detector used in Astronomy is a light sensitive layer of small size 0·5×0·5 mm or smaller, deposited on glass with electrodes usually of gold.

The illumination of a semiconductor may be followed by various consequences. Generally, quanta of wavelength larger than 1μ do not excite photo-electrons sufficiently to obtain a metal to vacuum transition. However, they can produce an internal photo-effect which in semiconductors results in an increased population density in the conduction band and a directly enhanced conductivity. The electrons are excited to an energy state which is unstable and in due course revert to their ground state. While in the conduction band they are free to move and to contribute to the conductivity under an electric field. Such a process is termed intrinsic photoconductivity. Moreover the vacancy, positive hole, left in the otherwise full valence level can also be displaced by the field.

There may also be energy levels associated with impurities and defects in the lattice. The former case is classified as a donor level. The general phenomenon is termed impurity photoconduction. Clearly this can be established by photons of lower energy.

It is possible that as a result of processing (sublimation or chemical deposition) and baking of the surface in air or oxygen that the surface layer is oxidized. Unoxidized films have been shown to be n-type. The addition of the oxidant serves to change the film to p-type. The action of the oxide layer may therefore produce optimum conditions. The chemical deposition method is more widely

used than the sublimation one. The former method results in a more uniform sensitivity over the surface while variations of up to 50% in signal from point to point across the surface have been reported (Kruse et al. 1962). The behaviour of the oxide layer is well described (Wilman 1948, Moss 1953, Young 1955, Scanlon 1956, and Slater 1956).

The upper limit for prolonged storage is about 100^{o}C. Performance will deteriorate under long exposure to ultra-violet radiation. A decrease in performance with time has been associated with migration of sodium ions from the glass substrate into the lead sulphide film. Some films have been found to polarize i.e. to exhibit resistance dependent upon the direction of current flow under prolonged electrical bias (Kruse et al. 1962).

The mechanism of the photoconductive response in lead sulphide has been described by two differing models. The usual theory of photoconductive response states that photons falling on the crystal liberate free carriers increasing the conductivity. While the opposing theory, the so-called barrier modulation theory, based on the crystaline nature of the film has that photons falling on the film produce carriers which are trapped at the ω potential barriers that exist throughout the material at the irregular boundaries of the crystalites. The space charge due to the trapped carriers reduces the potential barriers causing the conductivity to increase through an increased effective carrier mobility (Slater, 1956).

A simple quantitative theory of the intrinsic

photoconductive effect (Conn & Avery 1960) and a more complete study (Moss 1952) show that the responsitivity is determined by the carrier lifetime, the conductivity before illumination and the element thickness.

Consider a semiconductor with a concentration of electrons and holes n and p cm^{-3} respectively with mobilities μ_n and μ_p irradiated by an incident photon flux of Qs^{-1} cm^{-2}. Then the conductivity before irradiation is

$$\sigma = e(n\mu_n + p\mu_p) \qquad \ldots (2.1)$$

while the conductivity after illumination is

$$\sigma' = e[(n+\Delta_n)\mu_n + (p+\Delta_p)\mu_p] \qquad \ldots (2.2)$$

where Δ_n and Δ_p are the changes in the concentration of electrons and holes.

Define $\Delta\sigma$, the change in conductance by,

$$\Delta\sigma = \sigma' - \sigma \qquad \ldots (2.3)$$

then

$$\Delta\sigma/\sigma = e(\mu_n\Delta_n + \mu_p\Delta_p)/\sigma \qquad \ldots (2.4)$$

and if $\Delta_n = \Delta_p$ we have

$$\Delta\sigma/\sigma = e\Delta_n(\mu_n+\mu_p)/\sigma \qquad \ldots (2.5)$$

If the semiconductor has a quantum efficiency of ε and a thickness Z then the number of excitations per unit volume of semiconductor is given by

$$\text{nos of excitations } cm^{-3} = \varepsilon Q/Z$$

assuming that Q/Z is the number of photons absorbed per unit volume. The change in the number of holes and electrons is then

$$\Delta_p = \Delta_n = \varepsilon Q\tau/Z \qquad \ldots (2.6)$$

where τ is the carrier lifetime.

If the resistance of the element is R then

$$-\Delta R/R = \Delta\sigma/\sigma$$

which on substitution from equations (2.5) and (2.6) gives

$$-\Delta R/R = e\,\varepsilon Q\tau(\mu_n+\mu_p)/\sigma Z \qquad \ldots (2.7)$$

So for high responsitivity, we require τ large and Z and σ small.

This approach concentrates only on the change in density of the carriers in the crystallites. The role of the intercrystalline barriers and space charge regions is neglected. If it is assumed that the primary mechanism is the absorption of light and the production of electron-hole pairs, any increase in mobility from barrier modulation is a secondary process. However, the latter's influence on the change in conductivity should be taken into account.

The change in conductivity that occurs when radiation falls on a film can result from a change in the density of carriers and from a change in effective mobility. If we assume that all the holes take part in the conduction process but with a reduced mobility μ^*, then

$$\mu^* = \mu\exp(-e\phi/kT) \qquad \ldots (2.8)$$

where μ is the mean hole mobility, ϕ is the potential height of the barriers referred to the valence band and T is the absolute temperature. Then for small changes in conductivity

$$\Delta\sigma = e\mu^*\Delta p + ep\Delta\mu^* \qquad \ldots (2.9)$$

where $\Delta\mu^* = -\mu\exp(-e\phi/kT)e\Delta\phi/kT$.

Here we assume that the total change in the majority carriers contributes to the change in conductivity and minority carriers have a diffusion length longer than the detector thickness.

The majority carrier lifetime is assumed equal to the photoconductive response time. So the equation of primary photoresponse can be written

$$\frac{d\Delta p}{dt} + \frac{\Delta p}{\tau} = g \qquad \ldots (2.10)$$

where g, the rate of absorption of incident photons is given by

$$g = \varepsilon Q/Z \qquad \ldots (2.11)$$

where Δp is the increase in majority carrier density over the mean value, τ the majority carrier lifetime. Let us assume the radiation to be turned on at time t=0 and we have chopped the incident radiation with some angular frequency ω. Then g in equation (2.10) may be written in the complex form

$$g = g_0 e^{j\omega t}$$

and equation (2.10) becomes

$$\frac{d\Delta p}{dt} + \frac{\Delta p}{\tau} = g_0 e^{j\omega t}$$

and has a solution

$$\Delta p = \frac{g_0 \tau e^{j\omega t}}{1+j\omega\tau} \qquad \ldots (2.12)$$

If we now define B, the relative effect of barrier modulation by

$$B = (\Delta\mu^*/\mu^*)/(\Delta p/p)$$

then equation (2.9) may be written

$$\Delta\sigma = e\mu^*(1+B)\Delta p \qquad \ldots (2.13)$$

and on taking the amplitude of equation (2.12), equation (2.13) becomes

$$\Delta\sigma = (1+B)e\mu^* g_0 \tau/(1+\omega^2\tau^2)^{\frac{1}{2}} \qquad \ldots (2.14)$$

B = 0 means that there is no barrier modulation. Comparison of equation (2.14) with equation (2.7) shows the dependence of $\Delta\sigma/\sigma$ on time constant , detector thickness Z and the dark resistance $1/\sigma$. Rewriting equation (2.14) we have

$$-\frac{\Delta R}{R} = \frac{\Delta\sigma}{\sigma} = \frac{(1+B)e\mu^*\varepsilon Q}{\sigma Z} \cdot \frac{1}{(1+\omega^2\tau^2)^{\frac{1}{2}}} \qquad \ldots (2.15)$$

2.2 NOISE AND THE NOISE EQUIVALENT POWER

Noise mechanisms in a semiconductor can be classified in two general categories: electronic and modulation noise. The electronic noise includes all fluctuations inherent in the electronic system of a semiconductor. Modulation noise includes fluctuations in quantities which exert a control over the average current.

For a detector where the photoconductive effect is due to a change in the number of majority carriers it has been shown (Petriz 1956 and Lumis & Petriz 1957) that the noise in such a detector should have four components namely, 1/f, generation-recombination, Nyquist and Shot noise. The barriers between the crystals of the detector bulk material give rise to a Nyquist and a Shot component while the crystals themselves give rise to a Nyquist and a generation-

recombination component. The 1/f component is believed to arise from the surfaces and inter-crystal barriers in the detector bulk material. They (Petriz 1956 and Lumis & Petriz 1957) show that the 1/f component dominates at low frequencies and the Nyquist and Shot components at high frequencies. Generation-recombination noise, which establishes the fundamental limit of sensitivity, should be observable at intermediate frequencies in sensitive detectors. The Nyquist Noise of the cell is usually (Lumis & Petriz 1957) grouped with that of the load and the amplifier resistors. It therefore is treated as noise arising in a resistor when no direct current is flowing and is due to the random motion of electric charge in the resistor itself. A small fluctuating voltage is developed across the ends of the resistor.

Consider the circuit (figure 2.1) and let us suppose that the system is at some absolute temperature T, in thermal equilibrium with its surrounds. Voltage fluctuations in the resistance will lead to voltage fluctuations across the capacitor. The average value of this energy, $\frac{1}{2}C\bar{V}^2$, is given by

$$\frac{1}{2}C\bar{V}^2 = \frac{1}{2}kT$$

i.e.

$$\bar{V}^2 = \frac{kT}{C} \qquad \ldots (2.16)$$

Suppose the fluctuation is due to a random e.m.f generated in a resistor and the e.m.f is analysed into a frequency spectrum, giving the mean square value of the e.m.f corresponding to fluctuations in a small frequency internal

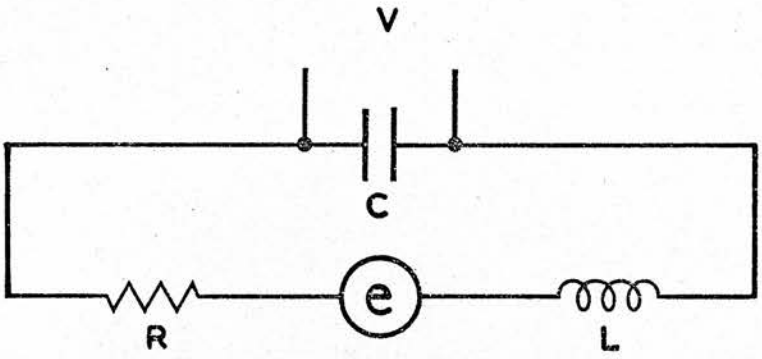

Figure(2.1)

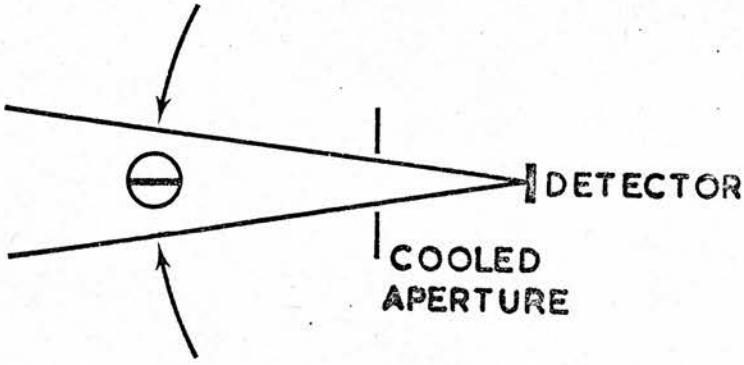

Figure(2.3)

Δf centered on some frequency f. Then for small values of Δf

$$\overline{e_f^2} \propto \Delta f$$

and

$$\overline{e^2} = E\Delta f \qquad \ldots (2.17)$$

where E is a function of frequency.

Now for the circuit shown

$$V_f = \frac{e_f}{LC\omega^2 - 1 + jRC\omega} \qquad \ldots (2.18)$$

and

$$\overline{V_f^2} = \overline{e_f^2} / (\omega^2 LC-1)^2 + R^2C^2\omega^2 \qquad \ldots (2.19)$$

now if $2\pi\Delta f = \Delta\omega$

$$\overline{V_f^2} = \frac{1}{2\pi} \frac{E\Delta\omega}{(\omega^2 LC-1)^2 + R^2\omega^2C^2} \qquad \ldots (2.20)$$

and integrating over all frequencies

$$\overline{V^2} = \frac{E}{4RC} \qquad \ldots (2.21)$$

where $\overline{V^2}$ is the mean square fluctuation. Then we have on substitution from equation (2.16)

$$E/4RC = \frac{kT}{C} \qquad \ldots (2.22)$$

i.e.

$$E = 4kTR \qquad \ldots (2.23)$$

then

$$\overline{e_f^2} = 4kTR\Delta f \qquad \ldots (2.24)$$

This is valid only where

$$hf \ll kT \quad ?$$

The Shot noise in the cell arises from the fact that electricity occurs in individual units of equal charge, e. These fluctuations would vanish if e were infinitesimal. Where the Shot noise is due to a barrier in series with a crystallite

and the barriers are thin compared to a mean-free-path in the crystallites, Petriz (1956) has shown that

$$I_b = I_s(\exp(e\Delta V_b/kT)-1) \quad \ldots (2.25)$$

and

$$I_s = A_b M_b \exp(-e\phi/kT) \quad \ldots (2.26)$$

where I_b is the current density at the barrier

I_s is the current due to the signal

ΔV_b is the voltage drop across the barrier

T is the absolute temperature

A_b is the area of the barrier

ϕ is the potential height of the barrier referred to the valence band.

M_b is a parameter describing the individual barriers

p is the mean density of majority carriers

e is the electronic charge

then the Shot theory of barriers implies that the Short circuit noise current generator $G(I^2)$ is given by

$$G(I^2) = 2e(I_b + 2I_s) \quad \ldots (2.27)$$

Define R_b the resistance of the barrier such that

$$1/R_b = \frac{\partial I_b}{\partial \Delta V_b}\Bigg| \Delta V_b = 0,\ I_b = 0 \quad \ldots (2.28)$$

then, $1/R_b = I_s e/kT$

and

$$I_s = \frac{kT}{R_b e} \quad \ldots (2.29)$$

So from equation (2.27)

$$G(I^2) = 2eI_b + \frac{4kT}{R_b} \quad \ldots (2.30)$$

and at zero bias this reduces to

$$G(I^2) = \frac{4kT}{R_b}$$

i.e. $$V^2 = 4kT\,R_b \qquad \ldots (2.31)$$

and $$\overline{V^2} = 4kT\,R_b\Delta f \qquad \ldots (2.32)$$

where $\overline{V^2}$ is the mean squared value corresponding to small fluctuations in a small frequency interval Δf. That is the Shot noise reduces to the Nyquist formula, equation (2.24). A large forward or reverse bias reduces equation (2.27) to

$$G(I^2) = 2eI_b$$

This is the Shot noise formula, which is expected since the kinetic basis is the random passage of electrons across a barrier.

In PbS detectors where the barrier is of thickness of 5-20$\overset{0}{A}$ the voltage drop across any one barrier is small compared to kT/e. This implies that $G(I^2)$ may be expressed as follows

$$G(I^2) = 2eI_s(1 + \frac{1}{2}\frac{I_b}{I_s}) \qquad \ldots (2.33)$$

and on substitution from equation (2.29)

$$G(I^2) = \frac{4kT}{R_b}(1 + \frac{1}{2}\frac{I_b}{I_s}) \qquad \ldots (2.34)$$

and $$\frac{I_b}{I_s} = \exp(e\Delta V_b/kT) - 1 \cong e\Delta V_b/kT \qquad \ldots (2.35)$$

hence

$$G(I^2) = (4kT/R_b)(1 + \tfrac{1}{2}e\Delta V_b/kT) \qquad \ldots (2.36)$$

so where $e\Delta V_b/kT \ll 1$

the Nyquist formula is a good approximation for each barrier.

Let the detector have width a and thickness Z. Let there be N crystallites in series with individual barrier area A_b. If ΔV_b is the voltage drop across each barrier then

$$\Delta V_b = V/N = V/nb \qquad \ldots (2.37)$$

where V is the total voltage drop across the cell,

n is the number of crystallites per unit length,

b is the length of the cell in the direction of current flow.

The total resistance of the cell is defined by

$$R = b/\sigma ad \qquad \ldots (2.38)$$

where σ is the cell conductivity.

The expression for the total noise due to the barriers is found by considering the number of barriers in series across the length of the cell and the number of barriers in parallel. There are N barriers in series and approximately

$$N_{\parallel} = ad/A_b$$

barriers in parallel with voltage, ΔV_b, across them. The resistance of the $N_{\parallel}$ barriers in parallel is

$$R_b/N_{\parallel}$$

So converting to voltage we have for the short circuit voltage generators on substitution from equation (2.36)

$$G(V^2) = NG(I^2)\ (R_b/N_{\parallel})^2$$

$$G(V^2) = \frac{NR_b}{N_{\parallel}}\ 4kT(1 + e\Delta V_b/2kT) \qquad \ldots (2.39)$$

This shows that the contribution of the barriers in the first order is a Nyquist term, and in the second order includes a term of order $e\Delta V_b/kT$ called a shot component. It can be

shown (Petriz 1956) that this shot component has a linear dependence on the bias current.

Generation-Recombination (G-R) noise is caused by statistical fluctuations in the rate of generation and in the rate of recombination of charged particles in the detector. These fluctuations are manifest as an electrical noise. The fluctuations can be caused by the random arrival rate of photons from the background.

In an attempt to describe G-R noise and how it depends upon the detector material parameters it has been widely accepted that the G-R noise voltage for any photoconductor is given by the expression, (Petriz, 1956, Lummis and Petriz, 1957, Limperis 1965, Humfrey, 1967)

$$V_{GR} = \frac{2IR\tau^{\frac{1}{2}}(\Delta f)^{\frac{1}{2}}}{N^{\frac{1}{2}}} \qquad \ldots (2.40)$$

where I is the bias current,

R is the detector resistance,

τ is the time constant,

N is the average number of carriers

Δf is the frequency band width.

It has been suggested (Long, 1967) that this relation holds for impurity photoconductors where the incident radiation excites electrons from donor levels to the conduction band and that it does not hold for intrinsic photoconductors where the incident radiation excites electrons from the valence band to the conduction band. It is also shown that the difference in V_{GR} for the two cases is due to the way in which the variance of the electron or hole population is estimated. The G-R noise voltage can be

written (van Vliet 1958), in the general case of a two-carrier semiconductor,

$$V_{GR} = 2IR\left(\frac{b+1}{bN+P}\right)\left(\frac{\tau(\Delta f)\langle(\Delta N)^2\rangle}{1+\omega^2\tau^2}\right)^{\frac{1}{2}} \quad \ldots (2.41)$$

where b is the ratio of electron to hole mobility

P is the average number of holes

$\langle(\Delta N)^2\rangle$ is the variance of the electron population.

This reduces to the simpler form above if $\omega^2\tau^2 \ll 1$ and there is little or no conduction by holes.

When the impurity levels are unavailable to the conduction electrons for recombination all the recombinations take place to the valence band in which case Long (1967) shows the variance to be

$$\langle(\Delta N)^2\rangle = \frac{NP}{N+P}$$

and

$$V_{GR} = 2IR\left(\frac{b+1}{bN+P}\right)\left(\frac{\tau\Delta f\ NP/(N+P)}{1+\omega^2\tau^2}\right)^{\frac{1}{2}}$$

and

$$V_{GR} = 2IR\left(\frac{b+1}{bN+P}\right)\left(\frac{NP}{N+P}\right)^{\frac{1}{2}}\tau^{\frac{1}{2}}(\Delta f)^{\frac{1}{2}} \quad \ldots (2.42)$$

if $\omega^2\tau^2 \ll 1$.

This then is the expression for the G-R noise voltage in the case of an intrinsic photoconductor where recombination of electrons takes place from the conduction band to the valence band. In the case where $N \gg P$ then $b \gg 1$ and equation (2.42) will reduce to

$$V_{GR} = 2IR\left(\frac{P}{N}\right)^{\frac{1}{2}}\tau^{\frac{1}{2}}(\Delta f)^{\frac{1}{2}} \quad \ldots (2.43)$$

That is where the enhanced conduction under illumination is

small compared to the noise generated in the detector by the random arrival of photons from the object being observed. It is advantageous to arrange for the operating conditions to be such that the limiting noise is due to the random arrival of photons from the background. The background is composed of the atmosphere, spectral filter, window material, mirrors and other objects besides the target in the detector's field of view. This type of performance can be achieved with lead sulphide detectors.

Treating black-body radiation as a photon gas with an energy distribution given by Bose-Einstein statistics and if

$$n(\lambda) = 2\pi c\lambda^{-4}(e^{hc/\lambda kT}-1)^{-1} \qquad \ldots (2.45)$$

is the number of photons per sec radiated into a hemisphere then the mean square fluctuation in the photon arrival rate is given by

$$(\overline{\Delta n^2}) = \bar{n}\left(\frac{e^{hc/\lambda kT}}{e^{hc/\lambda kT}-1}\right) \qquad \ldots (2.46)$$

where $\bar{n}$ is the average photon arrival rate. The mean square fluctuation in photon arrival rate of wavelength λ emitted by a black-body becomes

$$(\overline{\Delta n^2}) = \frac{2\pi c}{\lambda^4}\left(\frac{1}{e^{hc/\lambda kT}-1}\right)\left(\frac{e^{hc/\lambda kT}}{e^{hc/\lambda kT}-1}\right) \qquad \ldots (2.47)$$

For the limited range of detection of a lead sulphide detector, $<5\mu$,

$$hc/\lambda \gg kT$$

and

and

$$\exp(hc/\lambda kT) \gg 1$$

which allows the approximation

$$(\overline{\Delta n^2}) \cong \frac{2\pi c}{\lambda^4} e^{-hc/\lambda kT} \qquad \ldots (2.48)$$

If the detector is sensitive to radiation with a wavelength shorter than λ_c then the total mean square fluctuation in photon arrival rate limiting the sensitivity of the detector is given by

$$(\overline{\Delta n^2}) \cong 2\pi c \int_0^{\lambda_c} \lambda^{-4} e^{-hc/\lambda kT} d\lambda \qquad \ldots (2.50)$$

On integration

$$(\overline{\Delta n^2}) \cong 2\pi c \frac{kT}{hc} e^{-hc/\lambda_c kT} \left[2\left(\frac{kT}{hc}\right)^2 + \frac{2kT}{\lambda_c hc} + \frac{1}{\lambda_c^2} \right] \qquad \ldots (2.50)$$

For a detector with area A, quantum efficiency ε and measuring through a band width Δf about same frequency f the r.m.s. fluctuation in the rate of the photon arrival is given by

$$(2\Delta f (\overline{\Delta n^2}) A\varepsilon)^{\frac{1}{2}} \qquad \ldots (2.51)$$

For an incident power P_s the rate of generation of current carriers in the detector is given by

$$G_s = \varepsilon P_s \frac{\lambda}{hc} \qquad \ldots (2.52)$$

where there are λ/hc photons sec^{-1} W^{-1} at wavelength λ. In the photon limited case the generation rate G_s must be the same as the generation rate of the noise source so that, for a signal/noise ratio of one

$$\varepsilon P_s \frac{\lambda}{hc} = (2\Delta f (\overline{\Delta n^2}) A\varepsilon)^{\frac{1}{2}} \qquad \ldots (2.53)$$

Then in this case, P_s is by definition the Noise Equivalent Power so that

$$NEP = P_s = \frac{hc}{\lambda\varepsilon} (2\Delta f(\overline{\Delta n^2})A\varepsilon)^{\frac{1}{2}} \quad \ldots (2.54)$$

then on substitution for $(\overline{\Delta n^2})$ from equation (2.50) the NEP for photon noise limitation becomes

$$NEP = 2(\frac{A\pi kT\Delta f}{\varepsilon h})^{\frac{1}{2}} e^{-hc/2\lambda_c kT} \left[2(\frac{kT}{hc})^2 + \frac{2kT}{hc\lambda_c} + \frac{1}{\lambda_c^2}\right]^{\frac{1}{2}} \quad \ldots (2.55)$$

The equations derived are valid when background fluctuations only contribute to the noise. Photoconductive detectors depend upon the change in concentration of change carriers upon irradiation.

In the dark, the concentration of free carriers is determined by thermal excitation, the lattice vibrations causing electrons to acquire sufficient energy to break electron bonds and become free. The concentration of free carriers is determined by both the generation and recombination rates. Fluctuations in these rates are termed noise. When radiation falls on the detector, the carriers are undergoing photoexcitation and recombination both spontaneous and induced. It has been shown (van Vliet 1958) that at equilibrium the total noise power can be no less than twice the photon noise power alone. Since the N.E.P calculated here depends on the square root of the noise power, the photon noise limit is root two times poorer than shown. That is the N.E.P shown should be multiplied by root two.

In a photon conductor, photons arriving from any

direction will be absorbed to produce free carriers. However the back hemisphere of a cooled detector will contribute relatively few excitations and no other correction is necessary.

Having determined the NEP for monochromantic signal radiation, let us consider radiation from a black-body.

The rms fluctuations in the arrival of the background photons remains the same and we still assume a quantum efficiency of unity or less for wavelengths shorter than the cut off and zero elsewhere. We wish to determine the rate of photon absorption emitted from a black-body of some temperature T having wavelengths in the spectral sensitive range of the detector.

$$G_s' = \frac{1}{h} \int_0^{\lambda_c} \varepsilon(\lambda) \frac{\lambda}{c} \frac{2\pi hc}{\lambda^5} \frac{d\lambda}{e^{hc/\lambda kT} - 1} \qquad \ldots (2.56)$$

in terms of P_s' the total radiant power from the black-body we express the signal photon rate as

$$G_s' = \frac{1}{h} \int_0^{\lambda_c} \varepsilon(\lambda) \frac{\lambda}{c} \frac{2\pi hc}{\lambda^5} \frac{d\lambda}{e^{hc/\lambda kT} - 1} \quad \frac{P_s'}{\sigma T^4} \qquad \ldots (2.57)$$

where σ is Steffan's Constant.

Comparing G'_s and G_s, we can express G_s' in terms of G_s by

$$G_s' = G_s \frac{P_s'}{P_s} K \qquad \ldots (2.58)$$

where K is given by

$$\frac{h\lambda c}{\sigma T^4 c} \int_0^{\lambda_c} 2\pi c \, \lambda^{-4} e^{-hc/\lambda kT} d\lambda \qquad \ldots (2.59)$$

if $\varepsilon(\lambda)$ is independent of wavelength and $\lambda = \lambda_c$.

Then on integration

$$K = \frac{2\pi k\ \lambda_c^3}{\sigma T^3 c}\ e^{-hc/\lambda_c kT}\left[1 + 2\frac{kT}{hc}\lambda_c + 2\left(\frac{kT\lambda_c}{hc}\right)^2\right] \quad \ldots (2.60)$$

Proceeding as we did before we equate the rate of absorption of signal photons to the rms photon noise. The value of the NEP = P_s' is

$$NEP' = P_s' = \frac{P_s}{K} = \frac{NEP}{K} \quad \ldots (2.61)$$

The dependence of the factor K upon detector cut off wavelength (Kruse et al 1964) is shown in figure (2.2).
For this derivation the detector has been illuminated by π steradians of background. In Astronomical work the field of view of the detector is limited by a cold stop in the focal plane of the telescope where it will be cooled or by a field stop in the optical arrangement of the telescope. In both these cases the field of view will be very much less than π steradians. If the fieldstop is circular the solid angle field of view is given by

$$\Omega = \pi\sin^2(\theta/2) \quad \ldots (2.62)$$

and the effects of field of view changes in NEP can be expressed by

$$NEP(\theta) = \left(\frac{1}{\sin\ \theta/2}\right)^{-1} NEP(\pi) \quad \ldots (2.63)$$

where θ is defined in figure (2.3). In low signal applications, frequently the rule in observations of Galaxies and faint astronomical sources, the expected signal level is fairly near to that of the detector noise, so that the form and magnitude of the noise voltage is of paramount interest. The spectrum of the short circuit noise current generator,

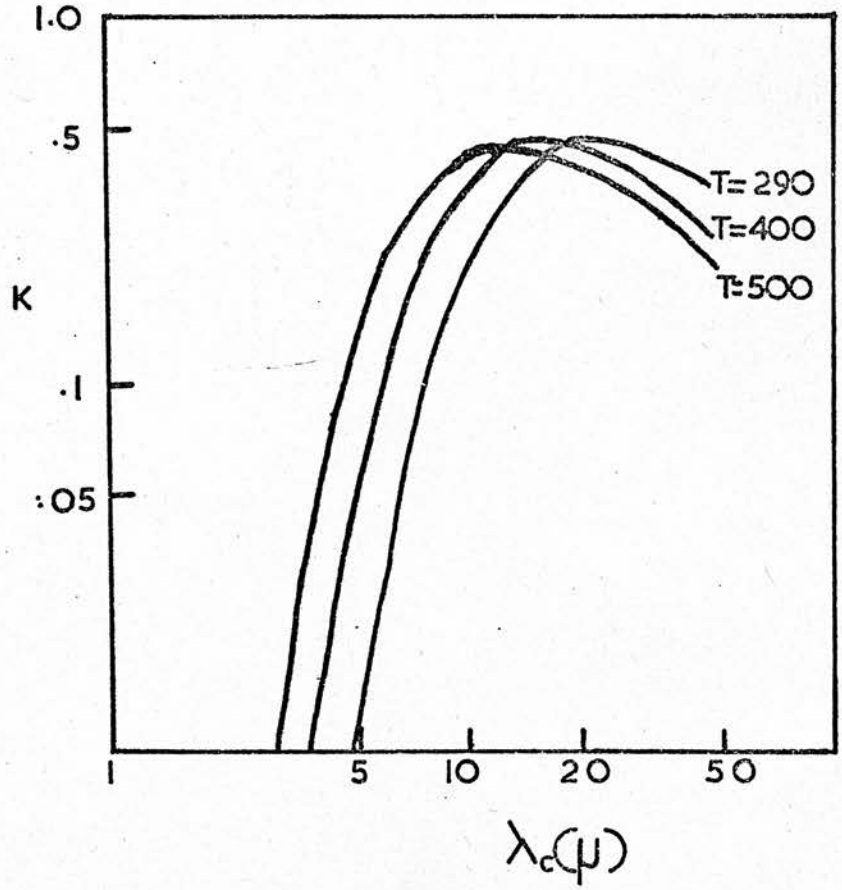

Figure(2.2)

$G(I^2)$, gives the distribution of noise power over the frequency range of interest. The term $G(I^2)\Delta f$ is the spectral noise power density in the frequency band Δf about some frequency f. The principal components of this noise spectrum, discussed above in terms of the detection mechanism, are Nyquist or Johnson noise, generation recombination noise and 1/f noise. In the case of a photoconductor the generation recombination noise is intimately associated with photon noise, as the charge carriers are generated and recombined in the random character of the incident photon stream. The total noise power spectrum is the combination of all these and in the discussion below this quantity is detailed as a function of the operation parameters of voltage bias, chopping frequency, dark resistance and time constant.

The NEP derived above in the photon noise limit is given by

$$NEP'(\theta) = \left(\frac{1}{\sin \theta/2}\right)^{-1} \sqrt{2}\, \frac{NEP(\pi)}{K} \qquad \ldots (2.64)$$

and, where the signal comes from a black-body with temperature $500^{o}K$, the photon noise in the background comes from a black-body with a temperature of $290^{o}K$, the detector is shielded to subtend an f/6 beam at the cooled aperture, the detector area is $5\times10^{-3}cm^2$ the quantum efficiency is assumed to be unity, the noise band width is unity, $\lambda_c = 4\mu$

$$NEP'(\theta) \simeq 3{\cdot}5\times10^{-14}WHz^{-\frac{1}{2}} \qquad \ldots (2.65)$$

It is assumed that the detectors used operate under the above limitations and the value given in equation (2.65) is the

theoretical limit to the NEP.

The evaluation of the NEP, sometimes referred to as the minimum detectable, power requires the measurement of two quantities: the signal produced by the detector when illuminated by modulated radiation from a calibrated source; and the detector noise when it is shielded from the source. Among the conditions of measurement which must be specified are the temperature of the radiation source, the modulation frequency and the amplifier bandwidth. Since both signal and noise may be frequency dependent, the modulation frequency must be specified. The amplifier bandwidth must be known because it determines the magnitude of the measured noise. In order to minimize the noise variations within the frequency interval over which the noise is measured, the amplifier bandwidth must be made as narrow as is practical.

The standardization of the source temperature at $500^{o}K$ (Levinstein 1970) has been suggested. For Astronomical purposes the most relevant basis for comparison is the minimum value of NEP under identical conditions. Thus any meaningful comparison of detectors must be made as close as possible to the actual conditions under which the detectors will operate namely, low background conditions and large f/no. To this end the comparison of the two types of detector made here includes, in the description of the operating parameters, a statement of f/no of the incident beam of radiation.

The NEP expressing a particular set of measurement

conditions is written

$$NEP = \frac{P_{incident}}{S/N(\Delta f)^{\frac{1}{2}}} \text{ W Hz}^{-\frac{1}{2}} \quad \ldots (2.66)$$

where $P_{incident}$ is the Power incident on the detector causing the signal. S and N are the Signal and Noise under the conditions of measurement. Δf is the amplifier bandwidth through which the noise is measured.

Another relation commonly used for the comparison of detectors is their normalized detectivity, D*, defined by,

$$D^* = A^{\frac{1}{2}}(NEP)^{-1} \text{ cm Hz}^{\frac{1}{2}}\text{W}^{-1} \quad \ldots (2.67)$$

where the area, A, of the detector is measured in cm. This convention may be misleading since the NEP may not be strictly proportional to area over the range of interest. In particular in Astronomy, the detector size is determined by the Fabry optics and the sensitivity improvement afforded by the reduction in detector size. The increase in NEP due to the decrease in detector area is a property common to most detectors but only to a limiting size of a few tenths of a millimeter and a further reduction in size may even degrade the performance of the detector (Low & Rieke 1974).

The experimental set up used for the determination of S and N and for the determination of the optimum voltage bias and chopping frequency is shown in figure (2.4). The important components are the radiation source, the low noise amplifier in the Phase Sensitive detector (PSD) and the PSD itself. The PSD is described later. The lamp, an Osram - wi 41/v has a Tungsten filament operating at a temperature of 2200^{o}K and was calibrated out to 2·6μ using the data

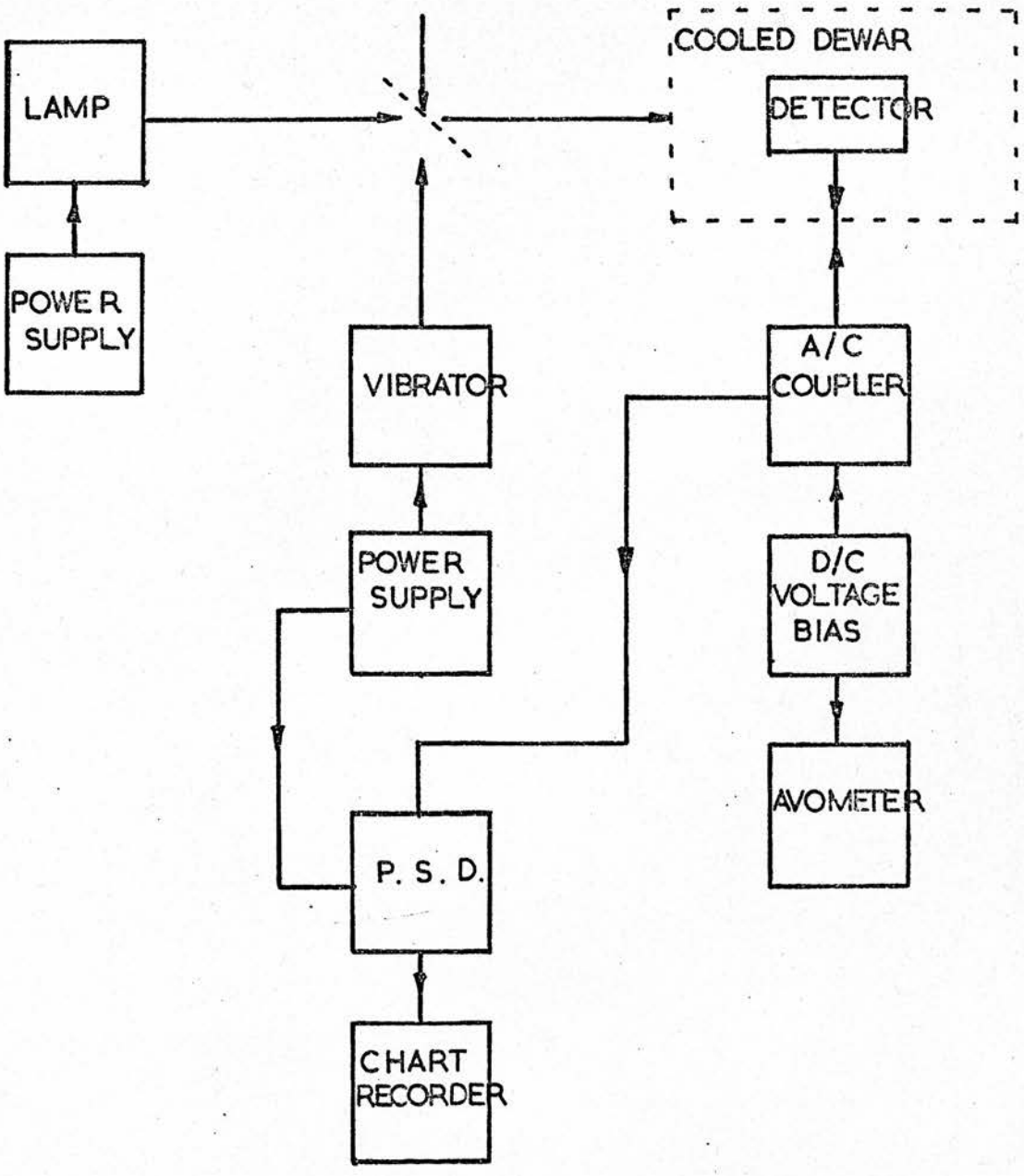
LAMP
POWER SUPPLY
COOLED DEWAR
DETECTOR
VIBRATOR
A/C COUPLER
POWER SUPPLY
D/C VOLTAGE BIAS
AVOMETER
P. S. D.
CHART RECORDER

Figure (2.4)

supplied by the makers, the emissivity of Tungsten at $2200^{o}K$ (Table 2.1) and the extension of the Planck function

$$B\lambda = \text{const } \lambda^{-5}(\exp(c_2/\lambda T)-1)^{-1}$$

where c_2 = 1·4388 cm deg, matched to the makers data. The source is mechanically chopped by the mirror. This chopper provides radiation modulated at frequencies of 1Hz to 50Hz. The chopped radiation generates an electrical signal in the detector which is then measured with the PSD. The PSD is then used to measure the in phase noise level when the detector is shielded from the radiation. The signal and noise are then determined as a function of voltage bias and chopping frequency (figure 2.5 a,b).

The primary purpose in measuring signal and noise, voltages with the equipment of figure (2.4) is to determine the detector's NEP. This can be done since the radiation intensity of the source is known from which the power density of radiation from the source falling on the detector can be calculated. The NEP is then given by equation (2.66)

$$NEP = P_s\ (S/N)^{-1}\ (\Delta f)^{-\frac{1}{2}}$$

where P_s is the power density from the source causing the signal,

S/N is the signal/noise ratio where S is taken as the signal voltage and N the noise voltage,

Δf is the electrical bandwidth through which the noise is measured.

The calibration of the source from the data supplied

TABLE 2.1 - EMISSIVITY OF TUNGSTEN AT 2200°K

λ(μ)	ε
0•7	•432
0•8	•414
0•9	•396
1•0	•378
1•1	•358
1•2	•341
1•3	•323
1•4	•308
1•5	•292
1•6	•278
1•7*	•267
1•8	•255
1•9*	•245
2•0	•235
2•1*	•227
2•2	•218
2•3*	•212
2•4	•206
2•5*	•206
2•6	•205

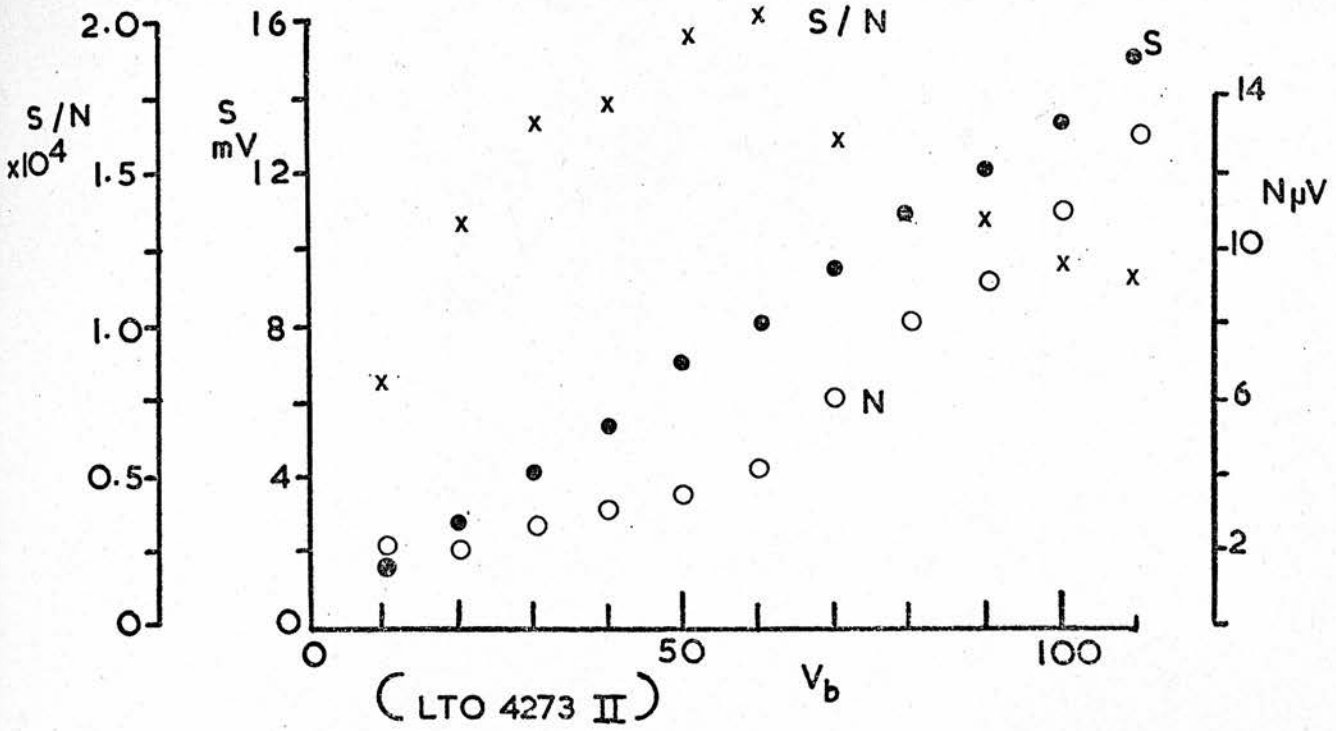
S / N
x10^4
2.0
1.5
1.0
0.5
0
S
mV
16
12
8
4
0
S / N
S
N
N μV
14
10
6
2
0
50
100
V_b
(LTO 4273 II)

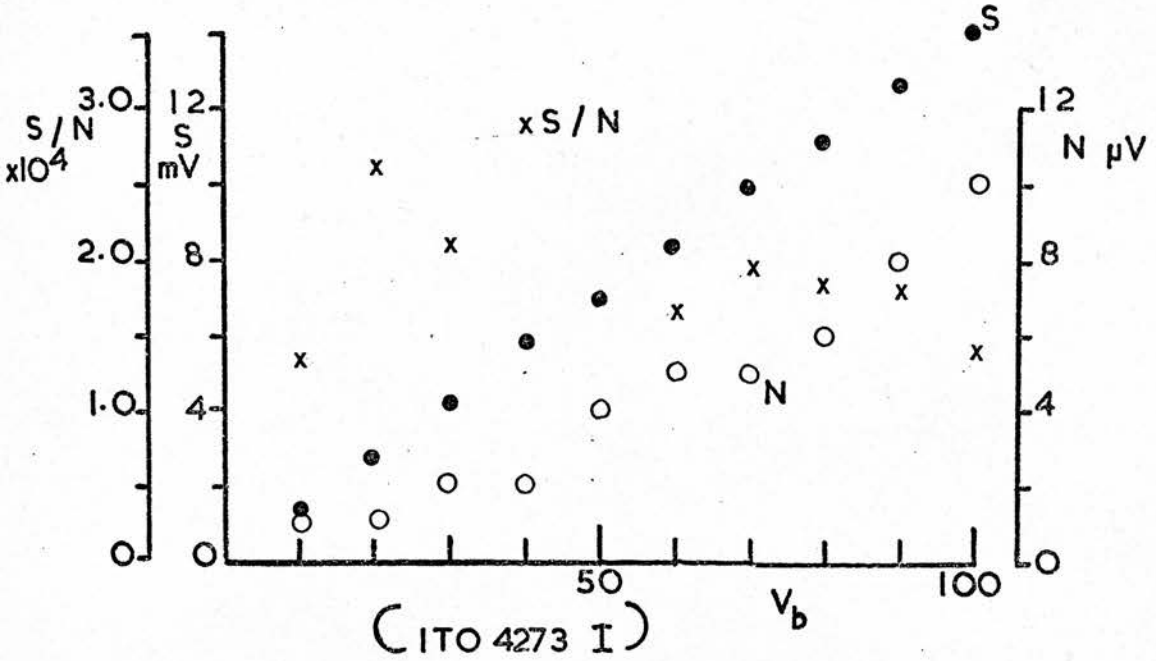
S / N
x10^4
3.0
2.0
1.0
0
S
mV
12
8
4
0
x S / N
S
N
N μV
12
8
4
0
50
100
V_b
(ITO 4273 I)

Figure (2.5a)

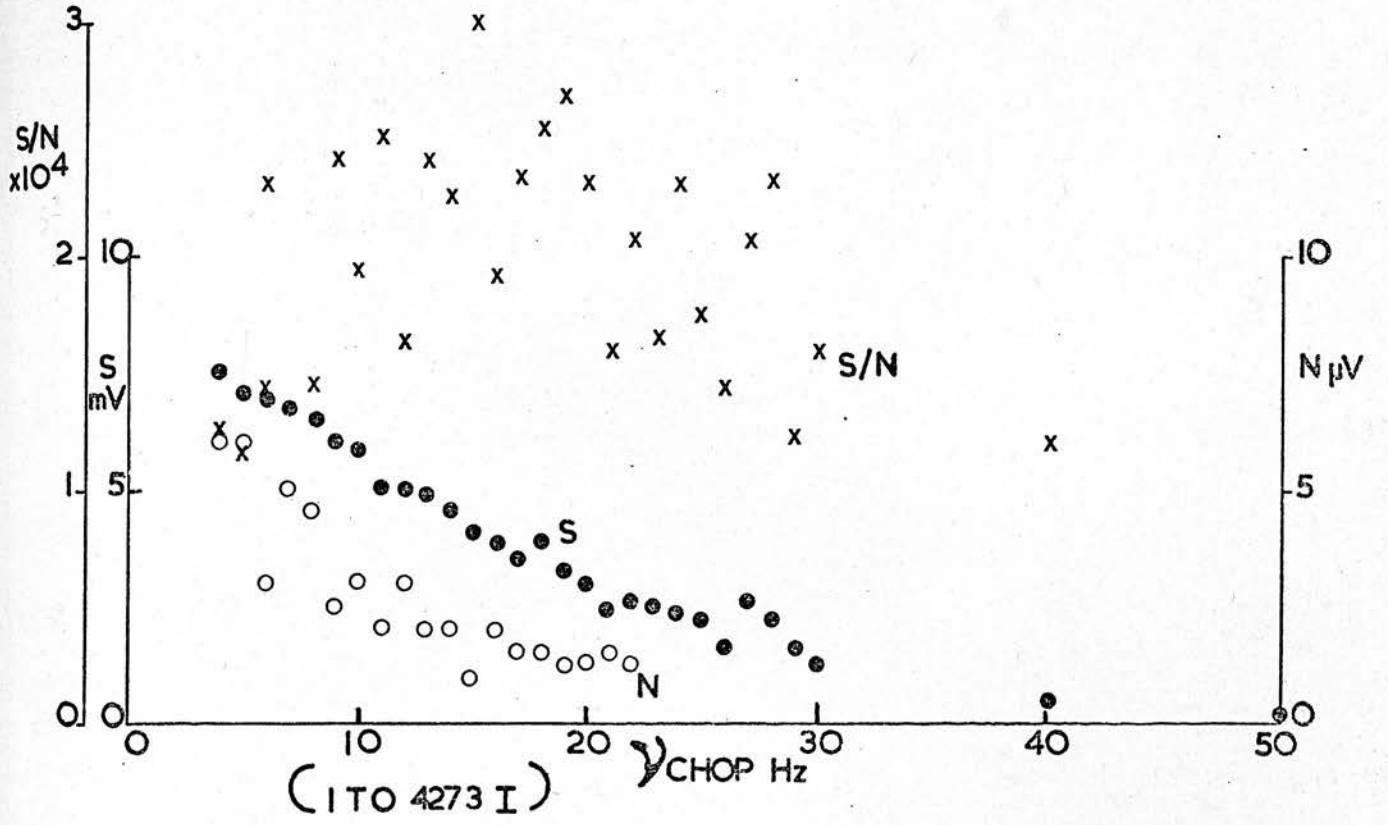
S/N x10^4
S mV
S/N
N μV
S
N
0
10
20
30
40
50
ν CHOP Hz
(LTO 4273 I)

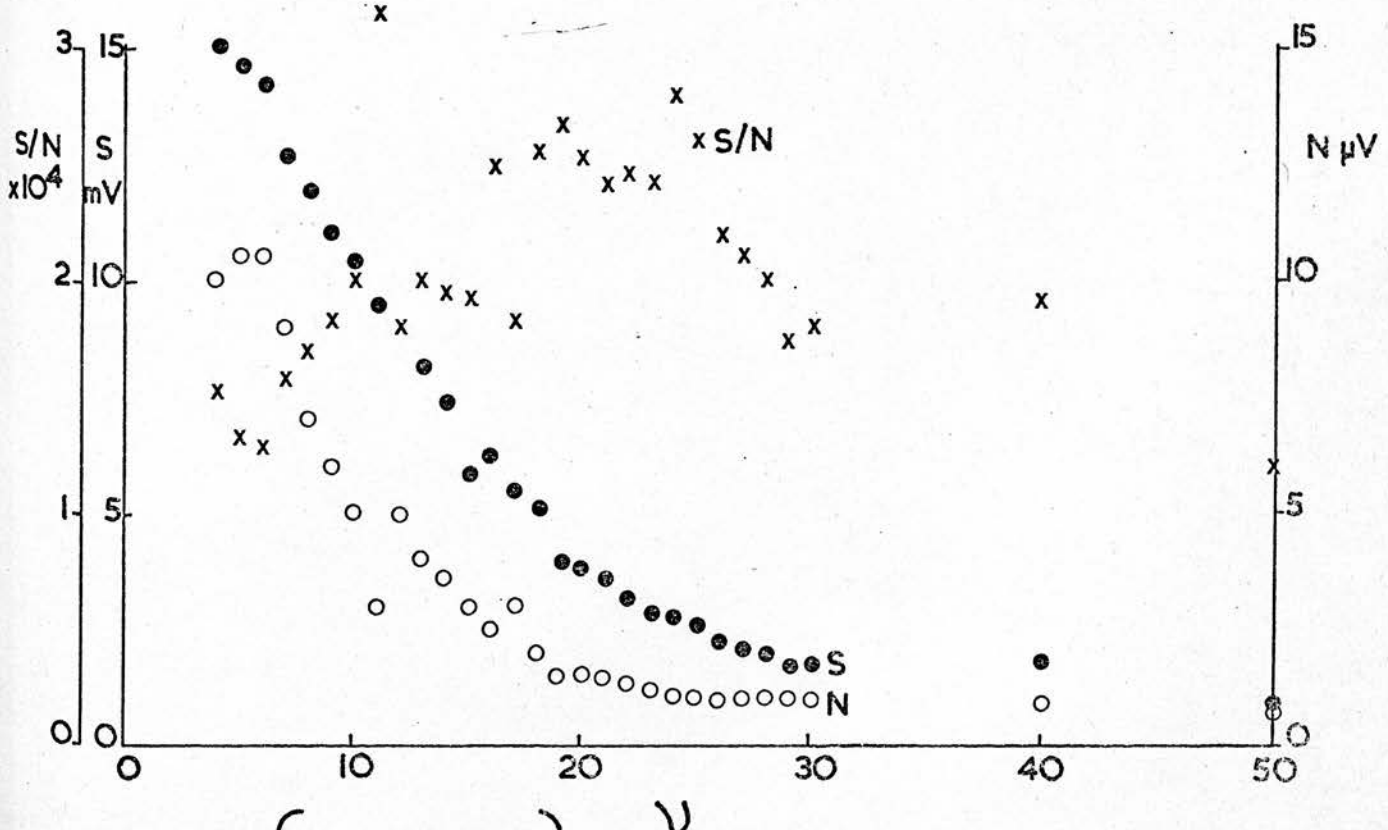
S/N x10^4
S mV
S/N
N μV
S
N
0
10
20
30
40
50
(LTO 4273 II)
ν CHOP Hz

Figure (2.5b)

by the manufacturer out to a wavelength of 2·6μ was done in the following way.

Assuming a Planck distribution then

$$B\lambda = \text{const} \times \lambda^{-5} \left(\exp(c_2/\lambda kT)-1\right)^{-1}$$

where $c_2 = 1{\cdot}4388$ cm deg.

For $T = 2200^{o}k$ and $\lambda = 0{\cdot}7\mu = 7{\cdot}10^{-5}$cm

$$B\lambda/\text{const} = 5{\cdot}211905543\times10^{-19}$$

$B\lambda(\text{lamp}) = 59{\cdot}01\times10^{-5}\,\text{Wst}^{-1}\text{nm}^{-1}\text{s}^{-1}$ from Manufacturer's data, table (2.1). From the tables the emissivity of Tungsten at $0{\cdot}7\mu = 0{\cdot}432$.

Then const $= 2{\cdot}620869106\times10^{20}$

and for $B\lambda(\text{lamp}) = 95{\cdot}82\ \text{Wst}^{-1}\text{nm}^{-1}\text{s}^{-1}$, $\lambda = 0{\cdot}8\mu$

and $\varepsilon(\lambda) = 0{\cdot}414$

then const $= 2{\cdot}692407758\times10^{20}$.

This method of calibration assumes that the area of the filament of the lamp is not known and that the radiation output from the lamp can be described by the Planck function given above. The calibration at shorter wavelengths $0{\cdot}5\mu$-$0{\cdot}8\mu$ matches the data supplied by the makers to better than 3%.

The values of the emissivity of Tungsten marked with an asterisk (*) are interpolated values using the interpolation formula

$$\varepsilon\lambda = (\varepsilon\lambda_2 - \varepsilon\lambda_1)\,\frac{\lambda-\lambda_1}{\lambda_2-\lambda_1} + \varepsilon\lambda_1 \qquad \ldots (2.68)$$

where $\lambda_1 \geq \lambda \geq \lambda_2$

The power density of the radiation (P_s) falling on the detector can then be found by integration of the curve (figure 2.6) over the limit $\lambda_{-\frac{1}{2}}$ to $\lambda_{\frac{1}{2}}$ defined by the filter

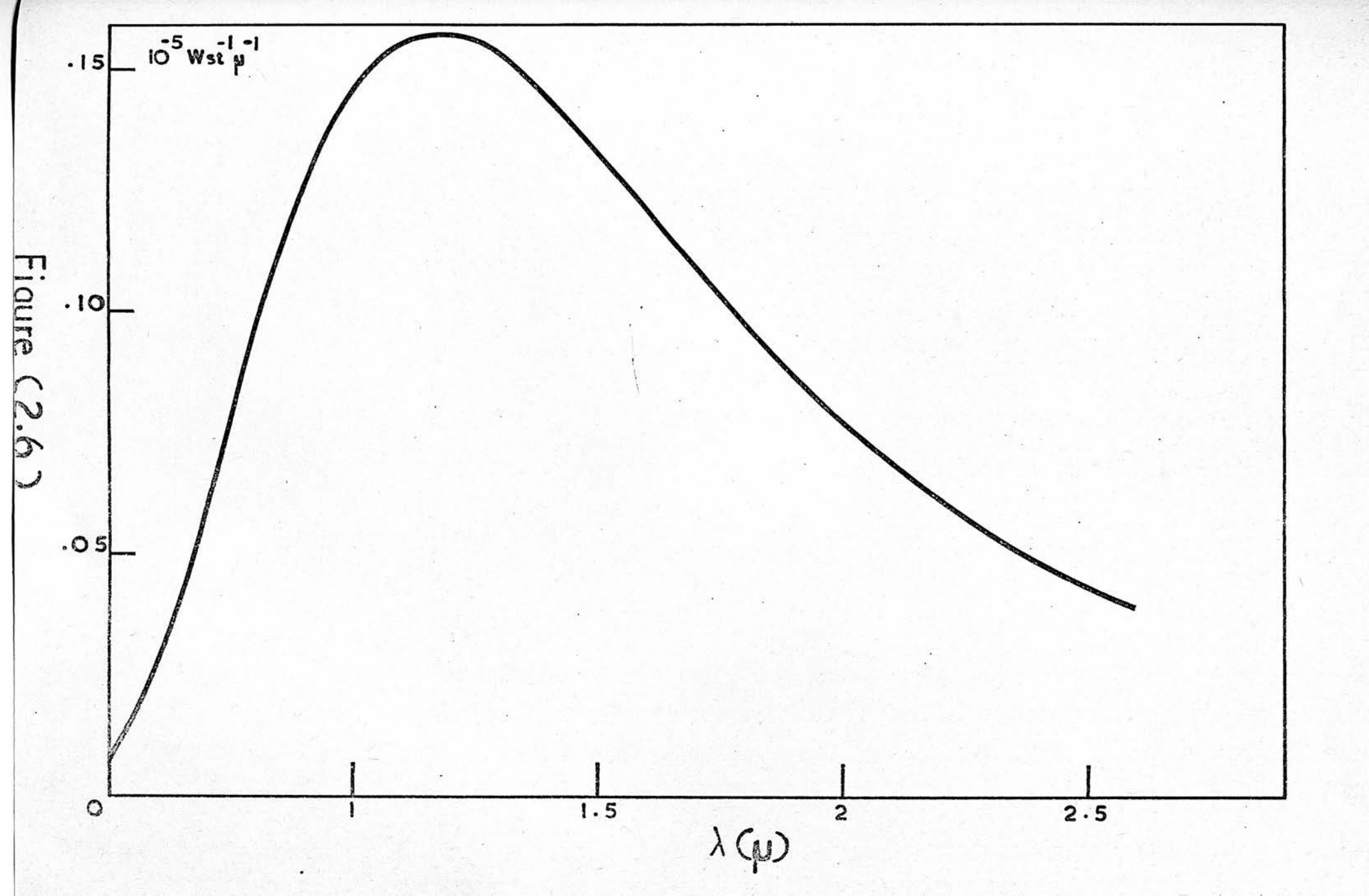

Figure (2.6)

used where

$$\lambda_1 \geq \lambda \geq \lambda_2$$

The power density of the radiation (P_s) falling on the detector can then be found by integration of the curve (figure 2.6) over the limit $\lambda_{-\frac{1}{2}}$ to $\lambda_{\frac{1}{2}}$ defined by the filter used where

$$\lambda_{-\frac{1}{2}} \leq \lambda_0 \leq \lambda_{\frac{1}{2}}$$

and the wavelength interval $\lambda_{-\frac{1}{2}}$ to $\lambda_{\frac{1}{2}}$ is the half power full bandwidth. The filter response is taken to be rectangular centered upon λ_0 with transmission given by the average transmission T_{AV} in the passband. For the filter used,

$$\lambda_0 = 2{\cdot}2\mu, \quad \lambda_{-\frac{1}{2}} = 2\mu, \quad \lambda_{\frac{1}{2}} = 2{\cdot}4\mu \text{ and } \quad T_{AV} = 60\%$$

Then

$$P_s = \int_{\lambda_{-\frac{1}{2}}}^{\lambda_{\frac{1}{2}}} B\lambda(\text{lamp}) T_{AV} d\lambda \frac{A}{(X_s)^2} \qquad \ldots (2.69)$$

where A is the area of the collecting aperture and X_s is the distance from the collecting aperture to the source. The error introduced in describing the filter response - figure (1.5) very nearly Gaussian - by a rectangle so defined is of the order of 5% in the area under the curve.

The integration equation (2.26) is done numerically by repeated application of Simpson's Rule with n+1 ordinates. The value of the integral is given by

$$I = \frac{\text{base}}{3n} [1,4,2,4,----,2,4,1] \qquad \ldots (2.70)$$

where 1/3n[1,4,2,4,----,2,4,1] is the weighted mean ordinate.

Equation (2.70) has a truncation error given by

$$E_{trunc} = -1/180 \text{ n base } f^{1V}(\zeta) \quad \ldots (2.71)$$

where ζ is the average of the ordinates and $f^{1V}(\zeta)$ is the fourth derivative of the function to be integrated evaluated at ζ. On investigation of the Truncation error given by equation (2.71) it can be shown that it is less than the error introduced in choosing the shape of the filter response function. Numerical integration of equation (2.69) gives a value of $1{\cdot}82\times10^{-9}$W.

The best signal/noise ratio achieved for both the detectors investigated is shown in figure (2.5 a,b) as a function of voltage bias and chopping frequency. The detectors, photoconductive lead sulphide, are commercially available and were obtained from Santa Barbara Research Centre. Their performance is compared to the manufacturers data in Table (2.2).

As can be seen in the above discussion, there are only a few possibilities for increasing the performance of a lead sulphide detector given that the manufacturing process remains the same for each. In general the following will have an effect

1) Increasing the time constant
2) Reducing the frequency band
3) Reducing the area of the detector
4) Increasing the quantum efficiency
5) Reducing the concentration of Carriers.

In particular, 1) and 2) are available to the user while 4) and 5) are fixed by the manufacturer.

TABLE 2.2 - COMPARISON OF MANUFACTURER'S AND EXPERIMENT OPERATING PARAMETERS.

SOURCE	MANUFACTURER		EXPERIMENT	
Detector	ITO	LTO	ITO	LTO
Temperature	193°K	77°K	77°K	77°K
R_d	0·4MΩ	1·5MΩ	1·5MΩ	1·6MΩ
R_L			1·5MΩ	1·6MΩ
f/no	π steradian	π steradian	11	11
ν chop			22Hz	16Hz
V_b	110V	110V	35V	60V

TABLE 2.3 - EXPERIMENTAL OPTIMUM OPERATING CONDITIONS AND NEPs.

DETECTOR	ITO	LTO
Temperature	77°K	77°K
R_L	1·5MΩ	1·6MΩ
f/no	11	11
ν chop	22Hz	16Hz
V_b	35V	60V
NEP $WHz^{-\frac{1}{2}}$	$6·8\times10^{-14}$	$6·5\times10^{-14}$

The two detectors were used at liquid nitrogen temperature although detector 4273-I was optimized for use at intermediate temperatures (193^{o}K). It was hoped that using this detector at low temperatures the time constant and dark resistance would increase substantially. The time constant of the ITO detector operating at 77^{o}K was very much the same as the time constant of the LTO detector. Similarly the dark resistance of the detector increased to much the same as the LTO detector. It had been hoped to use this method of obtaining a detector of intrinsically higher resistance and longer time constant, which in turn would lead to better performance. Also, the longer time constant would allow a lower chopping frequency. If the radiation is chopped at a frequency ν then the time constant can be determined (Humphrey, 1965) by

$$\tau = \tfrac{1}{2}\pi \nu_c \qquad \ldots (2.72)$$

where ν_c is the frequency at which the detector response is ·707 times its low frequency limit. Cooling of a detector increases the time constant and reduces the concentration of current carriers. Humphrey (1965) states that increasing the time constant by a process which also increases the current carrier density results in a decrease in performance. Clearly then it is desirable to match the operating frequency to the system and any optimization in performance results from an optimization of the operational frequency.

Cooling the ITO detector to liquid nitrogen temperatures should then increase the time constant. It was found that the time constant increased from 1·77ms to 7·96ms in this

case. There should also be an increase in dark resistance. The resistance increased from 0·6 MΩ at 193°K to 1·4 MΩ at 77°K. As can be seen from table (2.2) there was no perceptable increase in NEP over that quoted by the manufacturers. This detector has not, as yet, been used on a telescope on a faint source and it may be that in these circumstances there will be an increase in NEP.

The LTO detector was tested under the same laboratory conditions and an increase in NEP was seen over the manufacturers quoted value. Operation at the telescope viewing a faint astronomical source gave a further increase in NEP. It was also noted that the performance of the detector is variable in that the detector can be noisy on occasions. The best NEP obtained at the telescope is $\sim 5\times10^{-14}\,\mathrm{WHz}^{-\frac{1}{2}}$ which is an improvement on both the manufacturers data and the laboratory optimization.

It has been shown here that optimization of the detector performance is possible as a function of voltage bias and chopping frequency. The best value of NEP comes close to that predicted by the photon noise limit. As has been suggested 1/f noise is present in the noise spectrum at chopping frequencies below 100Hz but, in the case of the LTO detector, it is not serious enough to limit the detector performance to a great extent. It is therefore suggested that this detector is working in the photon noise limit under the conditions given in table (2.3). In the case of the ITO detector, the best NEP from the laboratory optimization show no such gains. In both cases deviations from the curves in figures (2.5 a,b) could be due to

the shape of the main body of the photometer. Certainly, the ITO detector was found to be microphonic and to exhibit a larger scatter from the smooth curves in figures (2.5 a,b). The lack of increase in NEP could be due to an increase in 1/f noise and a decrease in sensitivity. Both being a direct result of the lower operating temperature.

2.3 PHASE SENSITIVE DETECTION

The accurate measurement of a.c signals is often affected by the presence of noise, which may be reduced by special screening and earthing. However this does nothing to reduce random noise, the limiting factor to resolution in the measurement of small signals. A solution to this problem is the use of a Phase Sensitive Detector (PSD) and it is shown here how such an instrument can recover a.c. signals from both random and nonrandom noise.

Random noise can be divided into two categories:

1) noise generated in the source

2) noise in the signal recovery system.

Noise generated in the source has been described along with the noise inherent in the detector. Amplifying devices which carry direct current produce noise and it is important to know how the PSD copes with these noise signals.

The instrument used was a Brook deal Electronics Lockin Amplifier (LIA). The LIA consists of three main parts:

1) an amplifier

2) a PSD

3) a reference section.

The amplifier is normally necessary to increase the magnitude of the noisy signal to a level usually just below the overload level of the PSD. The Brookdeal 401A LIA has an input dynamic range of 100dB (10^5 voltage ratio), a low noise input with 1μV full scale sensitivity and wide-band operation from 1Hz to 50kHz. The Short circuit input noise is typically 20nV $Hz^{-\frac{1}{2}}$ at frequencies ∿10Hz. The low noise performance is useful since increased noise limits the recovery of very small signals and degrades measurement quality. The amplification is highly linear with typical nonlinearity of <0·01%.

Low noise filtering of the signal input takes place well away from the signal frequency. A Passive linear line frequency notch filter and low and high pass filters perform the functions of line rejection, Hi-Cut reduction of the response to 5kHz for operation at frequencies below 3kHz and Low Cut extension of the operational frequencies below 10Hz. The Low-Cut filter (LF) simply extends the 3dB points to 5Hz and can be adjusted to 1Hz if necessary.

The LIA has its own reference channel which is triggered by the positive going edge near to the mean level of the reference input waveform. This is accomplished by using a differential amplifier connected to a Schmitt Trigger. The input is differential in order to minimise ground loops. If the reference ground is connected to one side of the differential amplifier there is no way in which the reference

current taken by the LIA can return by the signal ground line. If this occurs an a.c. voltage is created which is indistinguishable from the signal voltage.

The reference waveform generated in the LIA is a square wave with the same frequency as the input reference signal. The control system used is called a mark space generator (msg). The msg provides two basic functions:

1) generation of symmetrical square waves
2) generation of a calibrated phase shift.

This system provides a symmetrical wave form and a phase shift control of up to 360^{o}. Thus the phase difference between the signal input waveform and the symmetrical reference waveform generated by the msg can be varied from 0^{o} to 360^{o}.

The PSD works on the principle of the synchronous switch (figure 2.7). The signal is periodically switched to the load resistors the frequency and phase of the switching being determined by the reference voltage. If the signal and reference voltages have the same frequency and phase the voltages across the load resistors will have the form shown in figure (2.8). It is seen that the balanced PSD gives fullwave rectification into the d.c. measuring device.

The bandpass characteristics of the PSD are determined by the output filters. In the 401A the main output filtering is determined by the time constant of the capacitor and the impedance of the resistor in the circuit figure (2.9) shown.

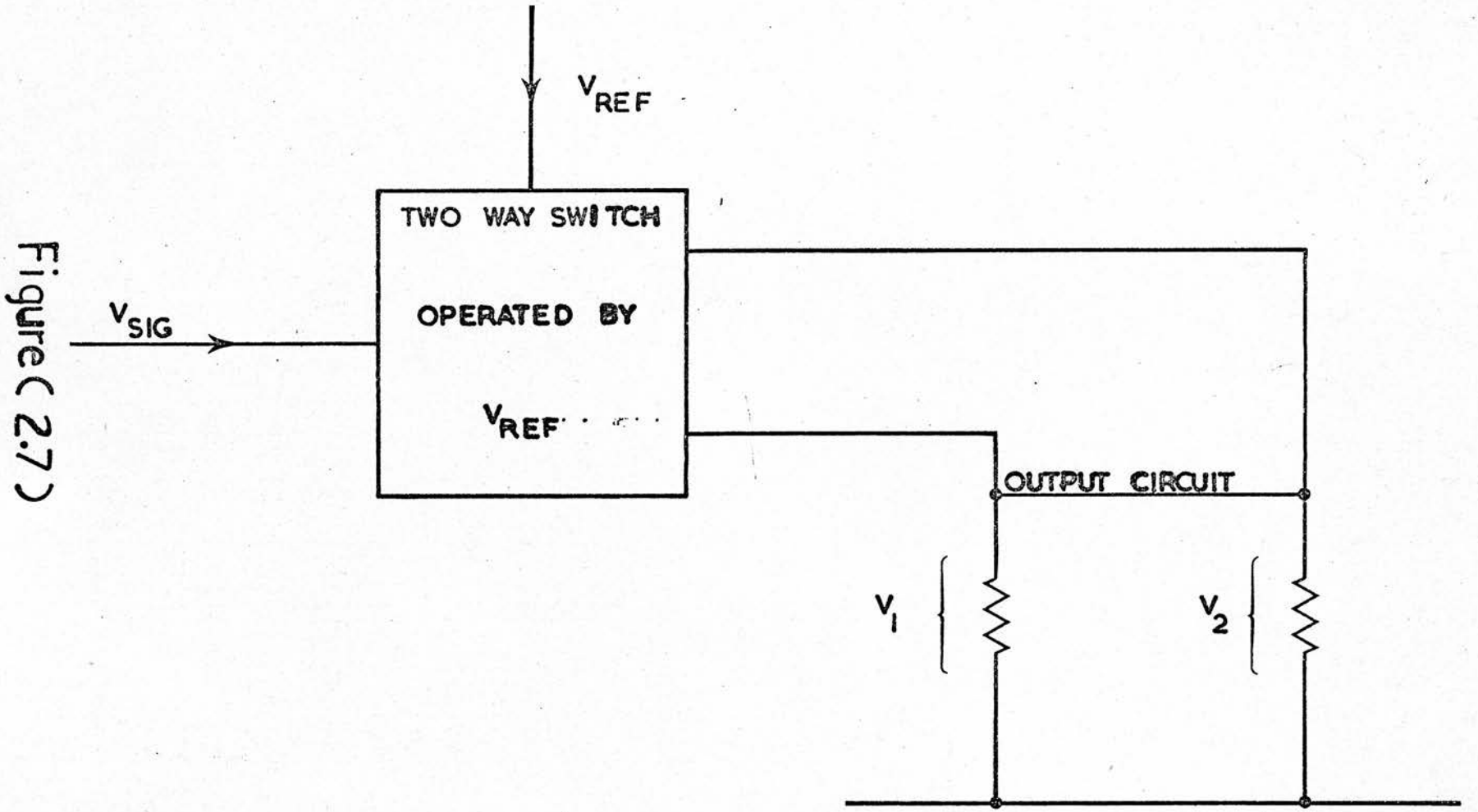
V_{REF}
TWO WAY SWITCH
OPERATED BY
V_{REF}
V_{SIG}
OUTPUT CIRCUIT
V_1
V_2

Figure(2.7)

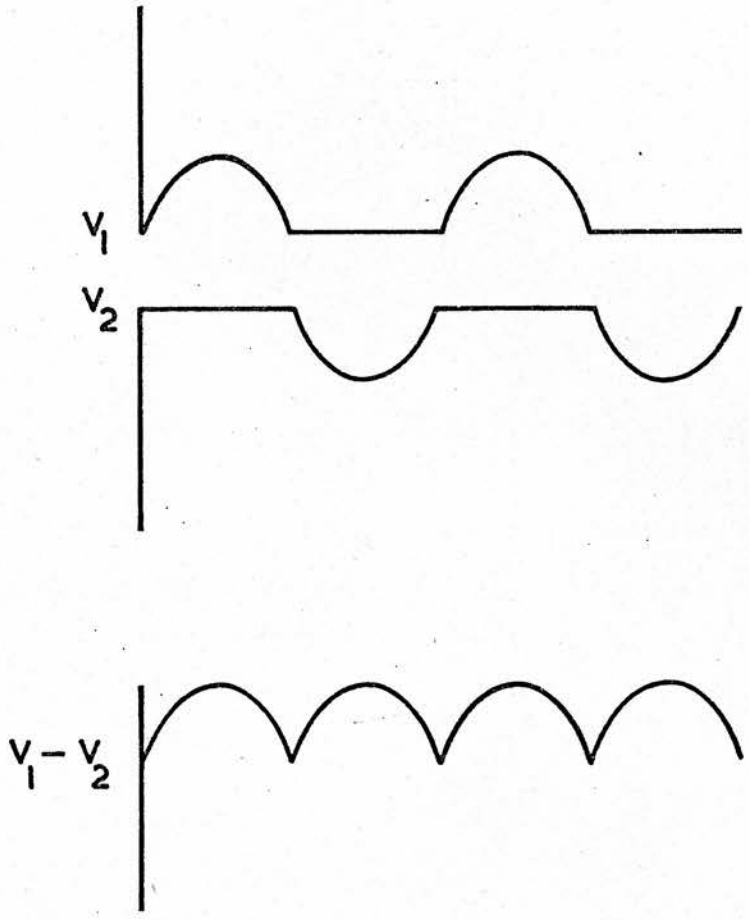

Figure(2.8)

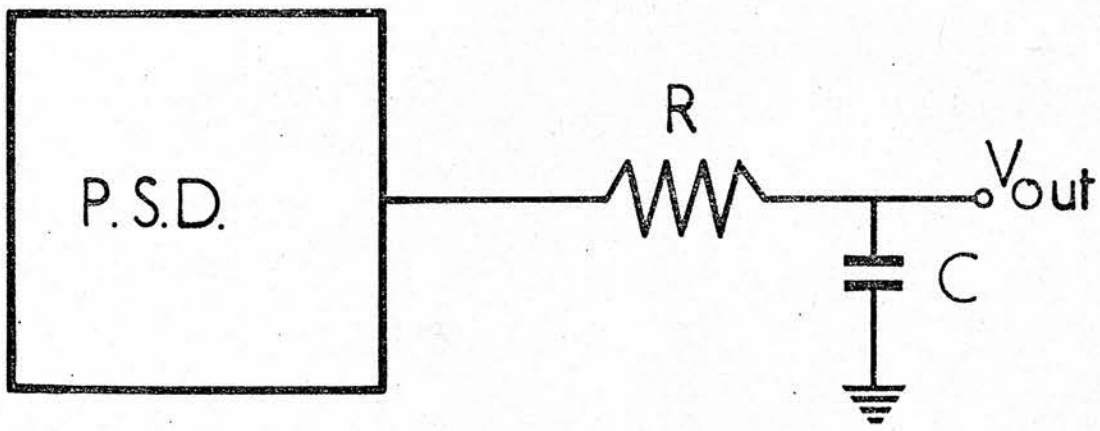

Figure (2.9)

Mathematically, the operation performed by the PSD corresponds to multiplying the signal input voltage by a square wave. Let the reference voltage be square with frequency ω_R. Decomposing the square wave into its Fourier components the reference voltage V(R) is given by

$$V(R) \alpha \cos\omega_R t + 1/3 \cos 3\omega_R t + \text{------}$$

Therefore all these components have contributions which diminish with their coefficients. That is, there are odd harmonic terms of ω_R.

If ϕ is the phase difference between the signal voltage and the reference voltage any term in the signal such as

$$V_S \cos(\omega_R t + \phi)$$

will give, amongst others, a product

$$V_S \cos(\omega_R t + \phi) \cos\omega_R t.$$

which is proportional to

$$\frac{1}{2}\left(V_S \cos\phi + V_S \cos(2\omega_R t + \phi).\right.$$

It can be seen that $V_S \cos\phi$ is a d.c. term and appears at the output while the other term is an a.c. component and, with a suitable filter time constant will be effectively rejected.

Any signal going to the PSD has components of signal from the object and noise. Let the signal be S with the star in and S' with the star out. Then let

$$S = S_0 + n_S + \bar{b}_S + n_{bS} + n_d \qquad \ldots (2.73)$$

and

$$S' = \bar{b}_0 + n_{b0} + n_d \qquad \ldots (2.74)$$

where S_0 is the star signal

n_S is the star noise

$\bar{b}_S$ is the sky signal, star in

n_{bS} is the sky noise, star in

n_d is the detector noise

$\bar{b}_0$ is the sky signal, star out

n_{b_0} is the sky noise, star out.

Approximate $n_{bS} \simeq n_{b_0}$ and let the mean of all the noise sources n's $\bar{n}=0$.

The signal then has a d.c. component given by

$$\tfrac{1}{2}(S_0 + b_S + b_0)$$

and an a.c. component with an amplitude given by

$$[\tfrac{1}{2}(S_0 + b_S - b_0) + n_S + n_b]d(t) + n_d$$

due to the motion of the chopper d(t).

The internally generated reference waveform is taken to be d(t). This is a square wave and is described for all integer n, by

$$\begin{aligned} d(t) &= 1 \quad nT \le t \le nT + T/2 \\ &= -1 \text{ otherwise} \end{aligned} \qquad \ldots (2.75)$$

The PSD multiplies the signal by d(t) and takes the average after some time t' using a filter $\omega(t)$ which removes the d.c. component.

Write the a.c. signal as

$$S + n$$

where $S = \tfrac{1}{2}(S_0 + b_S - b_0)$

and $n = n_S + n_b$

and

$$n = n_S + n_b$$

Let the filter function be normalized i.e.

$$\int_{-\infty}^{\infty} \omega(t)dt = 1$$

Then, the signal out of the PSD S_{out} is given by

$$S_{out} = \int_{-\infty}^{\infty} \{(S+n)d(t')+n_d\}d(t')\omega(t-t')dt' \quad \ldots (2.76)$$

$$S_{out} = S + \int_{-\infty}^{\infty} n\omega(t-t')dt' + \int_{-\infty}^{\infty} n_d d(t')\omega(t-t')d(t') \quad \ldots (2.77)$$

The noise component of S_{out} is given by the two integrals. We define the Noise Power Spectrum NPS in the following way. If n(t) is a stationary function, the output of a signal generator say, then $|N|^2$ the (NPS) is given by

$$|N|^2 = \lim_{T\to\infty} \left| \frac{1}{T} \int_{-T/2}^{T/2} n(t)e^{-2\pi i\nu t}dt \right|^2 = N(\nu) \quad \ldots (2.78)$$

and any particular sample can be expressed as

$$N(\nu) = N_0(\nu)e^{i\phi(\nu)} \quad \ldots (2.79)$$

The NPS is then the modulus squared of the Fourier Transform of the function n(t).

The associated NPS of the integrals in equation (2.77) are

$\|F[n*\omega(-t)]\|^2$	and	$\|F[n_d d*\omega(-t)]\|^2$
$\|F[n]\|^2 \ \|F[\omega]*\|^2$	and	$\|F[n_d d]\|^2 \ \|F[\omega]*\|^2$
$N\|W\|^2$	and	$\|N_d*D\|^2 \quad \|W\|^2$

where F implies the Fourier Transform of the function in

square brackets, N is defined by equation (2.78) and W, N_d and D are the Fourier transforms of ω, n_d and d. N is the NPS of star + sky and D is the Fourier transform of a square wave. If d(t) is defined by equation (2.75) then D is

$$D = \frac{2}{i\pi T} \sum_{n_{odd}} \frac{\delta(\nu - n/T)}{\nu} \qquad \ldots (2.80)$$

From equation (2.79) N_d can be written

$$N_d = N_{d_0} e^{i\phi(\nu)} \qquad \ldots (2.81)$$

then

$$|N_d * D|^2 = \frac{4}{\pi^2} \sum_m \sum_n \frac{1}{nm} N_{d_0}(\nu - n/T) N_{d_0}(\nu - m/T) e^{i(\phi(\nu-n/T) - \phi(\nu-m/T))} \qquad \ldots (2.82)$$

The ensemble average < > of this is given by

$$\int_0^{2\pi} d\phi$$

which gives at each ν a $\delta(\phi(\nu-m/T) - \phi(\nu-n/T))$ which reduces equation (2.82) to

$$|N_d * D|^2 = \frac{4}{\pi^2} \sum_{n_{odd}} \frac{1}{n^2} N_d(\nu - n/T) \qquad \ldots (2.83)$$

where N_d is the detector NPS.

In the particular case where N_d is flat and given by n_0 then

$$|N_d * D|^2 = \frac{4}{\pi^2} n_0 \sum_{n_{odd}} \frac{1}{n^2} \qquad \ldots (2.84)$$

Consider $$\sum_{n_{odd}} \frac{1}{n^2} = \sum_n \frac{1}{n^2} - \frac{1}{4} \sum_n \frac{1}{n^2}$$

then $$\sum_{n_{odd}} \frac{1}{n^2} = \frac{3}{4} \left(\sum_n \frac{1}{n^2} \right)$$

If the sum is over all n i.e. all positive and negative n then

$$\sum_{\substack{\text{all} \\ \text{n}}}^{\substack{+\text{ve} \\ -\text{ve}}} \frac{1}{n^2} = 2\left(\frac{\pi^2}{6}\right)$$

then

$$|N_d * D|^2 = \frac{4}{\pi^2}\, n_0\, 2\left(\frac{\pi^2}{6}\right)\frac{3}{4}$$

i.e. $$|N_d * D|^2 = n_0 \qquad \ldots (2.85)$$

The output of the PSD is a signal plus noise of two origins. The noise comes from the sky and star noises filtered by the time constant and the detector noise modulated by the chopper and filtered by the time constant. The resulting shape of the NPS is given in figure (2.10).

If the detector noise consists of white noise n_0 with a filter component (α 1/f) given by n_0 at some frequency $\nu' \simeq 10$Hz then with

$$M(\nu) = n_0 \nu'/\nu$$

$$|N_d * D|^2 |W|^2 = \left[n_0 + \frac{8}{\pi^2}\left(M(1/T) + \frac{1}{9}\, M(3/T) + \text{---}\right)\right]|W|^2 \qquad (2.86)$$

due to the square modulation of the chopper. Now with $\nu = \frac{2\pi}{T}$ equation (2.86) becomes

$$|N_d * D|^2 |W|^2 \simeq n_0\left[1 + \frac{4\nu' T}{\pi^2}\,(1 + 1/3^2 + 1/5^2 + \text{---})\right]|W|^2 \qquad \ldots (2.87)$$

then

$$|N_d * D|^2 |W|^2 \simeq n_0[1 + 0{\cdot}41\nu' T(1{\cdot}23)]|W|^2 \qquad \ldots (2.88)$$

$$|N_d * D|^2 \simeq n_0\left(1 + \frac{\nu' T}{2}\right)|W|^2 \qquad \ldots (2.89)$$

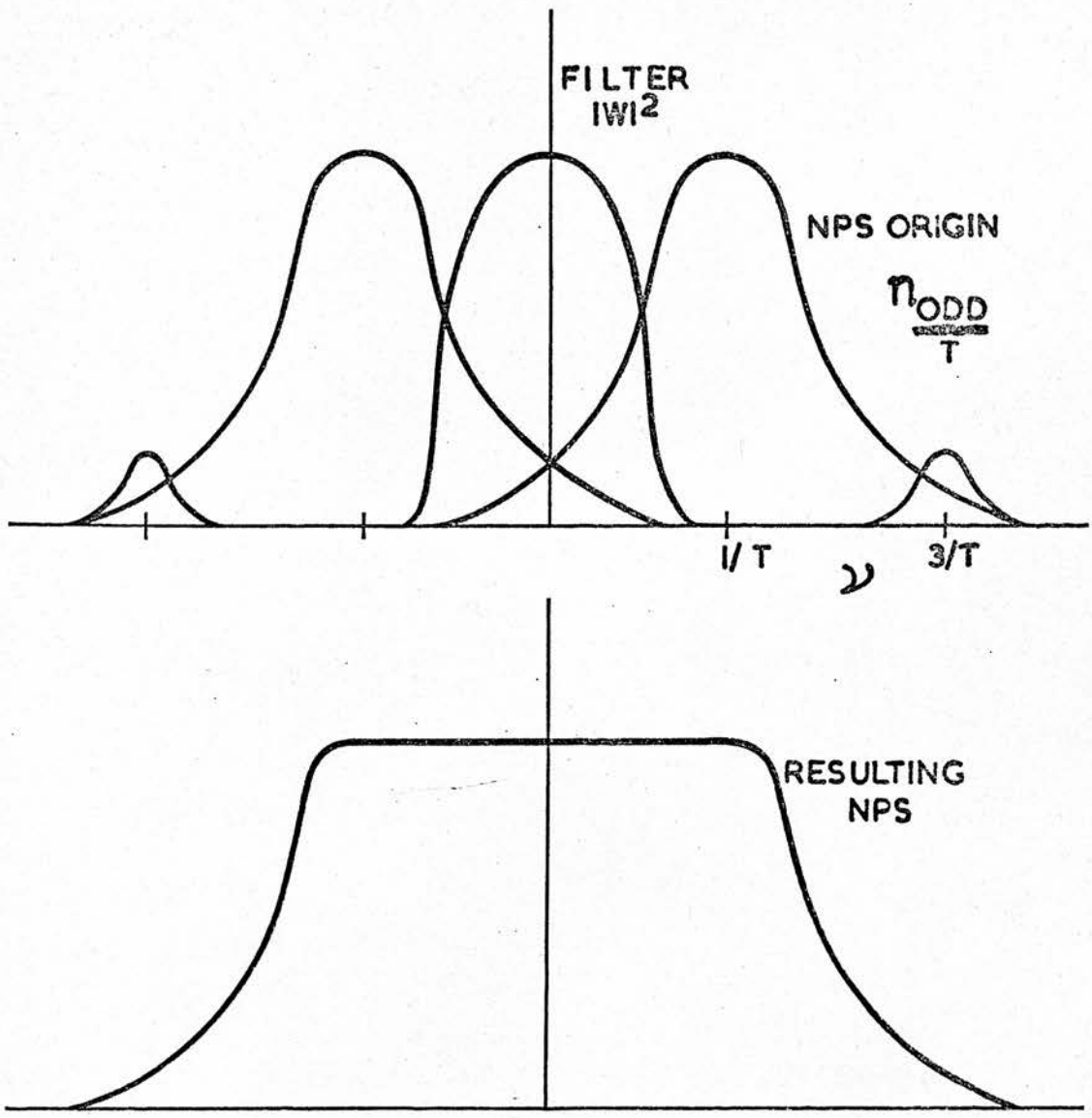

Figure(2.10)

Now if $T = (15Hz)^{-1}$ and $\nu' \sim 8Hz$ a good approximation to normal operating conditions, then

$$|N_d * D|^2 |W|^2 \simeq 1{\cdot}27 n_0 |W|^2 \qquad \ldots (2.90)$$

In the case of the 401A, the filter function is defined by the time constant of the RC circuit (figure 2.9). Let $\omega(t)$ have the form

$$\left.\begin{aligned} \omega(t) &= \frac{1}{\tau} e^{-|t|/\tau} \qquad t \leq 0 \\ &= 0 \quad \text{otherwise} \end{aligned}\right] \qquad \ldots (2.91)$$

where τ is the time constant. Then by definition of W

$$W(\nu) = \frac{1}{\tau} \int_{-\infty}^{0} e^{(1/\tau - 2\pi i\nu)t} dt \qquad \ldots (2.92)$$

and

$$W(\nu) = \frac{1}{\tau} \frac{1}{\frac{1}{\tau} - 2\pi i\nu} = \frac{1}{1 - 2\pi i\tau\nu} \qquad \ldots (2.93)$$

then

$$|W|^2 = \frac{1}{1 + 4\pi^2\tau^2\nu^2} \qquad \ldots (2.94)$$

This gives the value of the detector noise modulated by d(t) and filtered by $\omega(t)$ as

$$1{\cdot}27 n_0 \frac{1}{1 + 4\pi^2\tau^2\nu^2}$$

In general the LIA was used to recover signals modulated at frequencies 15Hz. The output filter time constant was usually 3s. In effect the LIA was used as a filter-cum-linear rectifier tuned to the reference used with a band width of $1/\pi\tau$ to enhance the sometimes poor signal/noise ratio of the signal input. The improvement in the signal/noise ratio depends on the bandwidth of the filter and the

noise distribution. If the low pass filter used at the output has a cut-off frequency significantly lower than the reference frequency then the only components of noise which get through unattenuated are those having frequencies well away from the signal frequency. That is the LIA is a bandpass filter which permits frequencies near the reference frequency only to appear at the output. The effective Q of the filter is

$$Q = \frac{\omega_R}{\Delta f} = \pi\tau\omega_R \simeq 3\tau\omega_R$$

The reference frequency was usually 15Hz and the time constant 3s which implies a Q of 135.

The LIA will automatically track changes in the signal frequency since it is locked to the reference frequency. It is this feature which allows the LIA to be used with such a narrow bandwidth and high Q in the effective recovery of noisy signals.

CHAPTER III

REVIEW

OF

INTERMEDIATE BAND INFRARED PHOTOMETRY

3.1 EXTERNAL GALAXIES

The first infrared observation of an extragalactic object was reported in 1964 (Johnson 1964) when a K magnitude of 9·5 was assigned to 3C 273. Confirmation of this result was reported later (Low & Johnson 1965) along with observations in the 7·5μ to 14μ window. These observations combined with optical and radio observations provided sufficient information to construct the spectrum of 3C 273. This in fact was the first such spectrum for a radio source. A tentative suggestion that the infrared emission could be due to synchrotron emission (Johnson 1964) was made.

The first infrared data on galaxies were reported in 1966 (Johnson 1966). Here eight colour photometry of 10 galaxies was reported. Infrared photometry of the central 35 arc sec of galaxies was carried out with a PbS photometer with an N.E.P reported as 1×10^{-14}W at 2·5μ. No correlation between long wavelength data and galactic type was reported nor was there any colour correlation with A/D(0). From the similarity in colours of the galaxies in the U to L photometric bands a stellar population was derived for the mean galaxy. Generally it was found that the energy distribution could be synthesized from K and M giants rather than dwarves which agrees with Arp's (1965) analysis of the stellar population of the nucleus of our own galaxy although the inclusion of some extremely red stars such as NML Cyg was required on the basis of the K-L index and would contribute about 20% of the light at 3·4μ.

The first observation of strong infrared radiation from a Seyfert galaxy was reported in 1967 (Pacholczyk & Wisniewski 1967). JHKL photometry of the central 15 arc sec of NGC 1068 revealed strong infrared emission. Multi-colour photometry of NGC 1068 and Johnson's (1966) mean galaxy were compared to reveal both short and long wavelength excesses which were strikingly similar to the spectrum of 3C 273. The radiation from a typical stellar component was subtracted from the nucleus of NGC 1068 and the resulting distribution of radiation strongly suggested a QSO-like component in the nucleus of the galaxy. These were probably the first attempts to separate the underlying galaxy from the nuclear core in a Seyfert galaxy.

The discovery of strong infrared radiation from NGC 1068 lead to the investigation of another Seyfert galaxy NGC 4151 in an attempt to strengthen the evidence for a possible relationship between Seyfert galaxies and Quasi-stellar sources. Observations of variability in the K magnitude of the central 15 arc sec of NGC 4151 (Fitch et al. 1967) were assigned to a variable nonstellar object in the nucleus although it was suggested on spectroscopic evidence that the intensity of the underlying stellar component may vary. However, they suggest that as the nonstellar object increases the stellar component is swamped by it.

That strong infrared radiation was not peculiar to NGC 1068 but was characteristic of Seyfert nuclei in general now became evident (Pacholczyk & Weymann 1968).

Further observations of another six Seyfert galaxy nuclei were presented. The infrared luminosity of these objects is very large and a model for their infrared emission compatible with the reported variability was, as yet, unknown. Pacholczyk & Weymann (1968) discussed two models for this type of emission based on observations of NGC 1068. The one associating the radiation with a dust cloud surrounding the centre of the galaxy, the other invoking the synchrotron mechanism. Both models were highly speculative at the time. The dust model being incompatible with the restrictions on the size of the emitting region imposed by the light variations, the synchrotron model invoking very large magnetic fields and neither model able to account for the millimetre radiation.

Further confirmation that Seyfert galaxies had enormously bright infrared continua and indications of variability in 3C 273 that could not easily be explained by observational errors (Low & Kleinmann 1968) was presented. Again the similarity between the central regions of Seyfert galaxies and quasars was highlighted although an observation that 3C 273 was highly polarized at 1·5μ (Low 1967) was unsupported by observations of Seyfert galaxies.

An intensive investigation of NGC 224 (Sandage et al. 1969) showed that the brightness distribution was the same at K as it was in B, V and R although the variation in U-B was not repeated in any other colour. The brightness profile of NGC 224 is similar to that of the Galaxy over the central 400pc while the surface brightness of NGC 224 is fainter than that of the Galaxy by a factor of 2·4. Since it is known

that the emission at $\lambda<0{\cdot}9\mu$ is due entirely to stars any similarity in the brightness distribution at $\lambda<0{\cdot}9\mu$ and $2{\cdot}2\mu$ would preclude nonthermal excess emission in the nucleus. No systematic difference between the brightness profiles in B and K was found. It must be added that the B profile was used to correct the zero level thus these two profiles should be the same at some level to $\sim \pm 10\%$ forcing agreement of the shapes. The agreement found over the entire range was to better than $\pm 10\%$. No colour variation was found in V to K.

The absolute energy distribution per unit frequency interval of the central 7·62 arc sec agrees well with that of K_0 III stars up to $\sim\lambda=6000\text{Å}$ and is considerably brighter at longer wavelengths. This seems to indicate divergence from a single spectral type.

Closer comparison of NGC 224 and the Galaxy shows that the central 7·62 arc sec of NGC 224 is fainter than the central 540 arc sec of the Galaxy by a factor of 2·4 in K and that the similarity in shape of the brightness profiles suggests that the Hubble type classification of the Galaxy is closer to early Sb than to Sc as in NGC 2403.

The absolute spectral energy distribution from $0{\cdot}32\mu$ to $2{\cdot}2\mu$ of quasi-stellar sources not measured before could now be investigated due to the development of infrared techniques for use with large aperture telescopes. Oke et al. (1970) presented results indicating that the continua of these objects could, in general, be described by a power law with indices ranging from -0·2 to -1·6. These observed values are in agreement with those obtained for objects where only K photometry and V magnitudes

(Burbidge 1967) was available. A large range of spectral index was found at all values of redshift. Objects with large visible variability showed continua which rose steeply into the infrared and a spectral index around -1·5.

The main character of the infrared spectrum of the nuclei of galaxies could only be established if a larger number of galaxies were observed. Kleinmann & Low (1970a) observed some 19 galaxies at wavelengths between 1·25μ and 3·4μ. These included real detections - 'intense radiation' - and possible upper limits. The best observations showed that from 5μ to 25μ the basic character of the continuum, $S(\nu) \propto \nu^{-3/2}$, to be the same while the continuum at shorter wavelengths is contaminated by the thermal radiation of stars. Variability was detected in NGC 4151. A bright discrete source was located in NGC 3034 at 1·65μ. The position of the infrared nucleus was determined by 2·2μ and 10μ observations. An upper limit of 3 times the luminosity of our own Galaxy was placed on NGC 224 and an estimate of the total infrared luminosity was made. These results combined with studies of the infrared radiation from the nucleus of our own Galaxy (Becklin & Neugebauer 1969 and Aumann & Low 1970) suggested that the infrared-galaxy phenomenon was a common physical property of the nuclei of galaxies and that the emission could be due to a common physical process.

Observations of the 10μ extended source in NGC 3034 (Kleinmann & Low 1970b) revealed a source with a half-power width of 200pc along the plane of the galaxy. This

was, in fact, the first 10μ observation of an extended extra-galactic source. New observations at 2·2μ were reported and the range of luminosities of the sources was extended. Kleinmann & Low (1970b) then suggested that the infrared phenomenon in galaxies was not describable by a single set of physical parameters. In fact a wide range of physical size, surface brightness and luminosity is observed.

The question of 2·2μ variability was by no means resolved. Observations of NGC 1068 (Pacholczyk 1970) indicated a time scale of a few days, implying a size of a few times 10^{15}cms for the emitting region. Observations of NGC 1068 at longer wavelengths (Kleinmann & Low 1970a) indicated no effect of beam size when diaphrams ranging from 4·5 arc sec to 35 arc sec were used. If this is the case at 2·2μ then centering of the object in a 15 arc sec diaphram should have no effect on the measurements of the flux from the star like nucleus. Differential extinction is also ruled out by Pacholczyk since the photometer used could repeat extinction measurements on stars of very blue and very red colours to better than 7%. The variability then is suggested as being intrinsic to the source.

The timescale of the variability reported severely restricts the size of the emitting region and seems to rule out both the dust model (Pacholczyk & Weymann 1968, Rees et al. 1969 and Burbidge & Stein 1970) and a homogeneous synchrotron model (Pacholczyk & Weymann 1968). The observations were described in terms of a nonuniform

synchrotron model in which the field decreases outwards. Radiation of a given wavelength emanates from a certain distance and the spherically symmetric model is optically thick to radiation of longer wavelength at smaller distances. Long wavelength radiation is emitted at longer distances. This model also implies that short wavelength radiation would have short timescale variability and long wavelength long time scale variability.

A detailed study of NGC 4151, a Seyfert galaxy with a bright stellar nucleus, presented observations at wavelengths from 0·3μ to 3·4μ made during the 1970 observing season (Penston et al. 1971). The nucleus of this galaxy was known to vary at optical wavelengths in a way reminiscent of quasars and N-type galaxies. The galaxy was known to have an infra-red excess and 10μ observations suggested variability within a timescale of about one year (Low & Kleinmann 1968 and Kleinmann & Low 1970a). Variability in excess of two standard deviations was observed in the one hundred day observing period. The largest variability was observed in the smallest apertures. This could be explained by poor guiding on a small resolved source. However it is clear that the optical and infrared magnitudes do not vary together. No deductions about the behaviour at 3·4μ were made.

Some evidence for rapid infrared variability is presented and timescales of the order of one week cannot be ruled out. If present, this would serve to distinguish between the differing emission mechanisms.

The purely optical colours U-B and B-V and the infrared colour K-L do not vary significantly and they suggest a greater contribution of the central source to the blue light. The method used to separate the central source suggested by the magnitude-aperture relation is based on the assumption that the underlying galaxy does not vary, has NGC 224 colours and a radial distribution of flux in a given aperture D proportional to D^{α} where the exponent α can be evaluated for each colour and each observing night. The underlying galaxy should peak around H to K and then drop off at longer wavelengths. The central source is then compared to 3C 273 (figure 3.1). The colours of the central source did not vary significantly in either the visible or the infrared. However the 2·2μ flux was found to vary by as much as a factor of 4. The independent variation suggested that the sources of optical and infrared emission are independent.

The observed time lag between maxima in the visible and the infrared can be due to the light travel time from a central source to a dust shell. For a dust shell whose emission peaks at around 3·4μ Rees et al. (1969) have shown that variations at a wavelength τ with a shorter timescale than

$$\tau = \left(\frac{\lambda}{2\cdot2}\right)^{5/2} L^{\frac{1}{2}} \text{ months} \qquad \ldots (3.1)$$

cannot be expected where, λ is the wavelength in microns, L the luminosity in units of 10^{44}W. If L = 0·1 then τ cannot be shorter than a month. Thus if the rapid

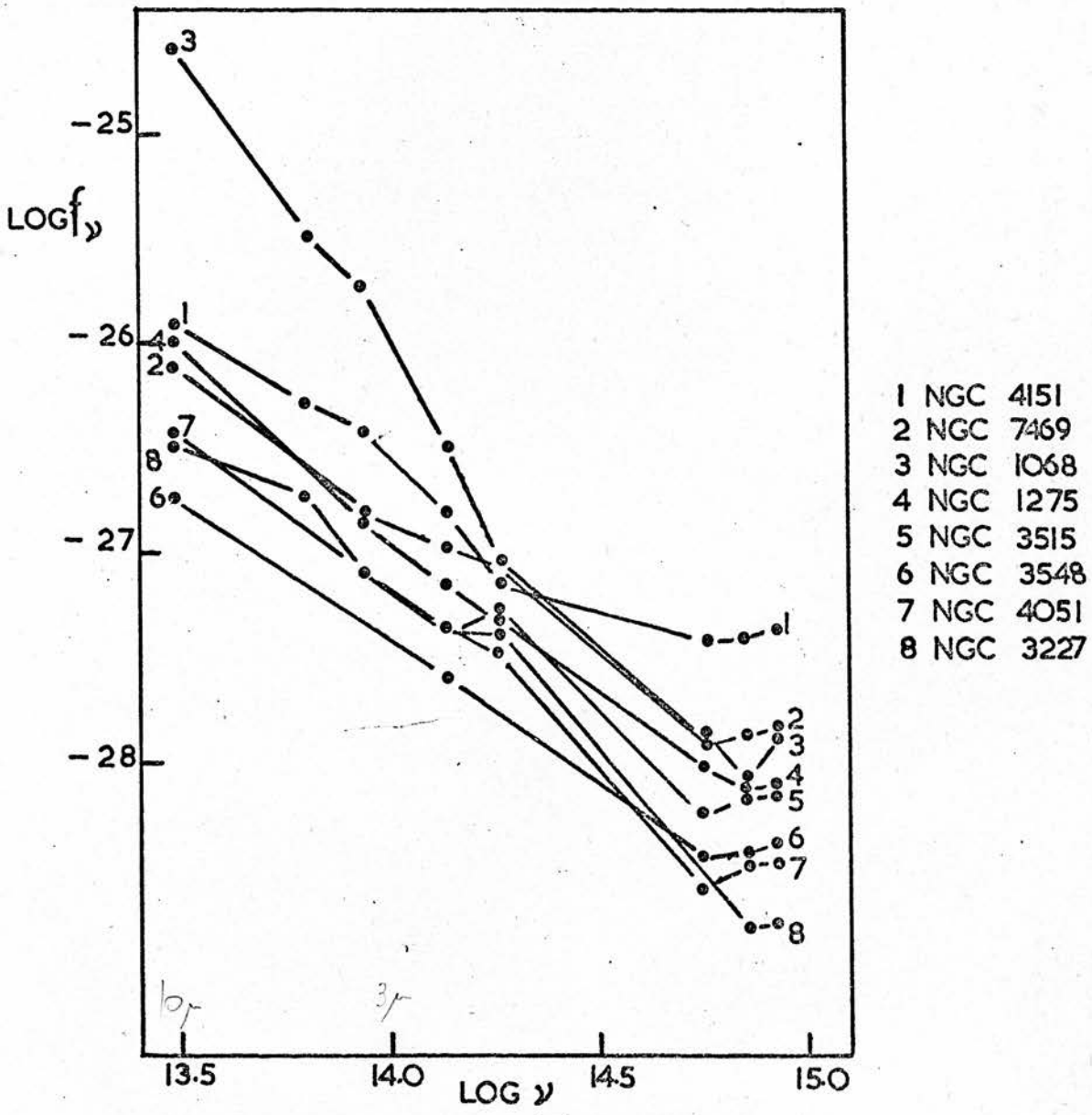
-25
LOG f_ν
-26
-27
-28
13.5
14.0
LOG ν
14.5
15.0
1 NGC 4151
2 NGC 7469
3 NGC 1068
4 NGC 1275
5 NGC 3515
6 NGC 3548
7 NGC 4051
8 NGC 3227

Figure (3.1)

variations with a timescale of a week are real this model of radiation by dust would have to be excluded.

A further study of the optical and infrared variability of NGC 4151 was carried out by Pacholczyk (1971). A 5·1 year period is suggested from the photographic data. The infrared observations presented are discussed to a fair degree of detail with respect to the effects of differential extinction and centering errors. Neither of these could cause the observed scatter and it is concluded that the observations are not incompatible with possible variability of the infrared flux at 2·2μ. The amplitude of the variability in flux found in NGC 4151 is similar to that found in NGC 1068 (Pacholczyk 1970).

An intensive study of Maffei 1 (Spinrad et al. 1971) included infrared photometry at 2·2μ. It was found that the fluxes from the central regions of Maffei 1 and NGC 224 are comparable. The data presented are consistent with a large normal elliptical galaxy. Photographically the galaxy could be either E3 or E4. The rapid drop in surface brightness is confirmed by the infrared data. The surface brightness at 2·2μ in an aperture of diameter D being proportional to $D^{-1\cdot0}$ compared to $D^{-0\cdot4}$ for NGC 224. The close similarity to NGC 224 confirms that Maffei 1 must be a massive galaxy. Photometry at 1·6μ and 2·2μ suggest $A_V \sim 4\cdot0 \pm 1\cdot6$ magnitudes. The infrared photometry indicates a core of radius <5·5 arc sec.

The flux from the nucleus of NGC 1068 at infrared wavelengths was reported to be independent of the field of

view (Kleinmann & Low 1970a) and although no similar work had been done at shorter wavelengths it was assumed that the flux distribution was the same. Neugebauer et al. (1971) showed that at wavelengths less than 3μ the object was definitely extended, whereas at wavelengths longer than 5μ the dominant source was, as yet, unresolved. The observations at 1·6μ, 2·2μ and 10μ were in general agreement in terms of flux with previous work. Pacholczyk (1970) observed variations at 2·2μ in the central 15 arc sec of NGC 1068 but pointed out that if the source were extended the variations could be due to setting errors. His reported drop in flux by a factor of 4 in less than one hour is questioned by Neugebauer et al. (1971).

If NGC 1068 is at a distance of 13 Mpc on cosmological interpretation of its redshift, a one hour variation cannot exist over an angular size of greater than 10^{-6} arc sec. The data presented by Neugebauer et al. (1971) shows that more than 50% of the radiation falling in a 15 arc sec aperture falls outside the smallest aperture used. Thus the observed short-term decrease in flux (Pacholczyk 1970) must be due to setting errors.

The observations are consistant with a point source in a normal galaxy. The separation gives a point source of 0·3 ± 0·1 f.u.* plus a diffuse component 0·8 times the flux density at 1·6μ. These can be compared to NGC 224

---

* 1 f.u. ≡ $10^{-26}\mathrm{Wm}^{-2}\mathrm{Hz}^{-1}$

where the diffuse component is 0·7 the flux density at 1·6μ and has a slightly bluer colour.

Scans and magnitude-aperture data of NGC 5128 (Becklin et al. 1971) revealed only one bright infrared region in the central 1 arc min of the galaxy. The data showed that from the visible to 1·6μ a power law dependence proportional to $D^{1\cdot25}$ adequately describes the shape of the flux distribution for 20 arc sec < D < ∿100 arc sec. For the outer regions of the galaxy the power law dependence changes to an exponential dependence. This is similar to NGC 224. Also the colours V-K, H-K and K-L are consistent with those of NGC 224 if a visual extinction of Av=3·0 mag is assumed.

The 2·2μ and 3·5μ aperture-size data indicates an infrared core with a diameter <7 arc sec. The rest of the data at these wavelengths indicate a normal galaxy with a surface brightness distribution given by the 1·6μ data. NGC 5128 differs from a normal galaxy as the discovery of the core which has a flux of 0·2 f.u. at 2·2μ and 0·5 f.u. at 3·5μ highlights. Similar separations have been discussed for NGC 1068 (Neugebauer et al. 1971) and NGC 4151 (Penston et al. 1971). In both these discussions it is apparent that the nonstellar core becomes pronounced at λ>3μ while in the case of NGC 5128 the entire flux at 10μ is confined to the core. It is possible then that there is a highly reddened stellar core in this galaxy.

The stellar core of NGC 5128 is 10 times brighter than the stellar component in the Galactic centre and 25

times brighter than the stellar component in the central 25pc of NGC 224. The core of NGC 5128 has a flux distribution similar to that of NGC 1275 and has a surface brightness at 3·5μ at least 10^3 times fainter than NGC 1275.

As can be seen from the above a large amount of observing time was used to study just two objects, NGC 1068 and NGC 4151, in an attempt to solve the problem of their apparent variability. It was left to Rieke & Low (1972a) to add significantly to the list of observations. Some 15 galaxies were observed in K and a few in K and L. These combined with longer wavelength infrared observations and radio spectra suggest a causal relationship between the radio and infrared spectra of the nuclei of Seyfert and related galaxies. The limit of ground based observations around 25μ severely restricts the estimation of the total infrared luminosity and its determination remains a problem.

The observations show that not all QSOs emit chiefly in the infrared but in the case of 3C 273 the energy loss in the infrared is 10 times the energy loss at all other wavelengths. Of the Seyferts observed, the infrared emission dominates over the total emission. The infrared observations of NGC 3504, 4194, 4385, 7714 and IIZw23 suggest a strong similarity to Seyfert type although they do not exhibit any broadening of emission lines. This could suggest that the broadening observed in Seyfert spectra is not a universal result of the highly energetic

phenomena present.

For those Seyferts and related objects observed containing compact radio sources Rieke & Low (1972a) were able to show that the infrared fluxes were proportional to the radio emission (figure 3.2). This is a direct comparison of the 10μ flux and the 21cm flux.

The outcome of these observations was that the infrared properties are added to the general characteristics of Seyfert galaxies. Seyfert galaxies were known to have

(a) Compact luminous nuclei

(b) Ultraviolet excess

(c) Strong emission line spectra

(d) Broadened permitted lines

(e) High infrared luminosity

(f) Radio flux proportional to the infrared flux.

Note that, as shown above, condition (d) may not be as fundamental a characteristic as the others.

Of all the observations made, only three Galaxies have been reported as variable, NGC 1068, NGC 4151 and 3C 273. An intensive study of NGC 1068 (Rieke & Low 1972b) revealed further changes in the flux from this object at 10μ. The observations were made relative to a system of standard non varying stars. The changes in flux during the three and one half year observing period are remarkable. The infrared luminosity of NGC 1068 is at least $10^{11}L_{\odot}$ and a change in luminosity of $7\times10^{9}L_{\odot}$ was observed at 10μ. This is an amount comparable with the total luminosity of our own Galaxy. If 3C 273 is at the distance suggested by a cosmological interpretation if its redshift then the change

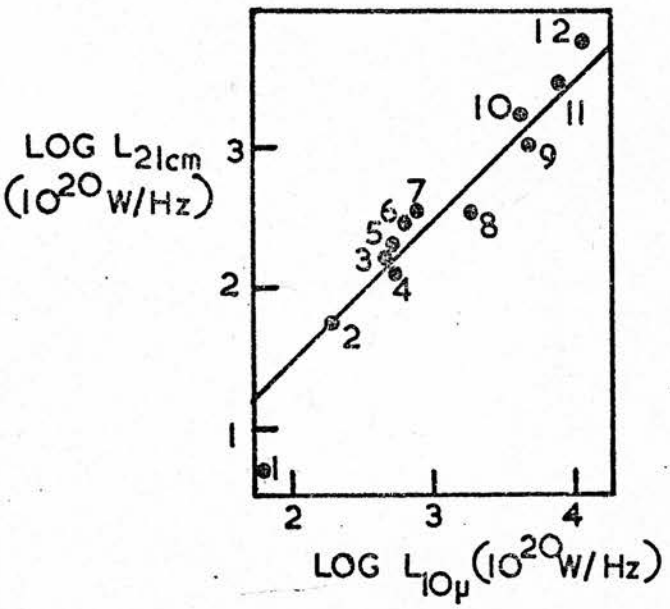

1	NGC 4051
2	NGC 3227
3	NGC 4151
4	M 82
5	NGC 3504
6	NGC 2782
7	NGC 7714
8	NGC 5548
9	MARKARIAN 79
10	NGC 1068
11	NGC 7469
12	MARKARIAN 9

Figure(3.2)

in luminosity at 10μ observed during a period of two months is of the order of $10^{12} L_{\odot}$. Variability at 10μ was also observed in NGC 4151 although no correlation with the 2·2μ variability (Penston et al. 1971) was possible due to the poor overlap of observing time.

Rieke & Low (1971b) pay due attention to the types of error which could reproduce the scatter in their observational data. They consider instrumental effects, the effect of extended sources, signal/noise ratio considerations and statistical effects. Their model is relatively simple. They choose a straight line fit to the data described by a mean $\bar{x}$ and standard deviation σ, then using the χ^2 test obtain a 1 in 10^3 probability that the scatter is due to chance. When observing a source in which there is no *a priori* reason to expect variability any single set of observations is accurate to better than 5%. Instrumental errors would appear equally in the observations and could be correlated. Any observation of a bright source will be achieved with a large instantaneous signal/noise ratio and it might be expected that a faint object like a galaxy would have a much smaller signal/noise ratio, small enough to degrade the photometric accuracy of the observation. However, Rieke and Low (1972b) show that in the case of NGC 1068 the instantaneous signal/noise ratio is so large that there is effectively no difference in the accuracy achieved on it or the bright standard source. However they do caution that this is not the case for the much fainter 3C 273.

If thermal, then the sources of these infrared fluxes must be as large as a black-body capable of emitting such a flux and smaller than $c\tau$, where τ is the period of the variations and c is the speed of light, from light travel considerations.

If the fluxes came from a cloud of dust then the temperature of the dust must be less than $1500^{o}K$ for the dust to exist and greater than $1000^{o}K$, the minimum temperature for Seyfert galaxy nuclei. These grains then would have to have anomalous emission properties being less efficient by a factor of 10 in the 2μ to 5μ region than they are at 10μ if they are to account for all of the radiation at these wavelengths. This type of grain with such a strongly wavelength dependent emissivity could be expected to show spectral features. Stein et al. (1974) obtained a spectrum of NGC 1068 in the 8μ to 13μ window which has no spectral features within the accuracy and resolution - $\Delta\lambda/\lambda = 0{\cdot}015$ - of their measurement.

A simultaneous search in the optical, infrared and radio wavelengths for variability in 3C 120, BL Lac, and OJ 287 revealed that no conclusions about infrared variability could be made about 3C 120, that there was infraday (timescale <24h) variability in the infrared in OJ 287 and that there could be interday variability but no infraday variability in the infrared in BL Lac (Epstein et al. 1972). All of the objects exhibited some kind of optical and radio (millimetre) variability.

A detailed study of the V-K colours of the nuclei

of bright galaxies (Penston 1973) was an attempt to use the infrared colours of galaxies as a baseline against which peculiar objects could be judged. Further, this gives a better understanding of the colours of the underlying galaxy when attempts to separate a Seyfert galaxy into a nuclear core and an underlying galaxy are made. Moreover the colours themselves will be constraints on attempts to sythesize the spectra of galaxies from stellar population models.

U,B,V,H,K, and L magnitudes of 5 galaxies, NGC 224,598, 5194,5195 and 5457 are given. The results for NGC 224 are compared with a predicted population model (Spinrad & Taylor 1971).

The H,K, and L observations were made with the photometer described by Becklin & Neugebauer (1968) and reduced to magnitudes using the system of Johnson et al. (1966) with the inclusion of the H magnitude. No correction was made to the data to allow for the infrared radiation in the reference beam. If the signal was large enough, each object was centred on the maximum signal found with the unfiltered detector.

The observations at K and L for NGC 224, NGC 598 and NGC 5457 agree with those of Kleinmann & Low (1970a,b).

Magnitude-aperture relationships were chosen from each set of observations. It was found that for ellipticals a Hubble (1930) type profile fitted while for spirals the flux was proportional to D^{α} where α was calculated for each set. The data were corrected for reddening using

van der Hulst (1949) no. 15 curve.

None of the galaxies was found to have an infrared excess in H,K and L except that NGC 5195 lay marginally outside the range of colours for normal stars. The 10μ excess found by Kleinmann & Low (1970b) was observed and if this has the same type of emission mechanism as the source in NGC 3034 (Kleinmann & Low 1970a) then it will contribute about 10% to the emission in K and L which is consistant with the high values of $(H-K)_0$ and $(K-L)_0$ found. The galaxies are all too red in $(V-K)_0$ compared with stars of the equivalent $(B-V)_0$. This is most probably due to the fact that red stars dominate at 2μ and contribute to $(V-K)_0$ but not to $(B-V)_0$.

The most important consideration is the constraint placed on stellar population synthesis by these values of $(V-K)_0$. The galaxies are all very red with values of $(V-K)_0$ ranging from 1·95 to 3·60. The colours are compared (Penston 1973) with four models (Spinrad & Taylor 1971). The models are all too blue. A further model privately communicated by Spinrad to Penston containing proportionately more K-type giants and subgiants and a bluer turn off to the main sequence predicted a $(V-K)_0$ in accord with that observed. Johnson (1966) colours do not cover such a wide range as do those of Penston (1973) and it may be that the range of energy distribution of the galaxies and their stellar composition may not be as uniform as Johnson supposed.

In an attempt to extend the knowledge of the infrared colours of galaxies Glass (1973b) observed 27 Southern

galaxies. J,H,K and L fluxes for NGC 7552 and 7582 and upper limits on the J,H and K flux of NGC 7590 were reported (Glass 1973a). These are the first examples of infrared observations of closely spaced galaxies which show infrared excess.

Observations in J,H,K and L are important for it is believed that this region of the spectrum contains the point at which ordinary radiation from stars starts to be overcome by the processes responsible for 10μ infrared excess.

The data were reduced to magnitudes using the system of Johnson et al. (1966) with the inclusion of H magnitudes. The photometer used was capable of J,H,K,L, M,N and Q photometry. No correction was made to the data for the infrared radiation in the reference beam. Standard deviations quoted arise from statistical fluctuations. Generally, systematic errors are expected to be small. The data were not dereddened since this is expected to be small also.

Compared to the K-L colours of Johnson (1966) there seems to be a high incidence of large K-L. The K-L colours range from about 0·4 to 1·86 which compare with 0·44 for ellipticals and 0·19 for spirals (Johnson 1966), 0·34 for NGC 224 (Sandage et al. 1969) and the large values for Seyfert galaxies (Pacholczyk & Weymann 1968 and Rieke & Low 1972a). The difference could be due to the choice of observed type, or the small apertures used which put more emphasis on the nuclear radiation. The largest

values of K-L were found in galaxies which appear in Sérsic & Pastoriza (1965) and have peculiar nuclei. Some of these have dust lanes but certainly most of those peculiar nuclei galaxies would seem to show evidence for the existance of highly energetic phenomena in their nuclei.

The general colour characteristics in J-H and H-K show peaks at positions characteristic of M-type stars. There is noticeable scatter in the K-L colour which could be due to the contribution at various power levels of a nonstellar source of infrared radiation at longer wavelengths. The marked dispersion of colour with increasing wavelength could be indicative of nonstellar type radiation being increasingly seen. K-L colours then are of little use in studying stellar populations since this tends to be contaminated by nonstellar radiation. It would be interesting to attempt a correlation of K-L and 10μ excess. The J-H, H-K colour-colour diagram (figure 3.3) shows a clumping around J-H = 0·8 and H-K = 0·2 characteristic of late-type giants.

The variation of flux with aperture size shows little concentration towards the nucleus except for NGC 1316.

The two Seyferts observed NGC 1566 and 3785 show no marked peculiarity in J-H or H-K. NGC 1566 has a K-L of 0·6 and a lower limit of 3·6 mag at 10μ. Rieke & Low (1972a) give an average value of 1·5 for K-L for the Seyferts they observe. However, NGC 1566 is sometimes quoted as being only a weak exhibiter of Seyfert characteristics.

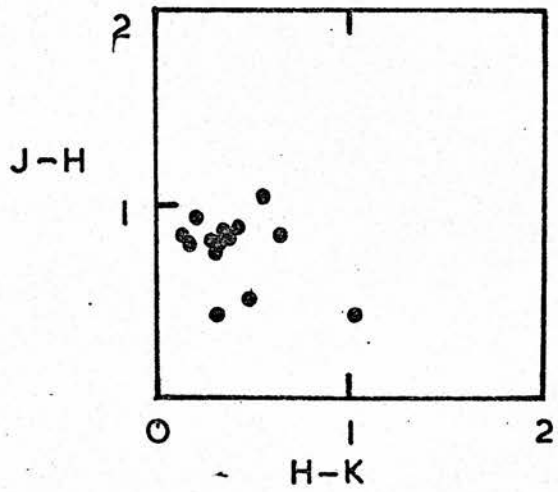

Figure(3.3)

From these observations Penston (1973) suggests that Seyfert spectral characteristics do not always imply strong infrared excess which stands with Rieke & Low's (1972a) comments on NGC 3504,4194,4385,7714 and IIZw23.

Direct comparison of the infrared and radio flux revealed that the infrared flux is linearly related to the high frequency radio flux with a few exceptions. NGC 5253 has a large 20μ excess and NGC 253 and 5236 both have long wavelength excesses, as could be predicted from their K-L colours.

NGC 253 is a bright spiral galaxy. Visually it is heavily obscured by dust lanes in the central region. 1μ to 20μ infrared photometry (Becklin et al. 1973) of the extended nuclear core revealed an infrared distribution very much redder than the energy distribution of stars or highly reddened stars. The infrared distribution is strikingly similar to NGC 1068 and 4151. However the radio distribution does not exhibit the same nonthermal characteristics of strong radio Seyferts. The existance of a nuclear core is substantiated by magnitude-aperture relationships and scans with a 5 arc sec aperture. There seems to be no significant difference between the spatial distribution at 2·2μ and at 2695 MHz.

Seyfert galaxies still remain the single most observed group of galaxies. The spatial distribution of the emitted flux shortward of 2·2μ suggests that the emission from a Seyfert galaxy can be decomposed into a nuclear source showing ultraviolet and infrared excess and

an extended source with normal starlike colours. A detailed study of 11 Seyfert galaxies (Penston et al. 1974) reported U,B,V,J,H and K broad band observations.

Magnitude-aperture relationships in the infrared showed clear signs of increasing brightness with increasing aperture. For each object however there is a wide range of slope for different wavelengths and a degree of scatter due to the suspected variability of some of the sources. The trend is that the slopes are flatter in U than in B and flatter in B than in V. In the infrared the slope of the magnitude-aperture relationship flattens with lengthening wavelength. It seems then that decomposition into a nuclear source having ultraviolet and infrared excess and an extended source with normal galaxy colours proposed by Penston (1973) can be extended to all Seyfert galaxies (Penston et al. 1974).

The infrared data, which are not corrected for radiation in the reference beam, reveal that the 2·2μ variability reported in NGC 4151 (Penston et al. 1971) is real and has a timescale of the order of one year and that the optical and infrared light curves differ. Pacholczyk (1971) suggested a 5·1 year period from optical variations but made no estimates of timescale at 2·2μ. The data at 3·4μ are not clear but NGC 4151 may be marginally brighter. The lag between the optical and infrared maxima reported as one month by Penston et al. (1971) is measured as two months. This seems to suggest that the optical and infrared emission have different mechanisms or emanate from

different regions and that the dust model suggested by Penston et al. (1971) does not hold.

The infrared observations of 3C 120 show no clear evidence for variability although it seems clear that optical variability exists. The difference between the infrared and visual light curves suggest that the emission mechanisms are different.

The optical light curves of NGC 1275 show irregular activity with a timescale of the order of one month which is quite clear in the blue but not in V. The infrared data are neither accurate nor numerous enough to cast much light on any possible variability.

The observations of NGC 1068 show no sure signs of either optical or infrared variability. A comparison of the rms residuals and rms error in each colour seem to preclude any observed variability.

Further examination of the view that the peculiar colours of Seyfert galaxies are caused by under luminous quasars (Pacholczyk & Wisniewski 1967 and Penston et al. 1971) was possible from the data. The colours of the central 10 and 20 arc sec of the galaxies show ultraviolet and infrared excess. The K-L colours which range from 1·3 to 2·06 are very large compared to Johnson's (1966) mean colours. The $(K-L)_0$ far exceeds the $(H-K)_0$. The energy distribution in this part of the spectral region differs from that of a single black-body for which these colours should be approximately equal.

The steep slope in the energy distribution in the

infrared of the nuclear source in NGC 1068 (figure 3.4) resembles a non-Seyfert type infrared galaxy while the others show great similarities to quasars. The scatter in the nuclear colour in the infrared is in marked contrast to the visible suggesting differing radiation mechanisms.

All the Seyferts studied (Penston et al. 1974) have spectra that turn upward in the infrared. This is not confined to Seyfert galaxies alone and most of the Seyfert galaxies studied have considerably weaker infrared excess than a number of optical and normal galaxies. Usually the infrared nuclear emission does not dominate the normal star light emitted by the galaxies shortward of 3μ.

It is interesting to contrast two galaxies, namely NGC 1068 and NGC 4151. The nucleus of NGC 1068 has been found to be extended at 10μ (Becklin et al. 1973) over a scale of 1 arc sec (60pc) and is interpreted as thermal emission. NGC 1068 shows no variability at 2μ. NGC 4151 on the other hand has a compact 2μ source which is evident from the variability at that wavelength. The observations of Penston et al. (1974) and the variability with a time-scale of about one year seem to point to a nonthermal model being more likely.

The NGC galaxies in the Virgo cluster and a group of galaxies taken from the HMS (Humason, Mayall and Sandage) groups for which photoelectric photometry exists were observed in the infrared and a V-K colour index formed for each (Grasdalen 1975). Some 28 galaxies were observed using a 30 arc sec aperture and an InSb detector. Using an

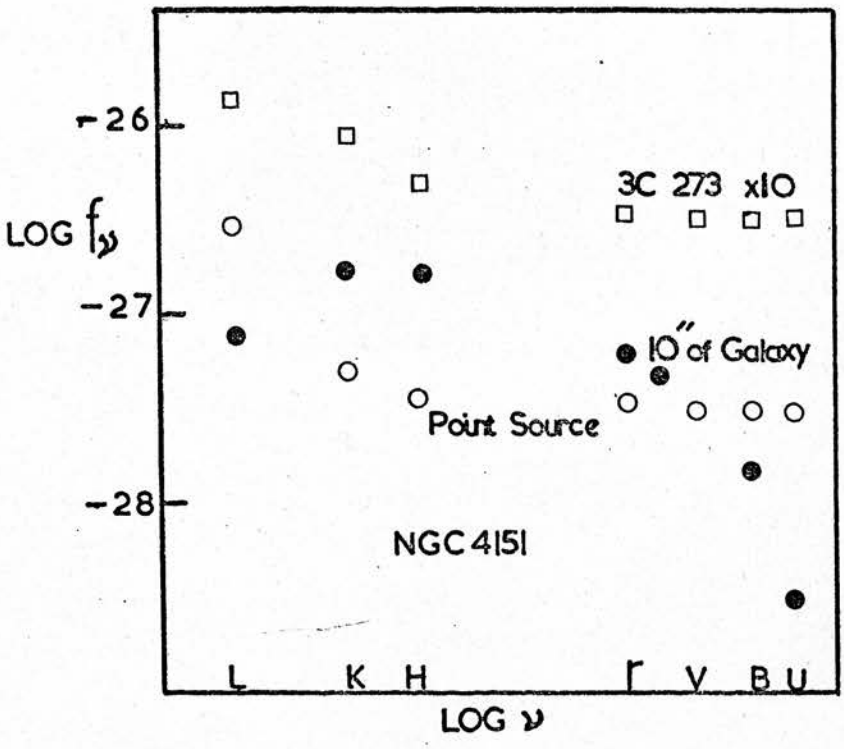
-26
LOG f_ν
-27
-28
3C 273 x10
10" of Galaxy
Point Source
NGC 4151
L
K
H
r
V
B
U
LOG ν

Figure(3.4)

aperture relationship from Sandage (1973), the shape of the light curve in B and a circularly symmetrical model, corrections to the K magnitude were made to include the infrared radiation from the reference beam and the apparent V-K colour index was formed. Further correction to the colour index is necessary to account for reddening and the red shift or K-correction to form the intrinsic spectrum at 2·2μ. This is beyond the maximum for all stars comprising a galaxy so a Rayleigh-Jeans distribution was choosen where $F(\lambda) \alpha \lambda^{-4}$. This yields a K-correction at 2·2μ of -3·252.

A wide range of colours was found in the spiral galaxies. Ellipticals have bluer colours than spirals. The range of colours, 2·8 to 3·5, correspond to a K_3 giant and a K_5 giant respectively. The extremely red colours are found predominantly in spirals presumably because of dust in the plane of the galaxy. The maximum effect would be 0·75 magnitudes i.e. half of the bluelight (visible) being absorbed and all of the infrared light being passed. However it seems unlikely that a thick cloud of dust like this could exist in the central regions of a galaxy.

Grasdalen (1975) finds that as the observing aperture is increased the V-K colour becomes bluer for the bright ellipticals and concludes that there is effectively no dispersion in the intrinsic colour and no dependence on absolute luminosity. This seems to indicate that a strong colour gradient exists in elliptical galaxies.

Detailed observations of NGC 4486 reveal that the

surface brightness distribution at 2·2μ can be described by the relationship

$$I_k(r) = I_0/(1+r/a)^2 \qquad \ldots (3.2)$$

where r is the radial distance to the nucleus, I_0 is the surface brightness of the nucleus and a is the characteristic radius with a value of 9 arc sec. These considerations lead to a model with a nuclear source unresolved by a 12 arc sec aperture where variability can take place.

Grasdalen suggests that the intrinsic dispersion in V-K in spiral galaxies is large and it is assumed that the colours refer to the stellar population within the galaxy and not just the effects of reddening, while the dispersion in bright ellipticals is very small and does not depend on total luminosity.

Since the discovery that 3C 273 and the nuclei of Seyfert galaxies emitted at infrared wavelengths it has become apparent that a large fraction of the luminosity from many extragalactic objects is emitted at infrared wavelengths. Early investigations of the source of the radiation by Rees et al. (1969) and by Burbidge & Stein (1970) have been published and the latter investigation showed that one important observational test for discriminating between thermal and nonthermal models for the sources is to determine whether or not variations of the infrared flux occur with time. The magnitude of the changes and the timescale in which they occur would allow limits to be set on the size of the emitting region. These size limits

could then be compared with the size required from the points of view of physical models.

Penston et al. (1971) have indicated that changes in flux from NGC 4151 have occurred at 2·2μ and 3·5μ; Stein et al. (1974) suggest variations to wavelengths as long as 11μ on NGC 4151; Rieke & Low (1972b) suggest a positive detection of small changes in the 10μ flux from NGC 1068 and NGC 4151; and Stein et al. set limits on the possible change of 11μ flux from NGC 1068.

The Seyfert galaxy NGC 1068 has a large infrared flux and consequently has been studied in great detail. The energy distribution is shown in figure (3.5). It has been shown that the 10μ radiation is extended (Becklin et al. 1973) with an angular radius of 0·5 arc sec. Stein et al. (1974) concluded that no flux changes occurred at 11μ in the case of NGC 1068 while cautioning that at least one example of discrepant measurement exists between their own data and that of Rieke & Low (1972b) and that the limits of possible changes allowed are consistent with those of Rieke & Low (1972b) who claim positive detection of small changes in flux. Stein (1975) sets the limit of the flux change in NGC 1068 to 10% on timescales shorter than one year.

The spectrum of NGC 1068 is given in figure (3.5) (Stein 1975 and Rieke & Low 1975). This shows a continuous smooth rise through 34μ and that there is a shallow absorption feature near 10μ. At longer wavelengths the spectrum may continue to rise but must ultimately fall below the

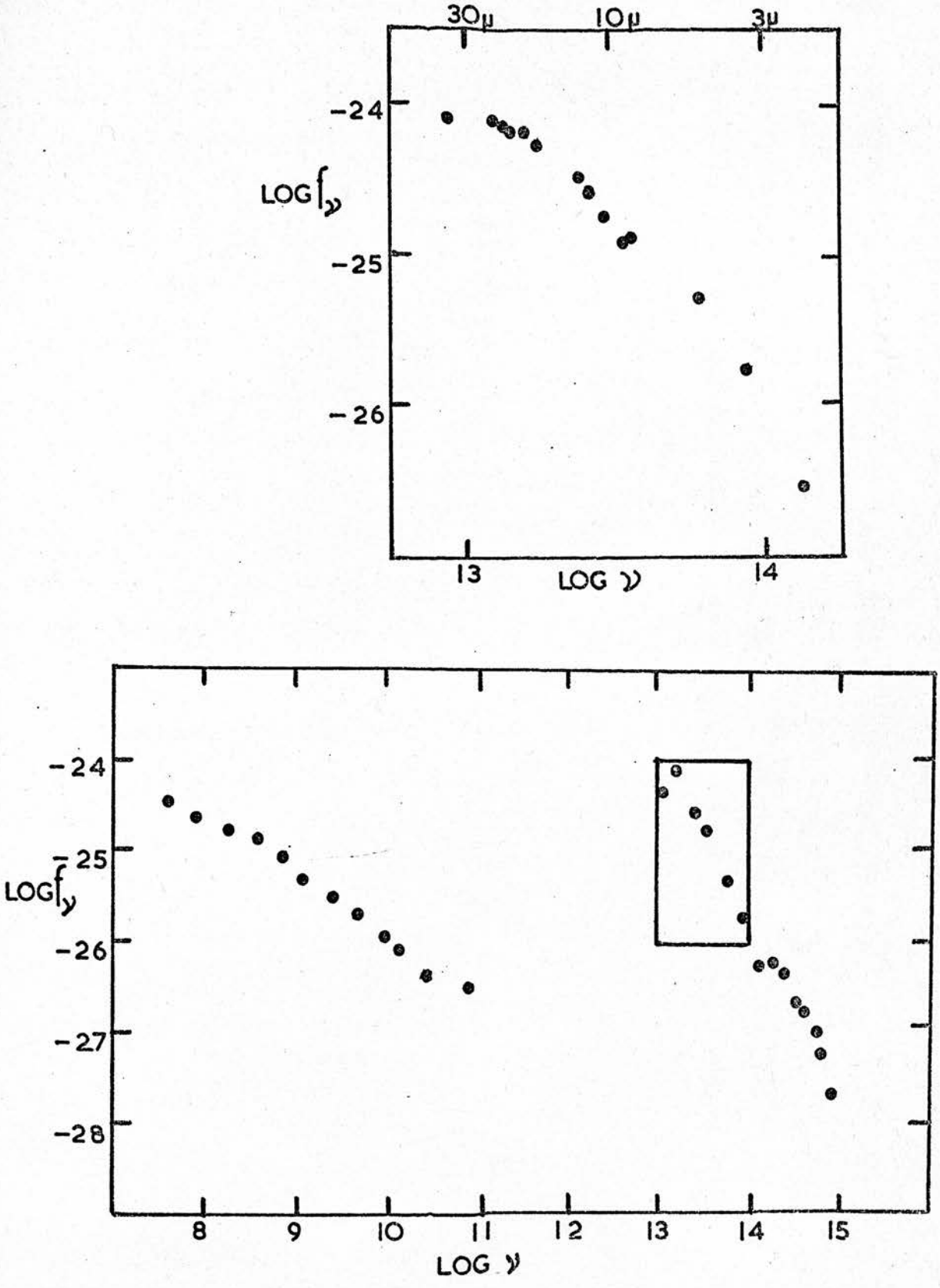
30μ
10μ
3μ
-24
-25
-26
LOG f_ν
13
LOG ν
14
-24
-25
-26
-27
-28
LOG f_ν
8
9
10
11
12
13
14
15
LOG ν

Figure(3.5)

observed upper limit at 3mm (Kellermann & Pauliny-Toth 1971). These results of Rieke & Low (1975) disagree with the observations of Jameson et al. (1974) where a turnover at around 18μ was reported.

The 3·5μ and 10·2μ infrared radiation from NGC 1068 has been found to be polarized (Knacke & Capps 1974). This observation was a result of the desire to distinguish between a thermal or nonthermal radiation mechanism in the infrared. The polarization at ultraviolet and visible wavelengths decreases with increasing wavelength due to dilution by the climbing stellar spectrum. If the polarization of the synchrotron component is constant, the net polarization should increase again in the infrared as the stellar component becomes weaker.

If the spectral turnover observed by Jameson et al. (1974) is real, it could be produced by several physical processes.

The turnover could be caused by a low energy truncation of the electron spectrum. The flux below the frequency of peak emission must decrease as

$$F(\nu) \propto \nu^{1/3}$$

However, a spectrum $\propto \nu^{1/3}$ extrapolated to radio frequencies would be inconsistant with the observed flux.

If the infrared source in NGC 1068 were a single source becoming self absorbed at 20μ it would have a maximum angular radius given by

$$\theta_{max} = \frac{c}{\nu_n} \left(\frac{F\nu}{\pi mc^2}\right)^{\frac{1}{2}} = 2\times10^{-6} \text{ arc sec}$$

where $F\nu = 4\times10^{-25}Wm^{-2}Hz^{-1}$ the observed flux.

The spectrum of NGC 1068 peaks in a mean surface brightness temperature of $\sim 100^{o}K$, whereas a self-absorbed source must have a brightness temperature greater than $mc^2/k = 6\times10^{9}{}^{o}K$ since the electrons are relativistic. Even if the turnover occurred at a longer wavelength, say 300μ, an angular size much smaller than the observed would be required (Jones & Stein 1975). Clearly, if the infrared emission is interpreted as synchrotron emission there must be several such sources distributed about the nucleus (Low 1970). Any nonthermal source with a spectral break at $\nu_b > 10^{12}Hz$ must be very small (Burbidge & Stein 1970). If there are several such small sources then variations in their properties would smear out the turnover as in nonthermal radio sources.

A low frequency turnover can be attributed to free-free absorption by plasma surrounding a nonthermal source. This kind of process is effective at low frequencies in HII regions, at low frequencies in nonthermal sources and at infrared frequencies in compact circumstellar regions surrounding Be stars. To have a reasonable luminosity the plasma cloud must be small because a large emission measure is necessary. For the plasma to become optically thick at 20μ it can be shown that, for reasonable estimates of temperature and emissivity and assuming that the plasma would not have a luminosity larger than the observed infrared luminosity, the angular size of the plasma cloud and the source must be much smaller than the observed angular

size (Jones & Stein 1975). It can be further shown that the required amount of gas necessary to produce the turnover at 10^{13}Hz in the 0·5 arc sec region would produce free-free emission well above acceptable levels (Stein 1975).

If the high energy electrons producing the synchrotron radiation radiate in the same region as that occupied by the ionized gas then the refractive index of the gas is less than one. The resulting energy loss due to collisions of the high energy particles with the plasma would heat the gas. The observed 20μ flux is such that the energy content of the high-energy particles and this heating would be very large. This would lead to a large observable radiation at visible and X-ray frequencies due to the cooling of the gas. Also, the plasma luminosity would be very large and, in order to avoid a large Compton luminosity, the angular diameter of the emitting region must be at least 10^4 times smaller than that observed for reasonable filling factors (Jones et al. 1974 and Jones and Stein 1975).

It seems then that there are serious defects in the nonthermal model if the spectral turnover observed by Jameson et al. (1974) is to be believed since there is no mechanism that can readily explain the infrared emission from NGC 1068 in this way.

In contrast to the nonthermal infrared model, a thermal model could explain the angular size of the 10μ emitting region in NGC 1068. The angular size of the 10μ emitting region is $\sim$ 50pc which is about half the diameter

of the long wavelength emitting region in the nucleus of our own Galaxy. If the emission was due to black-body grains then the observed luminosity and colour temperature ($\sim 200^{\circ}K$) indicates a source diameter of 20pc (Jones & Stein 1975).

If the radiation is thermal then there are several ways in which a nuclear cloud of dust could be heated. Stars in the nucleus could heat the dust as could a compact nonthermal source. The so called nuclear wind (Wolfe 1974) or the suggestion by Wickramasinghe (1971) of strong fluxes of nonthermal particles could be responsible for the heating. There are three plausible ways in which the gas could be ionized and the dust heated. These are a hot gas, stars or a nonthermal source and it seems that of the three a nonthermal source is the most likely in the case of NGC 1068 (Jones & Stein 1975). It seems unlikely that late-type supergiants would be the source of the stellar radiation heating the dust. The nucleus of NGC 1068 required only a small mass-to-luminosity ratio ($M/L < 0{\cdot}05$) and in this case the stars responsible must be early-type supergiants.

What is evident is that at 10μ nonthermal emission accounts for only 15% at most of the observed radiation. The major component of the 10μ emission comes from heated dust. The heating source also ionizes the gas which is responsible for the emission lines so characteristic of this class of spiral galaxy. The nature of this radiation is uncertain. It is most probably a nonthermal source

with a turnover at some frequency above 10^{11} Hz. The non-thermal source must have a small angular size and be very much smaller than the observed optical nucleus whose size is due to the scattered light in the nuclear dust cloud.

The observed energy distribution and angular size of the infrared emitting region can be interpreted in terms of silicate grain emission. The absence of a clear feature at 9·7μ could be interpreted in terms of a self-absorbed feature since the optical lines do not indicate abnormal abundances and the reddening observed in the spectral lines is interpreted as a visual optical depth of 7-15 indicating evidence for the presence of dust in NGC 1068. The silicate emission model provides a mechanism for the 20μ turnover since only modest optical depths predict such a feature. The precise shape and width of the feature could give a clue to the temperature distribution of the dust.

Calculations of the angular size from considerations of energy balance on small grains with reasonable assumptions for the physical parameters of the grains give values of >0·2 arc sec. However this will most probably be increased due to heating of the grains by trapped Lα photons in the HII region. This would bring the minimum size up to $\sim$ 0·5 arc sec.

If, as has been suggested, infrared emission from the nuclei of galaxies is characteristic of Seyferts and other energetic extragalactic objects it is likely that the physical phenomenon responsible may be repeated. To that end it is interesting to note that sources in other extra-

galactic objects are extended NGC 3034 (Kleinmann & Low 1970b) and NGC 253 (Becklin et al. 1973b).

Furthermore Knacke & Capps (1974) have observed a small amount of infrared polarization indicating that a nonthermal source is present in NGC 1068. However, there would appear to be no reason that the grains could not cause the observed polarization.

Recent observations by Rieke & Low (1975) (figure 3.5) show that the flux from NGC 1068 continues to rise approximately linearly above 25μ; there is a shallow feature near 10μ consistent with absorption by silicates within the nucleus; a substantial part of the infrared radiation is thermal and originates in a cloud heated by a nonstellar energy source.

These observations, combined with those of Rieke & Low (1972a,b), Stein et al. (1974) and Knacke & Capps (1974) on the radio-infrared relationship, the suggested 10μ variability and the polarization data, impose severe constraints on the models. It seems clear that nonthermal models of the type proposed by Fogarty & Pacholczyk (1972) may serve only to describe the nonstellar energy source.

3.2 THE GALACTIC CENTRE

The infrared radiation from the galactic centre region is strong and complex. High resolution maps at 2·2μ and 10μ (Becklin & Neugebauer 1975) and intermediate resolution maps at 3·5μ, 5μ, 10·5μ and 21μ (Rieke & Low 1973) show a complex of some 19 individual sources at 2·2μ

and 9 at 10μ. At each of the two wavelengths, 2·2μ and 10μ, there is an individual source which radiates at least 30% of the total radiation. At 2·2μ, the Becklin Neugebauer point source - BN point source - discovered by Becklin & Neugebauer (1968) is unresolved with a spatial resolution of ∿ 2·5 arc sec. At 10μ, the 10μ to 20μ dominant source Rieke & Low, source 1 - RL source 1 - (Rieke & Low 1973) is resolved and is 4×4 (R.A.×Dec) arc sec. (Becklin & Neugebauer 1975) and 4×6 (R.A.×Dec) arc sec. (Borgman et al. 1974).

At 2·2μ the dominant source (Becklin & Neugebauer 1968) agrees in position and extent with the radio source Sgr A. It has a full width at half maximum of between 3 and 5 arc min. and is extended along the galactic plane. Observations with differing aperture sizes reveal a magnitude-aperture relationship in which the flux within an aperture D is proportional to $D^{1\cdot2}$. This spatial distribution is non-Gaussian and follows a power law. Evidence of a nuclear core with a diameter of 18 arc sec. at 2·2μ was found.

The colour ratio of the mean surface brightness at 1·65μ and 2·2μ remains virtually constant over the entire dominant source implying a reasonably even distribution of any obscuring matter and little or no differential extinction in this region. The observed energy distribution is similar to that of a 900°K black-body.

Evidence for an extended source at 2·2μ has been found (Becklin & Neugebauer 1968, 1974). The 2·2μ emitting region is certainly extended on a scale of $1^{0}\times1^{0}$ but probably

not as large as the 100μ emitting region (Hoffmann et al. 1971a) which is of the order of $4^0 \times 2^0$ in extent. The large scale picture of the 2·2μ emitting region in the galactic centre clearly shows the source to be extended along the galactic plane. What is also interesting to note is that Sgr B2 does not show up on the map and the brightest portion of the map is located at the position of the radio source Sgr A.

The general background of 2·2μ emission which amounts to about one third of the total emission from the central 1 arc min. is of stellar origin (Becklin & Neugebauer 1968,1969,1974 and 1975 and Rieke & Low 1973). It is assumed that the observed energy distribution is that of a 4200°K black-body corresponding to a population of late-type stars and appears as a 900°K black-body distribution due to the effects of interstellar absorption. This is inferred from a direct comparison of the 2·2μ observations of the galactic centre degraded to match those of NGC 224 whose stellar population is known (Sandage et al. 1969).

Longer wavelength data on the background source in the central 3 arc min. of the galactic centre coinciding with the radio source Sgr A (Becklin & Neugebauer 1969) are consistant with the interpretation of the earlier 1·65μ, 2·2μ and 3·5μ observations as the energy distribution of K and M type stars.

On the basis of the mean 2·2μ surface brightness Becklin & Neugebauer (1968) estimated the mass within a

radius of 20 parsec to be $2{\cdot}3\times10^{8}M_{\odot}$. The power law dependence of the flux density implies that the mass density of the material falls from the centre approximately as $R^{-1{\cdot}8}$ since the surface brightness increases rapidly toward the centre the observed mass in a given diameter is equal to the mass within a sphere of the same diameter.

Most of the 2·2μ radiation from the central 2 pc of the galactic centre comes from individual sources unresolved at 2·5 arc sec (Becklin & Neugebauer 1975) rather than from an extended background. The brightest source is the BN point like source and is also seen at 10μ as expected if the emitted radiation was from a very luminous star (Becklin & Neugebauer 1975).

The BN point source is displaced from the centroid of the dominant source by about 10 arc sec. It lies 4 arc sec north east of RL source 3 which has been identified with the brightest 2·2μ source (Rieke & Low 1973).

The BN point source lies in the same region of space as the galactic centre on the evidence of the colour ratio, 0·20 for the galactic centre and 0·15 for the BN point source (Becklin & Neugebauer 1968). If it lies between the sun and the galactic centre then the radiation must come from a very cool object. The 2μ Sky Survey (Neugebauer & Leighton 1969) indicates that the number of stars of this colour and K magnitude in the galactic plane is 10^{4} sterad^{-1} so that the probability of finding an unreddened foreground star of this type within 18 arc sec of the galactic centre is less than 1 in 10^{4}. If the source is a single

very luminous star obscured by about 27 mag of visual absorption it would have an absolute magnitude of M_k=-11. The absolute magnitude of α Ori is M_k=-10·5 and if this kind of young Population I star can exist in the nucleus of a galaxy then the BN point could be a very young massive star.

The similarity in colour between the BN point source and the dominant source virtually implies that if the BN point source is nonthermal in origin then so is the radiation from the dominant source.

Long wavelength observations of the BN point source (Becklin & Neugebauer 1969 and 1975) show that the energy distribution follows the background rather than the central core thus strengthening the suggestion that the BN point source is a very luminous star.

Observations of the central 1pc core of the galactic centre from 3·5μ to 19·6μ can be represented as an energy distribution in which $F_\nu \propto \nu^{-1}$ (Becklin & Neugebauer 1969). This cannot be due to a reddened stellar continuum since that follows $F_\nu \propto \nu^{+2}$ and an increase in visual absorption from say 27 mag to 54 mag would change the slope of the continuum by about 30% only.

Any explanation of the energy distribution of the 1pc core in terms of thermal reradiation of star light by dust would require that the dust be more concentrated towards the centre than are the stars.

The fact that the 1pc core is not obviously associated with Sgr A precludes the infrared energy distribution from being a simple extension of the radio spectrum

if the latter is of synchrotron origin.

Assuming that the intrinsic energy spectrum of the nucleus of the galaxy is taken to be that measured in the nucleus of NGC 224 Becklin & Neugebauer derive a total absorption of 27 mag at 0·55μ in the direction of the galactic centre. The intrinsic surface brightness of the dominant source in the galactic centre at 2·2μ out to a diameter of 14pc is $10^{-17}Wm^{-2}Hz^{-1}$ $sterad^{-1}$ while that of NGC 224 is 0·4 $10^{-17}Wm^{-2}Hz^{-1}$ $sterad^{-1}$ (Sandage et al. 1969).

The detection of the galactic centre at around 1μ (Spinrad et al. 1971a) at wavelengths in the deep airglow minima lead to a prediction of about 29 mag of visual absorption. The observational data was consistent with the galactic centre having an intrinsic near infrared spectrum due to a highly obscured stellar system in general agreement with the observations of Becklin & Neugebauer and Rieke & Low.

The observations are interesting in themselves in that they were made taking advantage of the red tail of the FW-118 cell used with the Wampler Scanner. A search for the 1·083μ HeI emission was attempted but was unsuccessful. This was attempted since observations from 5μ to 1500μ (Low et al. 1969) combined with 1·65μ, 2·2μ and 3·5μ observations (Becklin & Neugebauer 1968 and 1969) produce a spectral power distribution of the galactic centre similar to that observed in the nuclei of Seyfert galaxies. The upper limits placed on $W\lambda(10830) \leq 19\mathring{A}$ from the observations are an order of magnitude below the NGC 4151 emission line

(Oke & Sargent 1968).

Rieke & Low (1975) discuss the question of extinction in the direction of the galactic centre. They adopt the value of A_V=29 mag rejecting the argument of Woolf (1973a) that the visible extinction could be as much as 200 mag. This, they argue, would assign unreasonably high luminosities to the 1μ to 3μ source of radiation.

The infrared observations of the galactic centre by Becklin & Neugebauer (1968 and 1969) were used by Sanders & Lowinger (1972) to derive a mass model for the galactic nucleus. They approximated the mass distribution as an inhomogeneous spheroid whose properties could be determined from the spatial distribution of infrared intensity. Using a value of A_V=27 mag, the smoothed elliptical intensity distribution obtained from the detailed distribution at 2·2μ was first converted into a two dimensional distribution, then to a column density and finally, by the application of Abel's theorem to a volume density. Using this mass distribution in the Schmidt model of the galactic mass distribution in place of the point mass a rotation law was derived consistent with the observed rotational velocities of neutral hydrogen.

The total luminosity of the extended 100μ source (Hoffmann et al. 1971a) was compatible with the total visual emission from the stars in the model. This Sanders & Lowinger (1972) suggest gives credence to the suggestion that this infrared radiation is the thermal reradiation of starlight. However this also implies a very efficient

mechanism for the absorption and reradiation of the star-light which may not be the case.

The incidence of stellar collisions will be too low to be important since the star density in the nucleus would be too low. However they suggest that a condensed object with a mass $Mp \equiv 6\times10^5 M_\odot$ might be associated with the BN point source. This arises from the conclusion that the BN point source could be a light spike due to stars surrounding the point mass.

Observations of the galactic centre over the range 5μ to 1500μ were combined with 1·65μ, 2·2μ and 3·5μ (Becklin & Neugebauer 1968 and 1969) observations to produce the spectral power distribution of the galactic centre (Low et al. 1969). The 1·65μ, 2·2μ and 3·5μ observations were corrected for the BN point source, aperture size differences and an interstellar extinction correction for A_V=27 mag. Becklin & Neugebauer (1969) had earlier shown that at 1·65μ and 2·2μ the flux density of the region centred on the maximum of surface brightness with the BN point source subtracted increased as a single power law of the observed area.

The observations (Low et al. 1969) showed that the galactic nucleus contained independent sources. There was an infrared source that corresponded spatially to Sgr A; there was an infrared core with a diamter of 15 arc sec; there was the general stellar background radiating predominantly in the 1μ to 5μ region; there was the BN point like source; and perhaps there was an ultraviolet source based on comparison with NGC 224 (Goldberg 1969).

The infrared luminosity of the 25 arc sec covered by the observations including the 100μ observation of Hoffman & Frederick (1969) is $8\times10^{6}L_{\odot}$ and a thermal model would require a central exciting source with a luminosity of $\sim 10^{11}L_{\odot}$ to produce the observed radiation. A non-thermal model would require a source consisting of many individual sources since the observations at 1200μ suggest a strong degree of self absorption.

Further observations of the galactic centre at long wave lengths (Aumann & Low 1970) resulted in a higher estimate for the total infrared luminosity of $8\times10^{7}L_{\odot}$. The 100μ extended source reported by Hoffmann & Frederick (1969) was not detected. The diameter of the galactic centre was found to be < 3 arc min. Thus the total luminosity from this 10pc region is five times more than the power radiated by stars in this volume and about 1% of the total power output of the galaxy. This upper limit on size strongly favours a nonthermal model for the galactic centre since an optically thick dust cloud heated to a temperature of $43^{\circ}K$ by an internal source would have to be larger than about 6 arc min.

The 10·5μ map of Rieke & Low (1973) with a resolution of 5·5 arc sec revealed 4 individual sources while that of Becklin & Neugebauer (1975) revealed 9 individual sources at 10μ. Of these sources all except two are resolved with a spatial resolution of 1 arc sec. The two sources unresolved at 10μ are the BN point source and RL source 3. One distinctive feature of the 10μ map is a curved ridge of

extended emission containing 3 individual sources and contributing about one half of the total 10μ emission from the region on the map.

The so called dominant source at 10μ - RL source 1 - is an extended object embedded in the ridge of 10μ emission coinciding with a compact radio source (Borgman et al. 1974). Its position agrees with a sharp maximum of the 6cm continuum flux (Ekers et al. 1974) very likely corresponding to the compact source in Sgr A West (Downes & Martin 1971). The total luminosity of the source from 3μ to 25μ observed with a 7 arc sec diaphram is $3\times10^5 L_\odot$.

The spectrum of this object from 3·7μ to 12·2μ is highly reminiscent of several infrared emitting HII regions e.g. W3 (Wynn-Williams et al. 1972 and Wynn-Williams & Becklin 1974). At 10μ to 20μ an infrared excess is observed of 2 orders of magnitude over the flux of ionized plasma responsible for the radio flux. In the near infrared the observed upper limits for the flux are lower than those predicted confirming the presence of absorption. The observed 3μ to 25μ luminosity is much larger than would be expected from the absorption of Lα photons by dust. This would seem to indicate that a significant fraction of the Lyman continuum photons is directly absorbed by the dust.

The possibility that this source could be a planetary nebula is raised since the shape of the spectrum including the supposedly flat radio spectrum is in good agreement with the spectra of some planetary nebulae (Gillett & Stein 1970). This possibility is however discounted by Borgman et al. (1974)

since some of the observed features are unknown in planetary nebulae viz. the 9·7μ absorption feature. The luminosity is most probably several orders of magnitude too high and several would be needed which makes the suggestion unlikely.

The properties of the 10μ source are compared with those of a prestellar object (Borgman et al. 1974). The two objects W3-IRS5 and the BN object in Orion show the 9·7μ absorption feature and are of stellar size - smaller than 2 arc sec in diameter. In addition they are both associated with OH and H_2O emission. The dominant source is not associated with molecular emission although observations of the 12·8μ NeII fine structure line have been reported (Aitken et al. 1974). The 9·7μ absorption feature is probably not associated with dust in the large cloud of cool stars.

On the basis of the evidence, Borgman et al. (1974) favour an explanation in terms of hot dust radiation for the 10μ to 20μ dominant source. The dust would be locally heated by an O star or protostar hot enough to locally ionize the hydrogen.

At 21μ the galactic centre is much more extended (Rieke & Low 1973) and the observed flux exceeds any extrapolation of the 5μ to 10·5μ spectra. The extended wings of the 21μ source are not seen at 10·5μ and therefore could be very cold and could be associated with the far infrared source.

At 100μ the first observation of Hoffmann & Frederick

(1969) has yet to be confirmed. This assigned a luminosity of $6\times10^8 L_\odot$ and an extent of $6^\circ.5\times2^\circ.3$. Later observations by Hoffmann et al. (1971a) produced a detailed map of the galactic centre region with a resolution of 6 arc min.. An emitting region of $2^\circ\times3^\circ.6$ was mapped yielding a luminosity of $3\times10^8 L_\odot$. The sources Sgr A and Sgr B2 are clearly resolved. The peak at Sgr A has a half power size of 38×15 arc min in direct contrast to the observations of Aumann & Low (1970) who place an upper limit of 3 arc min on the size of this source. The sources are connected by a continuous band of emission along the galactic plane. The extended nature of this source is confirmed albeit on a smaller scale than previously reported.

The detailed agreement between the 100μ and the radio observations reported by Hoffmann et al. (1971a) established the identification of the 100μ emission with the radio sources associated with the galactic nucleus.

The large size of the infrared emitting region for Sgr A brings into doubt the necessity of a nonthermal mechanism. If the mechanism is assumed to be thermal emission from grains with low infrared emissivity the grain temperature would be in the range $45^\circ K$ to $55^\circ K$.

Far infrared rocket (Houck et al. 1971) and balloon observations (van Duinen et al. 1972) confirm the observed structure (Hoffmann & Frederick 1969, Low et al. 1969 and Hoffman et al. 1971a) of the galactic centre at 100μ. From 40μ to 150μ the spectrum of the galactic centre would be approximated by a $60^\circ K$ black-body (Harper & Low 1973).

Rieke & Low (1973) were undecided as to whether there was a compact source in the galactic centre in the 40μ to 100μ region. They suggest RL source 3. It does not appear to rise steeply in the 10·5μ to 21μ range but this behaviour could be due to inadequate correction for extinction. If the deep absorption near 10μ (Aitken & Jones 1972 and Woolf 1973a) is due to silicates then another deep absorption might be expected around 20μ. However, later observations of RL source 3 (Becklin & Neugehauer 1975) show it to be spatially unresolved and to have the reddest 2μ to 10μ colour index of all the sources found in the galactic centre.

Observations of the central 30 arc sec of the galactic centre which include RL source 3 at 3·5μ, 4·8μ, 8·7μ, 12·5μ, 20μ and 34μ (Sutton et al. 1974) show the absorption feature at around 11μ and perhaps an absorption at 20μ. The energy distribution is very like that of an HII region and has a comparible luminosity. Sutton et al. (1974) suggest that these observations support the hypothesis that the infrared emission from the galactic centre is due predominantly to the thermal reradiation of heated dust.

The question as to whether or not the galactic centre is similar to compact HII regions has been raised by Pottasch (1974). There seems to be room for doubt.

At least six sources have been detected at 100μ in the vicinity of the galactic centre (Hoffmann et al. 1971b) and identified as HII regions because of the thermal nature of their radio spectrum and the presence of radio recombin-

ation lines. These sources all have an excess of infrared radiation for a given radio emission (Pottasch 1974) and deviate from the linear relationship between radio and infrared emission first pointed out by Harper & Low (1971). In fact Pottasch (1974) gives the observed radio emission in units of the Lα flux which an ionized region produces at the same time as it produces the observed thermal radio emission. This is essentially proportional to the radio flux because each recombination of an electron proton pair produces a single Lα quantum and the recombination rate is proportional to a slowly varying function of Te and to n_e^2. The two fluxes, radio and Lα, have the same n_e^2 dependence and almost the same Te dependence so that the two fluxes differ only by a constant.

In addition to the six sources there is an area of extended emission at 100μ covering a region of about $4^0 \times 2^0$ around the galactic centre. The problem is that this extended emission could be simply the sum of many smaller compact HII regions or the extension of the six observed sources in which case they are much larger than a compact region - or a general flux emitted by a continuous medium.

The luminosity of the extended region is about $8 \times 10^8 L_\odot$ while that of an average compact HII region is about $8 \times 10^4 L_\odot$. Thus if the energy source of an HII region was a hot star - O say - then at least 10^3 would be required.

There are two reasons for believing that an O star is the origin of the high luminosity in the compact HII region. Firstly, an O star is capable of emitting the

observed energy and secondly, the O star can account for the ionized gas which is observed in the radio continuum to be approximately coincident with the infrared emitting region.

There is also an extended region - $3^0 \times 2^0$ - emitting in the 12μ to 23μ region (Houck et al. 1971). It is interesting to note that there is less than a factor of three difference in flux between the central 30 arc sec core and this extended region which means that the ratio of the 100μ to 20μ flux is very different in the 30 arc sec core where it is less than 100 and in the extended region where it is at least 1000 (Pottasch 1974).

3.3 MODELS FOR THE GALACTIC CENTRE

The possibility that synchrotron emission is the source of infrared emission is suggested by the fact that it is probably responsible for most of the nonthermal radio emission. However Lequeux (1970) has pointed out that the low frequency part of the synchrotron spectrum of any distribution of relativistic electrons cannot be steeper than

$$S(\nu) \propto \nu^{+1/3}$$

if no low frequency absorption mechanism exists. Any such absorption mechanism operating on centimeter wavelengths would prohibit the observation of Sgr A and its associated sources in and around the galactic centre. Further, extrapolation following this law from 100μ would give radio fluxes

much in excess of those observed. Clearly, in the case of the galactic centre, synchrotron emission can be eliminated as the HII regions are seen clearly with a thermal radio spectrum.

But. No

The far infrared emission from the galactic centre might be due to forbidden fine-structure lines. These lines are formed by the collision of an electron with an ion in the ground state which raises the ion to an excited state from which only a forbidden transition can occur. These lines have been discussed by Petrosian et al. (1969) and Pottasch (1968) in connection with HII regions. There are no strong lines predicted near 100μ except the 0 III line at 88·1μ (Lequeux 1970) which can only be emitted in HII regions.

Lequeux (1970) estimates that the integrated flux of the principal lines in both HI and HII regions can be only 1% of the total 80μ to 120μ flux from the galactic centre, and there is no evidence for concentration into dense clouds which would increase the line intensity.

The mechanism of thermal emission from dust grains has been suggested by Hoffmann & Frederick (1969). They suggest that the observed far-infrared emission is thermal emission from interstellar grains heated by the absorption of starlight.

Stein (1966) has given a model for interstellar grain emission with which he estimates the intensity of the far-infrared radiation in the galactic plane. His model assumes that the grain size and density and the total

radiation energy flux in the solar neighbourhood represent a reasonable approximation to the mean over the galactic plane and he analyses thermal equilibrium of dust grains in the galaxy between the heating by stellar radiation and cooling by infrared emission. His estimate of thermal emission in the far infrared by dust grains in the galactic plane integrated over all wavelengths falls short by a factor of at least 30 from the intensity observed in the 8μ to 120μ band (Hoffmann & Frederick 1969 and Lequeux 1970). Hence if the data are to be reconciled to the model, a large fraction of the grains must be at a higher temperature than is suggested by Stein's (1966) analysis and the grains must be concentrated in dense clouds in the central regions of the galaxy where the radiation energy flux will be considerably higher than in the solar neighbourhood.

Burbidge & Stein (1970) discussed the explanation of the infrared observations of the galactic centre in terms of a dust model in the same way as galactic sources in terms of the mass of gas and dust required. The infrared characteristics are determined by the amount of dust present in the form of a cloud, the optical depth of the dust at different wavelengths and the temperature of the dust. They derive expressions for the mass of emitting dust as a function of τ the optical depth and R, the radius of the dust cloud and outline a method of deriving R by setting the rate of absorption of energy by the particle equal to the rate of radiation. A lower limit to R can be estimated from

$$\frac{L}{4\pi R^2}\,\pi a^2\,Q_{abs} < \frac{2\pi a}{\lambda_m}\,\sigma T^4 4\pi a^2$$

where L is the luminosity of the source of energy, a is the particle radius, Q_{abs} is the efficiency of absorption of shortwave radiation, σ is Steffan's constant and T is the temperature determined by the Wien law and the wavelength of observed radiation

$$\lambda_m T = 0{\cdot}3 \text{ cm deg.}$$

More rigorously, the grain temperature can be determined by the method of Krishna Swamy (1971) equation 1.

Taking $L = 10^9 L_\odot$ at 100μ, Burbidge & Stein (1970) find $R \sim 3\times10^{20}$cm = 100 parsec, $M = 5\times10^5 M_\odot$ and $Mgas \sim 10^8 M_\odot$ which seem to be reasonable estimates.

Treating the 100μ emitting region in the galactic centre as an HII region with the continuum emission due to thermal grain emission Harwit et al. (1972) proposed a model of grain heating through resonantly trapped Lα photons. They fit the model to the galactic centre and obtain an emission measure from the 100μ observations agreeing with an emission measure obtained from radio observations (Downes & Maxwell 1966). They obtain their emission measure in the following way:- the temperature of the grain is determined by the local Lα flux and depends on the Lα density N through the energy balance equation,

$$4\sigma T^4 \varepsilon_{ir} \sim \alpha c N \varepsilon_{uv}$$

where α is the Lα energy and ε_{ir} and ε_{uv} are respectively the infrared and ultraviolet grain emissivities. The

formation rate of the Lα photons integrated over the entire volume of the region equals the recombination rate and determines the Lα photon density.

$$\dot{N} \sim n_e n_p v \sigma_r V$$

where $\dot{N}$ is the formation rate of Lα photons, n_e and n_p are respectively the electron and photon number densities, v is the particle velocity, σ_r is the recombination cross section and V is the volume of the ionized region. When only grain absorption limits the L_α photon lifetime, it is given by

$$t \sim (c\, n_g \varepsilon_{uv} \pi a^2)^{-1}$$

where n_g and a are the grain number density and radius. Then

$$N \sim \frac{\dot{N}t}{V}$$

gives the Lα photon density and the temperature can be determined in the following way

$$4\sigma T^4 \varepsilon_{ir} \sim \alpha c \frac{\dot{N}t}{V} \varepsilon_{uv}$$

i.e.
$$4\sigma T^4 \varepsilon_{ir} \sim \frac{\alpha c n_e n_p v \sigma_r V \varepsilon_{uv}}{c n_g \varepsilon_{uv} \pi a^2 V}$$

i.e.
$$T \sim \left[\frac{n_e n_p v \sigma_r}{n_g \varepsilon_{ir} \sigma 4\pi a^2} \alpha \right]^{\frac{1}{4}}$$

In the case of the galactic centre where the luminosity is $\sim 10^8 L_\odot$ then the Lα energy creation rate and the grain emission rate give rise to values of n_e and n_p and an emission measure and, with considerations of chemical abundance, gives values of n_g and $\varepsilon_{ir} T^4$. These follow from

$$\alpha\dot{N} \sim \alpha n_e n_p v\sigma_r V \sim 10^{42} \text{ergs}^{-1} \sim n_g 4\pi a^2 \varepsilon_{ir} \sigma T^4 V$$

On substitution for $V = 3\times10^{62}\text{cm}^3$, $\alpha = 1{\cdot}6\times10^{-11}\text{erg}$, $v\sigma_r \sim 5\times10^{-13}\text{cm}^3\text{s}^{-1}$, ρ gas/ρ dust = 300, $\rho_g = 1$ g cm^{-3}, $m_H = 1{\cdot}6\times10^{-24}$g, $a = 5\times10^{-6}$cm gives $n_e \sim n_p \sim 20\text{cm}^{-3}$, $n_g = 2\times10^{-10}\text{cm}^{-3}$, $\varepsilon_{ir}T^4 \sim 5\times10^2$ and an emission measure of $12\times10^4\text{cm}^{-6}$pc.

A detailed model attempting to describe the infrared spectrum of the galactic centre on the basis of a dust model is discussed by Okuda & Wickramasinghe (1970). They assume that the central source has an effective temperature $\sim 50{,}000^{\circ}$K and radiates like a black-body enabling them to use the luminosity L, rather than the flux $F\lambda$, to characterise the central source. The results for the case where τ, the optical depth at $0{\cdot}5\mu$ is unity and $L = 10^7 L_{\odot}$ give a best fit to the observations with R = 100 pc. They suggest that it appears that the results favour a model in which the dust shell surrounding the central source has a more or less sharply defined outer boundary. This could be the case if the grains were decoupled from the surrounding gas which could be if there was a sharp reduction in photoelectric charge (Wickramasinghe 1970). For grains with $a = 5\times10^{-5}$cm and $\rho_g = 2{\cdot}5$ g cm^{-3} they find the total mass in a 100 pc emitting region to be $10^3 M_{\odot}$.

In an attempt to describe the observations of the galactic centre in a consistent way and not a collection of radiation sources which can be physically distinguished, Borgman (1974a) has suggested a radiation model based on an infrared picture of the galactic centre that can be

summarized as follows:

(1) There is an extended region of 100μ emission in which Sgr A and Sgr B2 are outstanding concentrations. Sgr A is a nonthermal radio source while Sgr B2 is a thermal HII region. The region has an overall extension of $2^0 \times 4^0$ and is extended along the galactic plane. The observed luminosity of this source in the 80μ to 120μ band is $5 \times 10^8 L_\odot$.

(2) There is an extended region of 1μ to 5μ emission strongly concentrated towards the centre and elongated along the galactic plane. This is probably a large concentration of stars in the nucleus of the galaxy whose observed energy distribution agrees with that of a stellar population whose energy distribution has suffered 27 mag of visual extinction (Becklin & Neugebauer 1968,1969,1974,1975). This emitting region is extended to the order of 1^0.

(3) There is an extended region of 10μ emission centered on Sgr A containing concentrations (Rieke & Low 1973 and Becklin & Neugebauer 1975). The emitting region is of the order of 30 arc sec in diameter.

(4) There is a point like source in source (3) most probably a highly luminous late-type star $M_k = -11$ and $L = 3 \times 10^5 L_\odot$. This source is the BN point source.

The model used is an attempt to fit the observations for $\lambda \leq 2 \cdot 2\mu$ as a continuum of late-type stars modified by interstellar reddening. Borgman claims a unique solution of

28 mag of visual extinction by fitting a typical late-type star energy distribution modified by an extinction law based on Van de Hulst's (1949) curve no.15 adjusted for large extinction, broad band response functions and a low temperature source to the observed 1·6μ and 2·2μ points in the galactic centre spectrum. This then requires 7×10^3 late-type giants at $M_{bol} = -1$ within the 22 arc sec region resulting in a luminosity of $1\cdot2\times10^6 L_\odot$.

The continuum emission from the above model at 4·8μ is very low and so Borgman (1974a) claims that the emission at longer wavelengths, $\lambda>5\mu$ say, can be dealt with separately. This radiation, he suggests, comes from thermal reradiation from a dust cloud heated by a dense cluster whose radiation characteristics are determined by late-type stars. By fitting the 4·8μ and 8μ points of the galactic centre spectrum and assuming that the cluster continuum is observed at 8μ and the dust cloud is far enough away from the cluster rendering thermal emission from the dust at $\lambda<8\mu$ negligible a value of 200 mag of visual extinction is found. This model requires 3×10^6 late-type giants and with $M_{bol}= -1$ gives a luminosity of $10^9 L_\odot$. This may be a lower limit to the mass of stars as there will be a reasonable number of early-type stars which excite the HII regions in the galactic centre.

This model fits the observations out to 12·8μ and takes only the infrared observations into account. It considers only the broad band work done. The fit to the 100μ observation is purely a justification of the luminosity

estimate for the primary energy source. If the 100μ emitting region is a large HII region then the ratio of the total flux in the infrared to the 75μ to 125μ flux is of the order of 2 to 4. From observations, the 100μ luminosity is $5\times10^{8}L_{\odot}$ (Hoffmann et al. 1971a) implying a total luminosity of between 1 and $2\times10^{9}L_{\odot}$ consistent with the model. At 100μ the stellar contribution would be rather small.

The observed 20μ excess and the deviation of the observation from the model could be due to the fact that more than 75% of the 10μ radiation comes from discrete sources and the extended ridge (Becklin & Neugebauer 1975) and it is reasonable to assume that the dominant sources at 10μ and 20μ are the same (Borgman et al. 1974). Therefore it seems that there would only be a low background at 10μ coming from the galactic centre. That it is extended and comes from a large area is clearly seen (Rieke & Low 1973, and Becklin & Neugebauer 1975).

It has been suggested that on the evidence of medium resolution maps (Rieke & Low, 1973 and Borgman et al. 1974) the dominant source at 10μ, the RL source 1, is a compact HII region superimposed on the much more luminous and extended source of cool dust heated by late-type stars (Borgman et al. 1974). High resolution maps (Becklin & Neugebauer 1975) show that this indeed may be the case and that there are additional sources. It may be that RL source 1 as observed by Rieke & Low includes radiation from the Becklin & Neugebauer (1975) 10μ ridge.

RL source 1 and the individual sources in the ridge

could be compact HII regions where the dust is heated either by O stars or by photostars hot enough to ionize the gas locally. It seems that a search in the region of RL source 1 and the BN 10μ ridge for molecular emission lines is called for. Neither of these suggestions are unreasonable. It seems very possible that in a dense dusty region like this star formation would be taking place and, where the ionizing centres in these regions O stars, a reasonable number could be accomodated into the model while maintaining the nuclear mass required within the limits set by observations of the rotation of the nuclear disc.

Observations of Sgr B2 (Rieke et al. 1973) show that the centre of the infrared emitting region lies to the north of the molecular core of OH and H_2O maser sources. The compact radio HII regions in Sgr B2 (Martin & Downes 1972 and Balick & Sanders 1974) are not prominent at 10μ to 20μ (Downes 1974) and this could be due to high extinction in the infrared quite consistent with the high density inferred from the presence of the Sgr B2 molecular cloud.

Radio results in the past few years have confirmed the picture of two main components in the 3 arc min source called Sgr A. There is a broad nonthermal eastern component with an angular size of 150 arc sec and a bright thermal western component with half width of 45 arc sec. These sources are respectively Sgr A East and Sgr A West.

The thermal source Sgr A West coincides with the maximum of 2·2μ surface brightness which suggests that this is the centre of mass of the galaxy. Radio continuum maps show that much of the fine structure is coincident with

infrared sources thought to be at the galactic centre (Balick & Sanders 1974). In fact the infrared sources are coincident with the fine structure Balick & Sanders (1974) call the northern complex.

Balick & Sanders (1974) assign a scale size of 1 pc and a density of $10^4 cm^{-3}$ for the northern complex. They suggest that ionized gas of this density might be present in the central 1 pc core of the galaxy if it is deposited by the stars by means of gradual or explosive mass loss. They suggest that in the inner 1 pc core there are $1\text{-}2\times10^6 M_\odot$ of late-type stars which is in good agreement with Becklin & Neugebauer (1968), Sanders & Lowinger (1972) and Borgman (1974).

Balick & Sanders (1974) suggest that the infrared point sources - RL sources 1 to 5 - could be thermal emission from dust surrounding massive stars forming in the gaseous disk and that the positional coincidence of RL source 1 and 5 with the brightest radio components in the fine structure could indicate that these objects are themselves sources of ionizing radiation. Further confirmation of these observations is provided by Downes (1974).

The radio point source found by Balick & Brown (1974) is assumed to be $\leq 0{\cdot}1$ arc sec in angular diamter and does not coincide with any of the infrared sources in the galactic centre. It does, however, coincide with the maximum in surface brightness at $2{\cdot}2\mu$ (Becklin & Neugebauer 1975).

CHAPTER IV

NARROW BAND OBSERVATIONS

4.1 THE CO INDEX

It has long been known that Carbon monoxide, (CO), is amongst the most abundant molecules in stellar atmospheres, it being the most stable of all diatomic molecules with a dissociation energy of ∿11·1 volts (Russell 1934). As is the case with H_2, all electronic transitions from the ground state lie shortward of the atmospheric cut-off in the ultra-violet. Those CO bandheads have been observed only in the sun (Goldberg et al. 1965).

The first overtone $\Delta v=2$ band sequence at 2·3μ is well placed for observation with PbS detectors. Several stars with strong CO absorption show at least 6 bandheads at 2·29μ, 2·33μ, 2·36μ, 2·39μ, 2·42μ, and 2·45μ these correspond to the (2,0), (3,1), (4,2), (5,3), (6,4) and (7,5) transitions. The relative strengths of each bandhead depend upon temperature and have been used for rough spectral classification (Johnson et al. 1968, Johnson 1968 and Frogel & Hyland 1972).

The behaviour of the CO bandheads as a function of spectral type is not clearly understood (Spinrad & Wing 1969). It has been reported that CO is detectable near K_0III and strengthens till M_2III where it remains constant till M_8III (Boyce & Sinton 1965 and Spinrad & Wing 1969). Johnson et al. (1968) report that the strengths of the CO bandheads increase with advancing spectral type and luminosity class. They also note that, among the giants measured, the CO bandheads are strongest in Mira stars. Three stars are compared by way of an example and are given here in increasing

CO strength. δ Oph (M_1III), α Ori (M_2Iab) and μ Cep (M_2Ia). The latter in Johnson et al.'s opinion having CO strength comparable with Mira. Spinrad & Wing (1969) report that the CO strength shows a strong positive luminosity effect among stars of classes III to Ia. They suggest that the luminosity effect is due to decreased saturation due to turbulence in the supergiant atmospheres. The luminosity effect is substantiated in the observations of McCammon et al. (1967) and Johnson et al. (1968).

In an attempt to make a quantitative estimate of the strength of CO absorption Frogel & Hyland (1972) defined a quantity,

$$\log \left[\frac{F\ Cont}{F\ CO}\right]_{\lambda = 2{\cdot}29\mu}$$

which was a measure of the depth of the first bandhead at 2·29μ below the continuum obtained by extrapolating the flux observed at wavelengths shorter than 2·29μ. This process was applied to medium resolution spectra of carbon stars.

In an attempt to establish a photometric technique that would measure the CO absorption exhibited by late-type stars in the K photometric band a system of two narrow band filters was used to measure the 'CO index'. The filters were obtained from O.C.L.I. and their transmission curves are given in figure (4.1). The filters have λ_0 of 2·30μ and 2·23μ, half power bandwidths of 0·09μ and 0·05μ respectively and are called the CO filter and the Cont. filter. These two filters were used uncooled in the photometer described previously. The filters have about 40% transmission and are fully

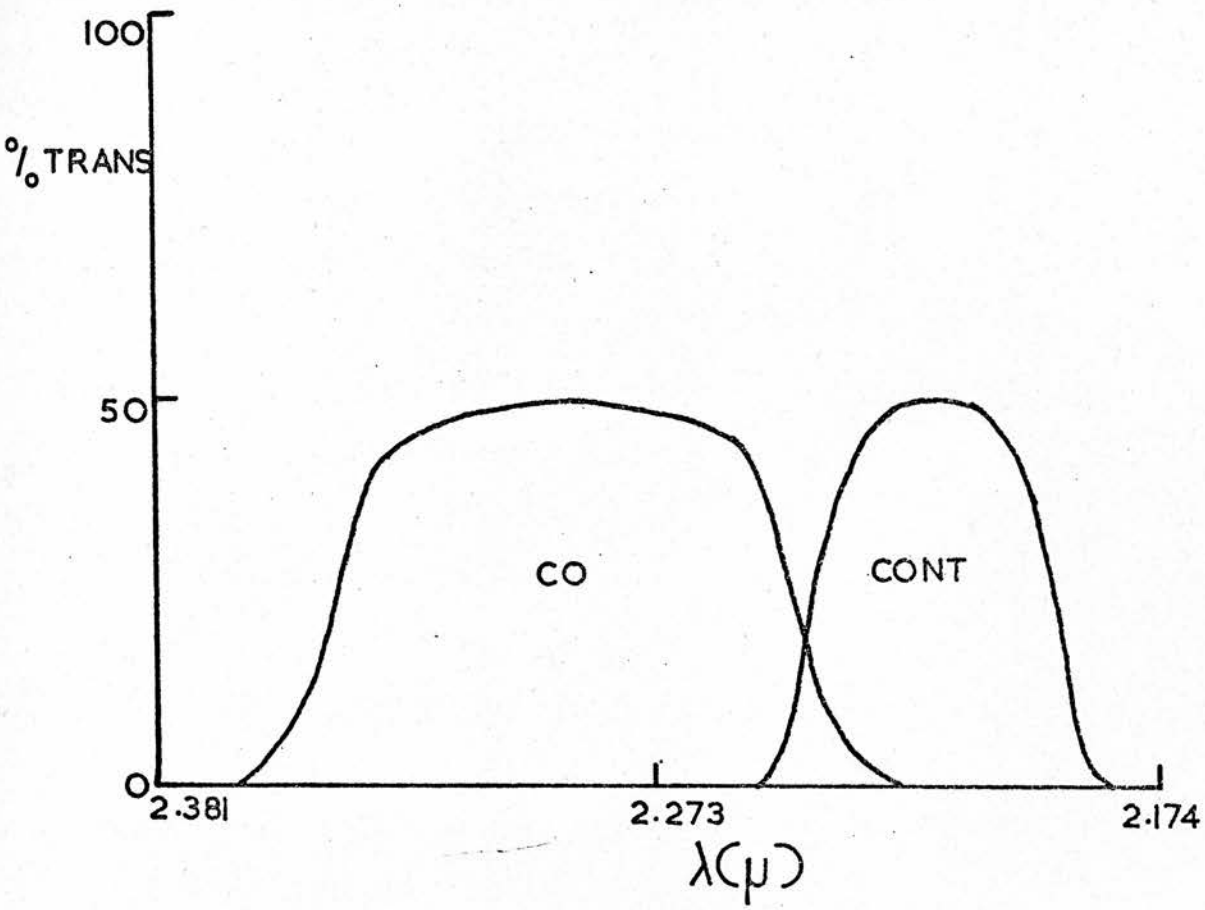

Figure (4.1)

blocked outside the band pass region. The CO filter is centred near the (2,0) bandhead at 2·29μ and also covers the (3,1) bandhead at 2·33μ of the first overtone band of $^{12}C^{16}O$. The CO filter also covers the (2,0) bandhead of $^{13}C^{16}O$ at 2·34μ. Note that the bandheads up to the (4,2) bandhead of $^{12}C^{16}O$ are well below the 10% transmission level.

The Cont. filter is centred in a region of the continuum close to the CO bandheads to be measured where there is no absorption of equivalent strength by any other molecule. The only absorption line that falls near the Cont. filter band is the Bγ(B_7) line in the Brackett series of hydrogen at 2·166μ. These lines occur in stars of spectral type A_0.

The CO index is a photometric measurement that attempts to represent the quantity described in Frogel & Hyland (1972) and is defined in the following way:-

Let the signal received be

$$I^{CO} = I_0^{CO} e^{-\kappa l \sec z} \qquad \ldots (4.1)$$

and

$$I^{Cont} = I_0^{Cont} e^{-\kappa l \sec z}$$

where I_0^{CO} and I_0^{Cont} represent the radiation from the object in the respective bands above the atmosphere and κlsecz is the effect of the atmosphere in terms of magnitudes of extinction per air mass. Since both the CO and Cont. filter lie inside the K intermediate band and measurements were made after each other in order that secz for each filter is

very nearly the same, then for each object the ratio defined from equations (4.1) as

$$\text{ratio} = I_0^{CO}/I_0^{Cont} \qquad \ldots (4.2)$$

is equal to the ratio (I^{CO}/I^{Cont}), the ratio of the quantities observed. This can then be converted to a magnitude difference in the usual way

$$\Delta m = -2{\cdot}5 \log (\text{ratio}) \qquad \ldots (4.3)$$

This magnitude difference for the star α Lyr(A_0V) is used as a zero point. The CO index of each object is defined normalized to α Lyr by

$$\text{CO index} = -2{\cdot}5 \log [(\text{ratio})/(\text{ratio})^{\alpha Lyr}] \qquad \ldots (4.4)$$

The CO index as defined in equation (4.4) assumes that $(\text{ratio})^{\alpha Lyr}$ measures only the instrumental response and sets the CO index of α Lyr at zero. α Lyr is used as a standard in these measurements because no features comparable in strength to those to be measured in late-type stars appear in its spectrum (Johnson & Mendez 1970). Where α Lyr was not available, α Boo was used as a secondary standard.

The use of the CO index (Frogel & Hyland 1972) in the interpretation of carbon stars resulted in the observation that the Miras have the weakest CO absorption while the irregular variables have the strongest. The dependence of the CO index on colour and carbon abundance showed that the reddest stars of the group observed, the Mira variables, had the smallest index and the CO index decreased rapidly with increasing J-L colour. There is also a strong suggestion

that there exists an inverse correlation between the absorption and the abundance of carbon determined from visual spectra. This, however, depends critically upon the behaviour of the CO index as a function of luminosity in carbon stars. Frogel & Hyland (1972) were unable to furnish direct evidence as to this point since there was little or no information about the luminosities of the individual stars in their group.

Their interpretation of these observations was that the variation of the CO bands as a function of colour and variability type was due to the filling of the bands by thermal emission of a circumstellar shell. Thus implying that the reddest of stars have the thickest shells and that the abundance of photospheric carbon determined from visual spectra is proportional to the optical depth of the circumstellar shell as measured by the CO index.

Stars cool enough to have strong CO vibration rotation bands - the red giants - cover a wide range of spectral types, G8 - M8. In the region 4230cm^{-1} to 4360cm^{-1} most of the CO opacity is due to a small number of saturated lines. The continuum can be estimated by assuming that there are no lines in the region 4400cm^{-1} to 4900cm^{-1}. In fact, any measurement made in that interval is taken to be continuum.

As is pointed out, the CO index measures bandheads which are most likely to be saturated and it should be expected that even large changes in CO abundance in stars will have no observable effect. This fact has been pointed out for K giants by Ridgway (1974). Thus any difference in

the observed CO index of a nonstellar object or group of nonstellar objects would be due to a change in stellar population. Similarly any observation of the CO index of a galaxy placing it in the domain of the late-type star is arguably a strong indicator of the stellar population of that galaxy.

4.2 OBSERVATIONS OF STARS

The observations described in this section were made with the 60 inch (1·5m) Flux Collector at Izãna, Tenerife. The data was obtained with the photometer previously described. Table (4.1) list the stars, their spectral types and CO indices. The spectral types are taken from The Bright Star Catalogue, Keenan (1963), Dentsch et al. (1969), Gillet et al. (1971) and Morgan & Keenan (1973).

Most of the stars observed are variable of one type or another as would be expected from their highly evolved types. η Gem (M_3III) is an eclipsing binary (McLaughlin & Van Dijke 1943) although Woolf (1973b) claims that the evidence that an actual eclipse takes place is slight and that the star is most likely an ellipsoidal variable. No spectral type is available for the companion if it exists and no effect of the binary system on the silicate emission of η Gem seems present (Woolf 1973b). The only estimate of spectral type for the companion is forwarded by Woolf as 'an even later M giant'. η Gem has a high CO index almost as high as RW Cyg (M_{3-4} Ia Iab). Most certainly the question

TABLE 4.1 - CO INDEX

BS	NAME	I-K	TYPE	CO INDEX	NO. OBS.
337	β And	1·64	M_0 III	0·11	10
2061	α Ori	1·50	M_{1-2} Ia-Iab	0·13	2
2216	η Gem	1·79	M_3 III	0·13	1
3748	α Hya	1·35	K_3 II-III	0·06	2
4057	γ Leo	1·19	K_0 III+G_7 III	0·03	1
5340	α Boo	1·33	K_2 IIIp	0·02	6
6056	δ Oph	1·65	$M_{0.5}$ III	0·04	2
6134	α Sco	1·98	$M_{1.5}$ Iab	0·15	2
6406	α Her	2·33	M_5 Ib-II+G_5 III	0·16	1
6526	λ Her	1·45	K_4 III	0·03	1
6603	β Oph	1·15	K_2 III	0·08	1
6695	θ Her	1·31	K_1 II	0·13	1
6746	γ Sgr	1·10	K_0 III	0·04	1
6752	70 Oph	1·04	K_0V	0·05	1
7001	α Lyr	0·08	A_0V	0·00	19
7009	XY Lyr		M_{4-5} II	0·14	1
7139	δ^2Lyr	2·12	M_4 II	0·10	1
8308	ε Peg	1·39	K_2 Ib	0·06	1
8316	μ Cep	1·96	M_2 Ia	0·11	1
8383	β Peg	1·81	$M_{2.5}$ II-III	0·13	9
	RW Cyg		M_{3-4} Ia-Iab	0·14	1
	RW Cep		K_0 O-Ia	0·09	1
	R Leo		M_8e	0·13	1

as to whether η Gem has a companion or not remains and it would seem that this could possibly be the cause of the high CO index. η Gem is reported by Woolf (1973b) as M_3III, as M_2III and M_3III by Jaschek et al. (1974) and as M_3III by Gillet et al. (1971). The spectral type assigned here, M_3III seems entirely reasonable on the available evidence. However, the high value of CO index could be due to a misclassification.

γ^1 Leo is classified as K_0 to K_1 III (Jaschek 1964) while γ^2 Leo is classified as G_7 III. Since the two stars are separated by 4·4 arc sec both will be visible through the 22 arc sec aperture used. The difference in visual magnitudes is small $\sim 1^m \cdot 5$ and in this case the companion, γ^2, will contribute significantly to the CO index. It seems reasonable to assume that the contribution from both stars in the Cont. filter will be the same and that the contribution to the CO filter in γ^2 will be at most 10% more than that of γ^1. Using these assumptions, the corrected CO index is given in table (4.1).

α Her is a visual binary with a separation of 5·3 arc sec. The companion, α^2 Her, is itself a spectroscopic binary being a G_5 III + F_2 (Jaschek 1964). In this case the effect of the companion stars will be to swamp the CO bandheads. The contribution to the Cont. filter will be dominated by α Her which is very bright in K, $-3^m \cdot 37$. The contribution to the CO filter from the companion star will tend to make the CO index too low and the corrected CO index is given in table (4.1).

70 Oph is a double star with a K_3-K_7 V companion (Jaschek 1964). The star itself is given as K_0V Jaschek (1964). The CO index measured for this star will be too large since the separation of the two stars is only 6·5 arc sec and they are of about the same magnitude in the visual. They probably both contribute the same amount to the CO index being of about the same spectral class and probably the same K magnitude. Notice that in this case the companion is of later spectral type. The corrected CO index is given in table (4.1).

There are two other stars worthy of note. One is θ Her classified by Morgan & Keenan (1973) as K_1 IIa cN+2. This star has an abnormally high CO index, higher that the luminosity class Ib star, ε Peg, of similar spectral type. This star is a Population II giant with a higher ratio of metals/hydrogen. This seems to be a high luminosity, slightly metal rich star (Williams 1975) and has Helium, λ 10830A^{o}, in emission (Vaughan & Zirin 1968). This suggests that this star has a highly active chromosphere and a high microturbulent velocity. All of these could contribute to the abnormally high CO index.

The other star of interest is RW Cep. This star is reported as M_0Ia-0 by Gillett et al. (1971) as $K_0$0-Ia by Morgan & Keenan (1973) and Keenan (1963) as K_5Ia-0 by Kennedy & Buscone (1974) and G8 Ia by Roman (1973). The classification reported by Gillet et al. (1971) is by Kukarkin et al. (1958) and would seem to be rather out. The CO index of RW Cep is consistant with a supergiant of spectral type

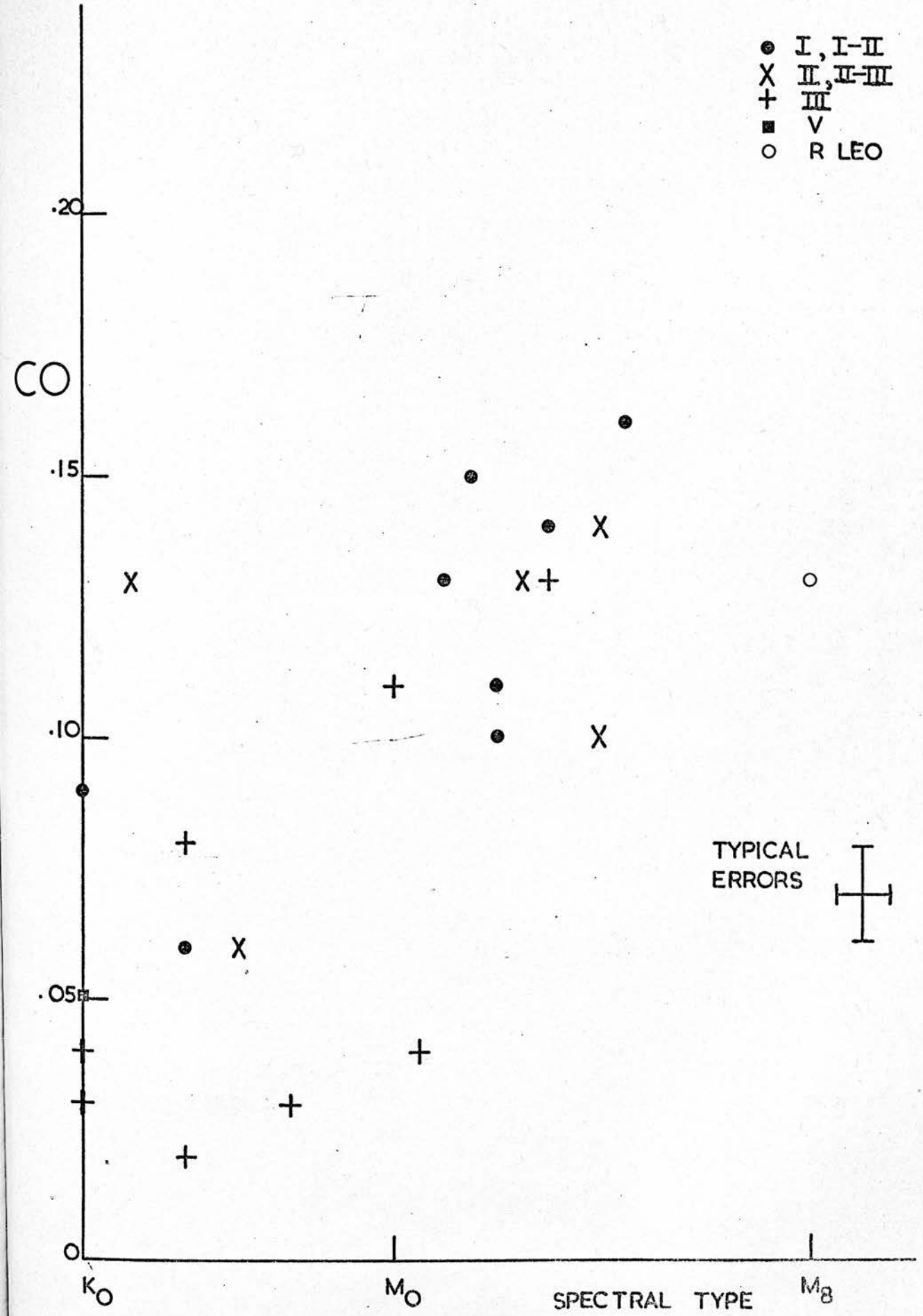
I, I-II
II, II-III
III
V
R LEO
.20
CO
.15
.10
.05
0
TYPICAL ERRORS
K0
M0
SPECTRAL TYPE
M8

Figure(4.2)

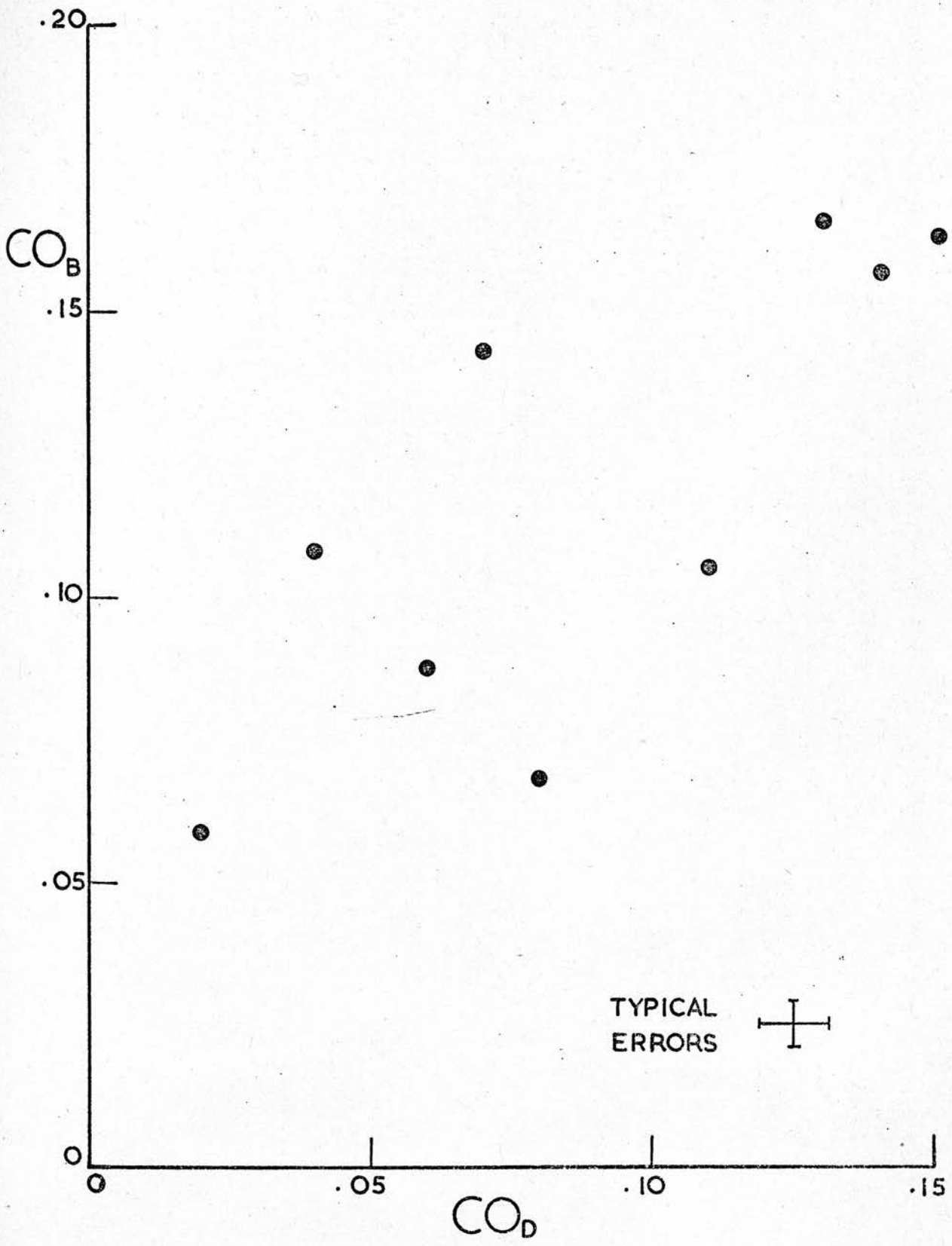

Figure (4.3)

K_0. This, in fact, is the type assigned here.

The rest of the spectral types given in table (4.1) are from the various sources shown in the table. Those marked with a dagger are members of the MK Dagger System (Morgan & Keenan 1973).

Figure (4.2) shows the observed CO index as a function of spectral type. What becomes apparent in figure (4.2) is that at around K_0 there seems to be little separation of luminosity class except that the luminosity class I seem to be consistantly higher throughout and that the CO index increases with spectral type in the range K to M_8 and luminosity classes I to III.

The observing time available and the development of the instrument meant that only 24 stars were observed with this filter combination and, with the exception of 70 Oph (K_0V), no dwarves were observed other than α Lyr (A_0V). Since the inception of this work, narrow band observations of dwarves later than K_0 have been published by Baldwin et al. (1973a) and updated by Frogel et al. (1975). Both sets of authors show that the dwarves lie significantly below the giants for types later than K_0. The position of the dwarves of later type than K_0 indicates a decrease in CO index with latening spectral type or perhaps more importantly decreasing temperature. Baldwin et al. (1973a) attribute this not to the absence of CO in dwarves but to a change in slope of the continuum in the 2μ region.

Figure (4.3) shows a plot of the CO index as measured by Baldwin et al. (1973a) and the CO index of this work.

The degree of correlation is measured by the correlation coefficient r, which is given by

$$r^2 = \frac{\left[\Sigma xy - \frac{\Sigma x \Sigma y}{n}\right]^2}{\left[\Sigma x^2 - \frac{(\Sigma x)^2}{n}\right]\left[\Sigma y^2 - \frac{(\Sigma y)^2}{n}\right]} \quad \ldots (4.1)$$

which in the case of figure (4.3) is r = 0·78. This is a positive correlation indicating a trend. If the Student's t test is applied

$$t = \frac{r\sqrt{n-2}}{\sqrt{1-r^2}} \quad \ldots (4.2)$$

then t = 3·31 which indicates that the correlation is significant, the 5% level being t = 2·37 and the 1% level being t = 3·50.

Thus it seems clear that there is an underlying trend being measured by both, but it cannot be said that there is a one-to-one correspondence between the systems.

The difference between the CO index as measured by Baldwin et al. (1973a) and that reported here lies in the characteristics of the filters used. The filters used by Baldwin et al. (1973a) have λ_0 = 2·31μ and 2·2μ and half-power bandwidths of 0·095μ and 0·090μ respectively while those used in this work have λ_0 = 2·30μ and 2·23μ and half-power bandwidths of 0·092 and 0·047μ respectively. Thus the two filters used in this work are closer than those used by Baldwin et al. (1973a) and the Cont. filter used in this work has a smaller half-power bandwidth.

This difference means that the CO index measured in

this work contains a component due to the colour of the object observed ∿60% of that of the CO index given by Baldwin et al. (1973).

Figure (4.4) shows the CO index of this work plotted against I-K (Johnson et al. 1966). The line drawn in this figure is the contribution to the CO index due to the colour of the object as measured by the CO and Cont. filters. This component is estimated assuming that the central wavelength λ_0, of each of the I, K, CO and Cont. filters represent the characteristic wavelength so that neither the shape nor the bandwidth of the filters need be considered. Thus the radiation may be represented as a monochromatic flux at wavelength λ_0. Figure (4.5) shows the CO index of Baldwin et al. (1973) plotted against I-K (Johnson et al. 1966). Again, the line drawn in this figure is the contribution to the CO index due to the colour of the object.

The corrected CO indices, CO', for Baldwin et al. (1973a) and this work are shown plotted against I-K (Johnson et al. 1966) in figures (4.6) and (4.7). The corrected CO index, CO', is formed by removing the colour component from the CO index. As can be seen from figure (4.7) there seems to be a well defined region occupied by the luminosity class III stars and only the class I stars separate, the class II and V stars from Baldwin et al. (1973a) with a Johnson I-K occupying the same region as the luminosity class III stars. Note also that the stars in this strip are of types K_0 to M_6. Thus it would seem that the Baldwin et al. (1973a) CO index,

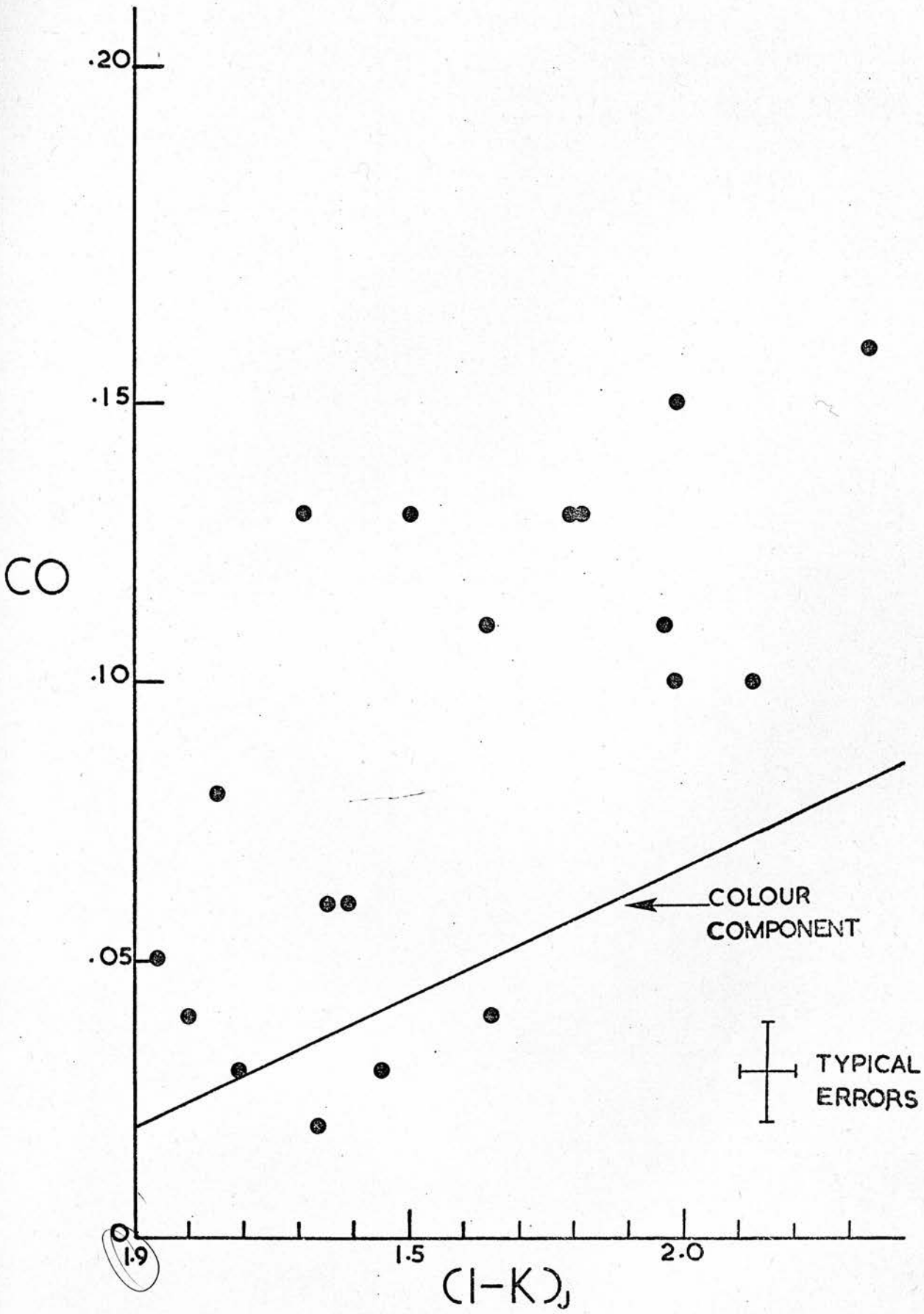

Figure(4.4)

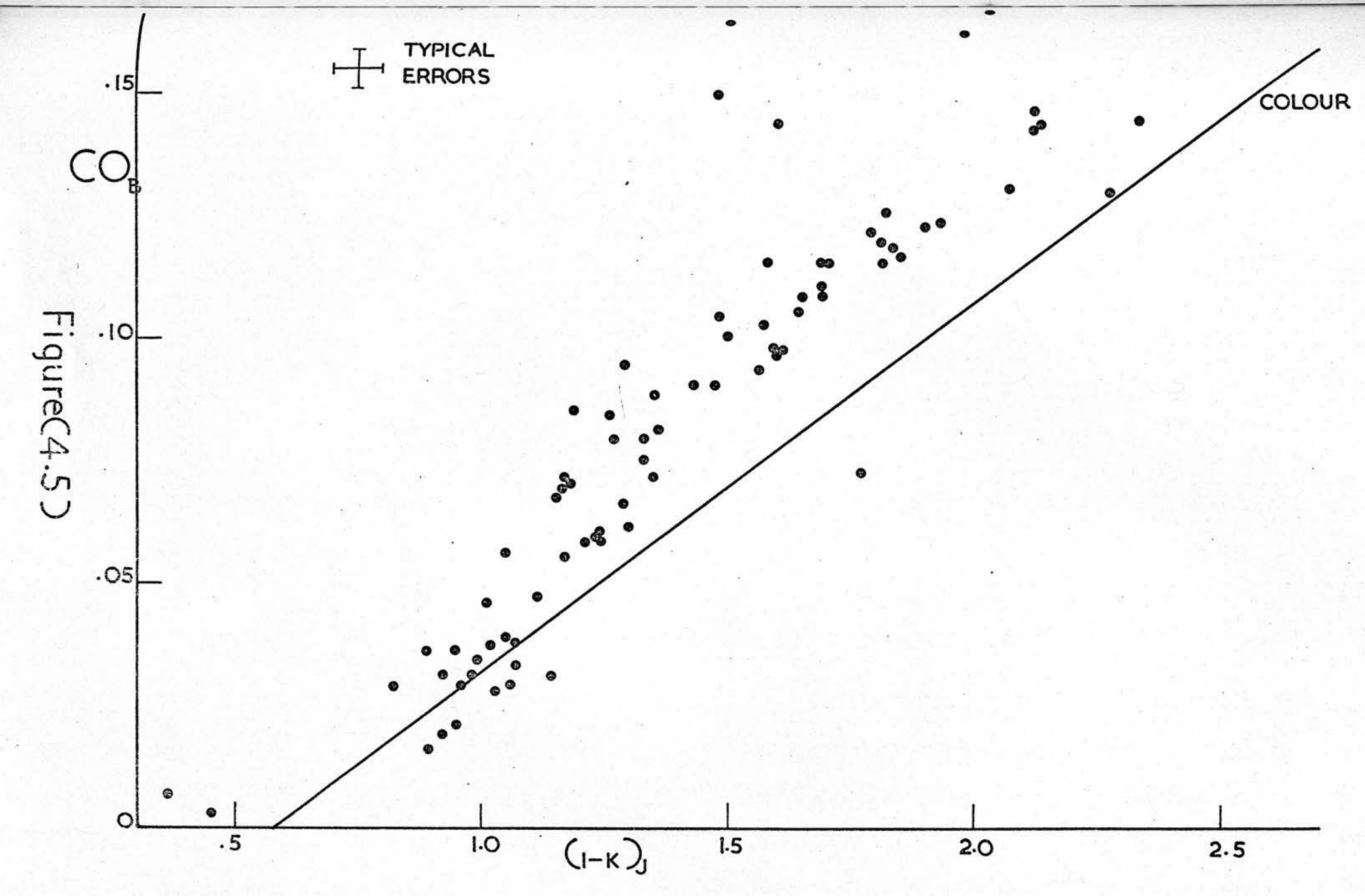

Figure(4.5)

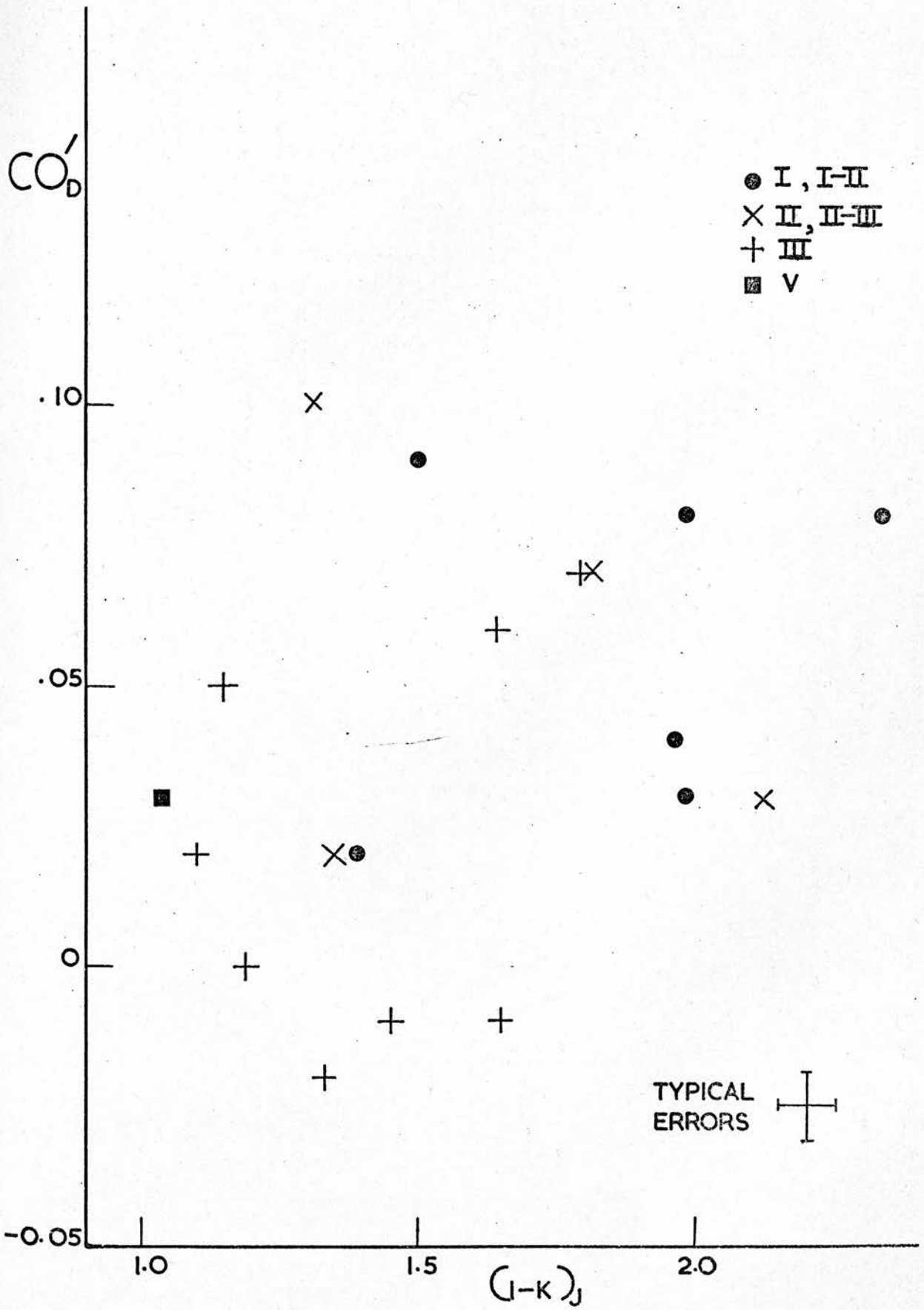

Figure(4.6)

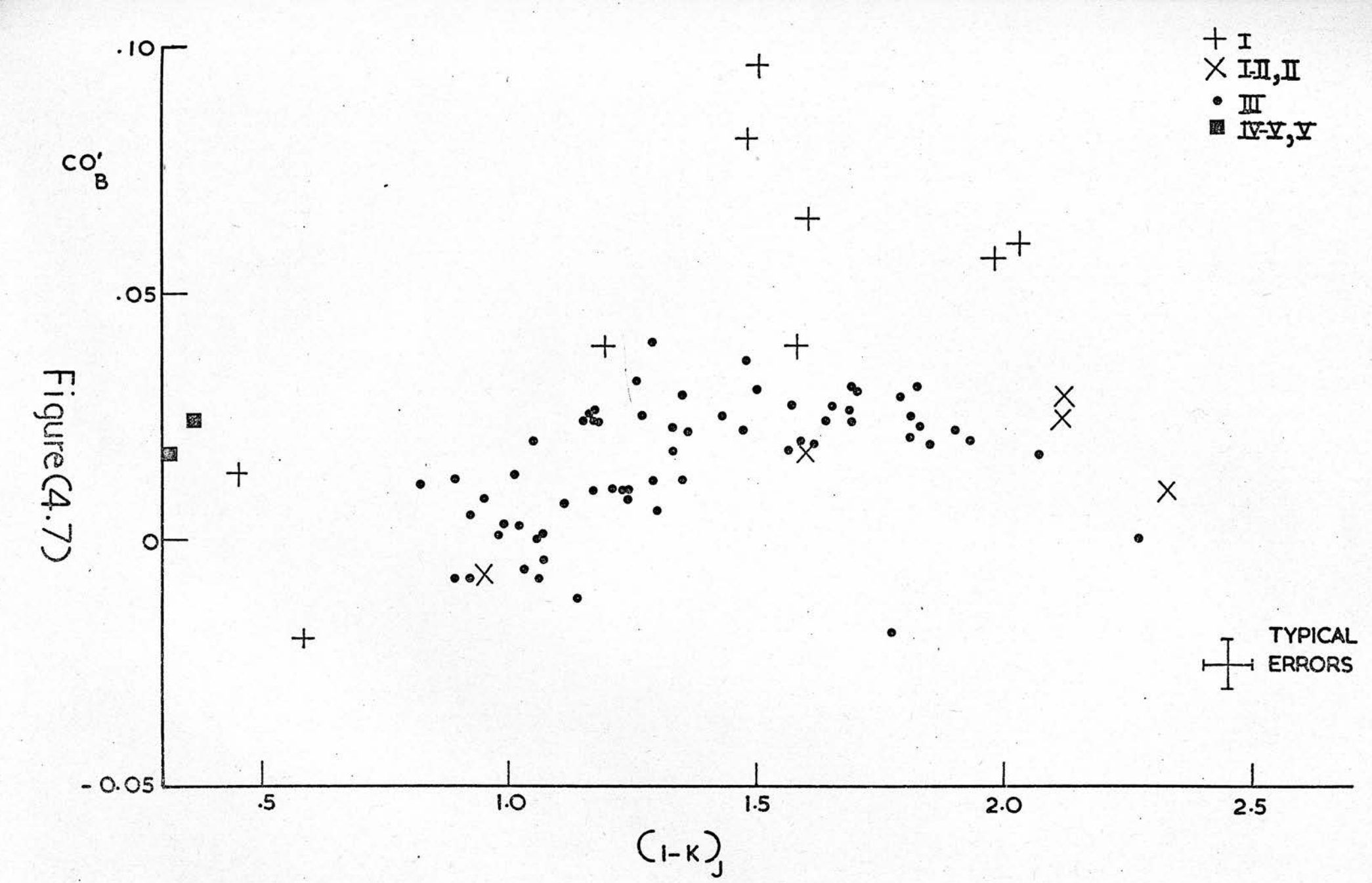

Figure(4.7)

even in the corrected from does not resolve spectral type and luminosity class except that it can be used in conjunction with colour, e.g. Johnson et al. (1966) I-K, to separate luminosity class I from all others. Further, figure (4.8) showing the corrected CO index, CO', for the Baldwin et al. (1973a) observations plotted against spectral type indicates the way in which luminosity classes II and III merge. This figure also shows that the colour corrected CO index of the Baldwin et al. (1973a) observations is not a good indicator of spectral type. Figures (4.5, 4.7 and 4.8) show that the Johnson I-K colour is as good an indicator of spectral type as the Baldwin et al. (1973) CO index. Therefore, any estimation of spectral type from these observations (Baldwin et al. 1973a, Figure 3) is highly uncertain. Figure (4.8) shows that the corrected CO index, CO', for M stars has less dispersion than that of the K stars. This, coupled with the impression that the index seems to increase from K_0 to K_5 and decrease from M_3 to M_6 for the class II and III stars, seems to suggest that the bandheads measurable with the Baldwin et al. (1973a) system are saturated by about M_2.

Figure (4.6) shows the corrected CO index, CO' of this work plotted against I-K. Here it can be seen that there is a large amount of scatter. Comparison with figure (4.7) shows no clustering of class III, all classes of luminosity being mixed. This suggests that the corrected index of this work is not so dependent on colour as that of Baldwin et al. (1973). In fact, there is a very low degree

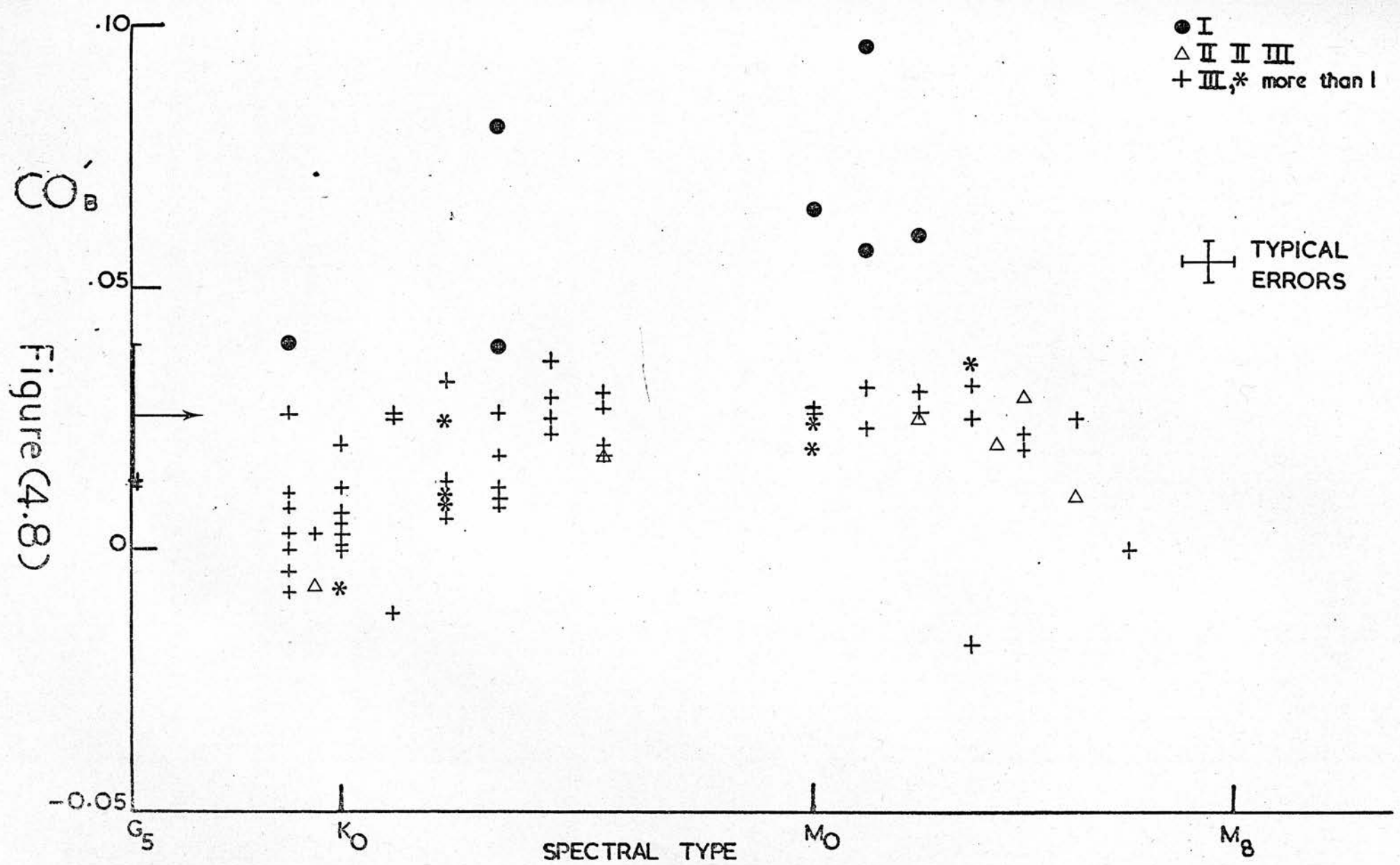
.10
.05
0
−0.05
$(C_B')_0$
● I
△ II II III
+ III, * more than I
TYPICAL ERRORS
G_5
K_0
M_0
M_8
SPECTRAL TYPE

Figure (4.8)

of correlation. Figure (4.9) shows the corrected CO index, CO' of this work plotted against spectral type. Not all of the points from figure (4.2) are used since some have no I-K colour available. It can be seen from figure (4.9) that, in general, the supergiants have a higher index than the giants and that the index increases with spectral type for a given luminosity class. What is not clear is the separation of luminosity clauses as well as spectral types. This could be due to the fact that the number of observations is too small or that the system is not capable of this.

It could be then that the form of figure (4.9) is due to observational error, the apparent separation of types being a direct result of this. Of the stars in table (4.1) four were observed on several occasions spread over two years namely α Lyr, α Boo, β And and β Peg. In every instance the individual observations were made with a signal/noise ratio of 40 or greater. α Lyr was observed 19 times, α Boo 6 times, β And 10 times and β Peg 9 times. In each case the CO index given in table (4.1), the mean of the observations, has a 1σ level of $\pm 6\%$. The rest of the objects in table (4.1) were observed only once or twice though, since they are all bright in the infrared, the instantaneous signal/noise ratio was of the same order as that of α Lyr. Thus, the typical errors given in figures (4.2), (4.6) and (4.9) are based on the 1σ level of the well observed stars. The spectral types of figures (4.2) and (4.9) have errors of about plus/minus one half of a subdivision though the members of the MK Dagger System may be even more accurate (Morgan

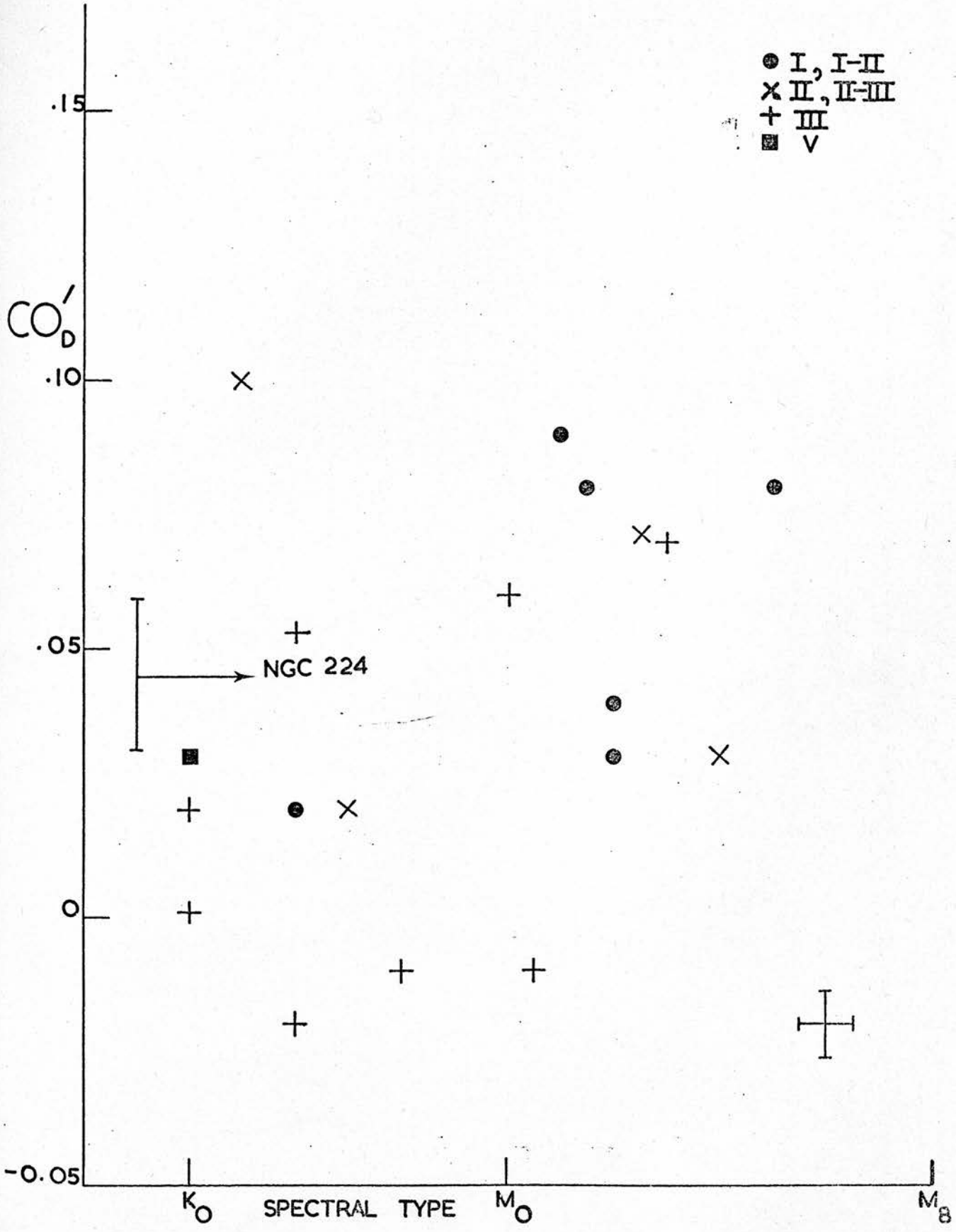
I, I-II
II, II-III
III
V
.15
.10
.05
0
-0.05
CO'_D
NGC 224
K_0
SPECTRAL TYPE
M_0
M_8

Figure(4.9)

& Keenan 1973). The typical errors shown in figure (4.9) suggest that the apparent separation is not due to observational error.

4.3 OBSERVATIONS OF NGC 224 AND THE GALACTIC CENTRE

In an attempt to estimate the stellar photospheric contribution to the 2μ radiation from the galactic centre, observations of the nucleus of the Galaxy and NGC 224 were made with the narrow band system. These observations were made with the 60 inch Flux Collector in Tenerife in October 1973 and July 1974.

The observations were made with a 22 arc sec diameter aperture and, in the case of the Galactic centre, were centred on the 2·2μ maximum - the BN point source. An attempt to make observations of the centroid of the extended 2·2μ source using the position given by Spinrad et al. (1971a) was made. Unfortunately these observations had a signal/noise ratio very much less than 3.

The observations of NGC 224 were also made with a 22 arc sec diameter aperture and were centred visually on the nucleus of the galaxy. In all, 11 observations of NGC 224 were made with the narrow band system of which all have a signal/noise ratio close to or less than 3. Taking the mean of the observations, a CO index of 0·09 is found for NGC 224. A corrected CO index, CO' can be found using the values of I-K of 1·54 (Johnson 1966) for a 35 arc sec aperture and 1·53 (Spinrad et al. 1971) for a 7 arc sec aperture and gives a value of CO' = 0·045.

The CO index of 0·09 for NGC 224 compares with the CO index of 0·098 of Baldwin et al. (1973b) and the corrected CO index, CO', of 0·045 compares with one of ·026 for Baldwin et al. (1973b). Placing these observations on figures (4.9) and (4.8) respectively puts the indices in the domain of the giants. In the case of the Baldwin et al. (1973b) corrected CO index, CO', and the I-K colour, the observation would seem to be certainly not equivalent to a supergiant being in the strip defined by the class II and III stars.

The CO index and the corrected index, CO', of this work again place the observation in the domain of the giants and, from figure (4.9), suggest a range of spectral types from K_4 to about M_3. The corrected CO index of Baldwin et al. (1973b) placed in figure (4.8) suggests a much wider spectral range of K_1 to M_5.

It would seem that neither work can predict an accurate estimate of luminosity class. What is certain is that it is not luminosity class I.

The indices of this work suggest that the stellar population of the central 22 arc sec of NGC 224 contains a higher concentration of late-type giants precluding a dwarf-enriched lower main sequence (Spinrad & Taylor 1971) and would presumably require a much lower mass-to-luminosity ratio. It is suggested here that the photospheric contribution to the 2μ radiation from the nucleus of NGC 224 comes from stars of integrated spectral type in the range K_4 to M_3 and luminosity class II or III.

The observations of the galactic centre were such that no such estimate could be made. Only one observation made on July 1974, has a signal/noise ratio near 3. This gives a CO index of 0·189. This is in error by 33% or more. In fact this observation has a signal/noise ratio of 2·3 and so the error is of the order of 43%. This observation was centred on the 2·2μ maximum, taken with a 22 arc sec aperture and a 52 arc sec chop in declination. Two observations were made of this region while two were made centred on the position given by Spinrad et al. (1971a). The latter observations had a signal/noise ratio of about one and are not used here.

This raises an interesting question. Why does an object with a K magnitude of 4·83 not give a signal when one with a magnitude of 6·55 does? This could be due to the fact that, even at the latitude of Tenerife, the galactic centre does not rise much above the horizon. The observations being taken with a secz of between 1·7 and 1·9 while those of NGC 224 were taken with a secz of between 1·0 and 1·2. Thus observations of the galactic centre were taken with the object at highest, 36^{o} above the horizon while observations of NGC 224 were taken with the object all but overhead.

The faintest stellar object observed with the narrow band filter system was RW Cep, K magnitude 2·45. The observation had a signal/noise ratio in excess of 20 though the gain setting was only 20dB less than that for the galactic centre. It seems clear that the system is capable

of observing a faint source so that the one detection of the galactic centre at such a low level of certainty must indicate that the observations are of poor quality due to the large zenith distance or that there is no flux to be detected. That there is no flux must be ruled out since observations in the infrared tend to rule out line emission in the 2μ region.

4.4 CONCLUSIONS

The narrow-band observations of stars were used to set up a system of colour corrected CO indices in an attempt to classify the infrared radiation from the nucleus of our own galaxy and the nucleus of NGC 224 with an integrated spectral type. No serious attempt was made to set up a system of spectral classification in any way similar to those in existance for late-type stars. The behaviour of the first overtone bandhead at 2·293μ was investigated as a function of spectral type in late-type stars. What has become obvious is that the super giants have the highest CO indices most probably due to the fact that the high turbulent velocities decrease saturation. Indeed, stars with highly active chromospheres tend to have high CO indices, not just supergiants.

The CO index of Baldwin et al. (1973a) was found to be highly colour dependent in comparison to the CO index of this work. Thus the predictions of Baldwin et al. (1973b) and, to some extent of Frogel et al. (1975) are called into question. The final conclusion made here on the observations

of NGC 224 compares well with the work of O'Connell (1974) and Frogel et al. (1975) indicating a significant contribution from giants cooler than K_4. It seems that the conclusions of Spinrad & Taylor (1971) based on narrow band scanner observations from 0·33μ to 1·07μ that no giants cooler than K_5 are significant contributers in NGC 224 and that a strongly enhanced lower main sequence is present should now be reviewed in the light of these observations.

The consequences of this issue, particularly their extension to elliptical and giant elliptical galaxies, are of importance since evolutionary effects on the luminosities of distant galaxies are determined by the ratio of contributions of giant to dwarf stars (Tinsley 1973). Because of the brighter galactic luminosities in the past the cosmological deceleration parameter, q_0, must be corrected downward by an amount that depends directly on the initial mass function (Rose & Tinsey 1974). Tinsley (1973) has shown that the correction to q_0 is in the first approximation, proportional to the relative contribution of giants to infrared light. She also suggests that, if gE galaxies have strong CO bands, as strong as the nucleus of an Sb galaxy, NGC 224 say, the rate of evolution is very great. This argument does not say that the nuclei of spiral galaxies have the same stellar content as whole elliptical galaxies but should be a proviso to many claims that the population of spiral nuclei based on dwarf rich models are consistent with non-evolved ellipticals.

The observations of the CO indices by Baldwin et al.

(1973b) and Frogel et al. (1975) of elliptical galaxies and the scanner observations by O'Connell (1974) of luminosity sensitive TiO bands suggest giant dominance. However, the CO indices of Frogel et al. (1975) may not be the observations required by Tinsey (1973) as the apertures used were on the small side. However if the CO indices remain constant with increasing aperture then a significant negative connection to q_0 is implied. A result not yet verified.

The non observation of the galactic centre was most probably due to the observing conditions at the time and the extended nature of the source. Any infrared photometer involving chopping techniques as this one does, will detect flux gradients. The extended nature of the galactic centre, its half width and zenith distance at the time of observation conspired to produce the null result. It is suggested here that, given better observing conditions, a CO index for the galactic centre would fall in line with those of NGC 224 and other spiral galaxies. The consequences of which are discussed later.

CHAPTER V

BROAD BAND OBSERVATIONS

5.1 INTRODUCTION

Astronomical measurements in the infrared have received increased emphasis during recent years. To a great extent this increase is due to the advance of the infrared detector and the development of the required photometric techniques. What the photometrist is interested in is the brightness of an object as a function of certain parameters, wavelength, time and so on. In infrared photometry, where the ratio of the half power band width to the effective wavelength lies between 10% and 20%, the reduction of the data consists primarily of an adjustment for atmospheric extinction and a transformation to a suitable system of magnitudes. In addition to the brightness of different objects at a given wavelength, the ratios of the fluxes at two different wavelengths are often compared. These ratios, called the colours, are usually expressed as the differences of the magnitudes in the two photometric bands. Thus, the principal parameters in any consideration of the objects are fluxes and colours.

The photometer measures the difference in the energies received from two circular regions of sky 22 arc sec in diameter with centres separated in declination by the same amount. This simulates a photometer having two focal plane apertures. The output of the photometer is proportional to the difference between the energies in the quasi-apertures. These energy differences are then related to the magnitude scales and fluxes are assigned.

A system of standard stars was set up based on α Lyr

in order to interpret the photometric results physically. Basically the zero points of the magnitude scale used (Johnson 1965) are such that for an average A_0V star all magnitudes are the same. From the standard system, magnitudes are assigned to the observed stars some of which are used as comparison stars for the galaxies observed.

The galaxies observed are discussed in terms of their colours and, for the case of NGC 224 and the galactic centre, in conjunction with their CO indices.

5.2 ZERO POINTS AND CALIBRATION

Physical meaning, interpretation in physical terms and astronomical cogency can be attributed only if the data is related to a system of physical units. This can only happen if a set of bright stars are selected as standard and are used in conjunction with zero points. These stars should be bright, accessible and, if possible, non-variable. Thus they will most probably be K or M giants.

Because of the problem of relating the flux and magnitudes of other workers, the zero points and standards are here related in detail.

The photometry of Johnson & Morgan (1953) and Johnson (1962 and 1965b) used the set of A_0V stars to define a group whose average member's colours were zero. This photometry and later work by Johnson et al. (1966) revealed that individual stars of type A_0V have departures of up to 0·07 mag from the mean zero. So, to this extent, they do

not form a well defined group. Here the problem is approached in a slightly different way. It was the aim of this work to use to the largest possible extent, the system of Johnson et al. (1966). To this end the detectors, filters and photometric techniques were a close copy of Johnson et al's (1966). However, a single star, α Lyr, is utilized here in place of the group and it is assumed that α Lyr is well represented at all wavelengths by the model of Schild et al. (1971). The star, α Lyr is then assumed to have H, K and L magnitudes of 0·02, 0·02 and -0·02 respectively.

In order to establish the magnitude scale in the H band it was necessary to interpolate between the J and K fluxes of the standard star. The J and K fluxes are taken from Johnson et al. (1966) and the linear interpolation function used is given by

$$f\lambda = f\lambda_0 + \frac{\lambda-\lambda_0}{\lambda_1-\lambda_0} (f\lambda_1 - f\lambda_0) \qquad \ldots (5.1)$$

where λ_0 and λ_1 are the logs of the effective wavelengths of the J and K bands respectively, $f\lambda_0$ and $f\lambda_1$ the logs of the fluxes of α Lyr in J and K using the magnitudes and zero points of Johnson et al. (1966), and λ is given by $\lambda_0<\lambda<\lambda_1$. Then for the star α Lyr, a magnitude can be assigned. The zero point for the H filter can be assigned in the same way using the zero points for the J and K bands.

The assumption being made here is that for a star of this effective temperature, Te = 9650^{o}K (Schild et al. 1971), observations in the J K and L bands are far enough away from

λ_m defined by Te and the Wien displacement law so that the Rayleigh-Jeams formula may be applied. Thus a log log plot of flux against frequency gives a straight line with a slope of +2 and linear interpolation, equation (5.1), can be used.

This then sets the magnitude for the standard star α Lyr in the H band, and the zero point. They are 0·02 mag and 1069 f.u. respectively. The magnitudes of α Lyr of Johnson et al. (1966) are accepted as standards in the K and L bands. Table 5.1 summarizes the zero points of the magnitude scale used in this work.

These zero points compare well with those of Low & Rieke (1974) and Thomas et al. (1973). There being about a 2% difference between the sets. Another method of obtaining H magnitudes is given by Glass (1974) although the set of 20 or so stars for which the formula

$$H = 0{\cdot}19J + 0{\cdot}81K \qquad \ldots (5.2)$$

holds are not given. One can only assume that this formula holds for early type stars. Certainly, if the values for α Lyr are inserted 0·02 for both J and K the value for H is as assigned here. However, for later stars α Boo or α Ori say the formula does not hold. The formula predicts H magnitudes of -2·90 for α Boo and -4·05 for α Ori which are 0·1 and 0·05 magnitudes in error compared to the values given by Thomas et al. (1973) and this work.

The H K and L photometric bands lie in regions of maximum atmospheric transmission. Nonetheless, all contain wavelengths where there is atmospheric absorption particularly the L band. Observations at different zenith distances are

TABLE 5.1 - ZERO POINTS

λ_0 (μ)	1·65	2·2	3·5
Flux (f.u.)	1069	630	310

TABLE 5.2 - STANDARD & COMPARISON STARS

BS	NAME	TYPE	H	K	L	No. Obs.
337	β And	M_0IIIa	-1·43	-1·80		11
911	α Cet	$M_{1.5}$III	-1·64	-1·68		1
1457	α Tau	K_5III	-2·89	-2·87	-3·08	1
2061	α Ori	M_{1-2}Ia-Iab	-3·81	-4·00	-4·30	2
3748	α Hya	K_3II-III	-1·51	-1·31	-1·39	4
5056	α Vir	B_1V	1·57	1·68	1·67	1
5340	α Boo	K_2IIIp	-3·09	-2·99	-3·14	10
6746	γ Sgr	K_0III	0·67	0·65	0·49	9
7001	α Lyr	A_0V	0·02	0·02	-0·02	25
8775	β Peg	$M_{2.5}$II-III	-1·96	-2·09	-2·31	9

made through atmospheric paths of different lengths and are thus subject to differing atmospheric absorption. As a result it is necessary to correct the observations for atmospheric extinction. Clearly, a measurement of extinction is essential where the observations are made in a region where it is high, particularly M or Q. In regions where the extinction is low such as H, K, and L average values can be used if a direct measurement is not available. Low & Rieke (1974) have shown that the dependence of λ_0 on extinction in the H, K and L bands is very small. The change in λ_0 at high extinction being less than 1%.

The observations described in this chapter were made with the 60 inch Flux Collector in Tenerife. No thorough attempt was made to study the properties of the atmosphere above the telescope in this work. The extinction in K was measured but no estimate is made here. In the reduction of the data, average values from Low & Rieke (1974) are used. They are 0·13, 0·15 and 0·23 mag/air mass respectively for the H, K and L bands.

5.3 DATA REDUCTION

The first step in making an observation in the infrared after the photometer has been aligned, the signal maximized and the telescope focussed (Appendix 1) is to check the performance of the detector. This is done in order that a record of performance may be kept, changes in the performance noted and any necessary adjustments made.

It was normally assumed here that the system was performing well if when the cooled detector was tested with a Brookdeal LNA an output of less than 0·2V on a gain setting of 80dB was obtained. Next, a standard star was measured, usually a star from table (5.2). The observing conditions were noted and compared with previous records. Then the sky close to the star was measured. This set of measurements determine the modulator noise, the sky noise and the system noise.

If these steps reveal no serious errors then photometric observations can begin. As has been shown in Chapter 2, the modulation of the beam produces two images of the object 180^{o} out of phase. Therefore, the phase detected signal from one of these images will be positive if the signal is very large compared to the contribution from the telescope and the sky, while the phase detected signal of the other image will be negative under these conditions. The desired signal is obtained by subtracting one from the other. Thus each data point comes from a pair or several pairs of observations designated Left and Right. Observations are carried out by centering one image and integrating the deflection for a set period of time (usually 40 sec), then centering the other image and integrating. During the integration the tracing made from the deflection can be used as a check.

At this stage sources of noise can be spotted. Figure (5.1) shows the typical tracing from a good observation of a star and can be compared with figure (5.2) which is a

Figure(5.1)

Figure(5.2)

tracing from a noisy signal. These tracings reflect only differences in instantaneous signal/noise ratio. Again these can be compared with figures (5.3) and (5.4) typical tracings of a galaxy and the galactic centre. These are all acceptable tracings in their own right and do not show any distortions due to drift, wind shake or offset. Examples of each of these are given in figures (5.5), (5.6) and (5.7).

The raw data, the numbers resulting from the integrations, are treated in the following way: let the results of the subtractions be a set of readings Ni(i=1,---n) for an object. Averages are formed in the usual way

$$\langle N \rangle = \frac{1}{n} \sum_{i=1}^{n} N_i \qquad \ldots (5.3)$$

and mean square deviations

$$\langle \Delta N^2 \rangle = \frac{1}{n} \sum_{i=1}^{n} (N_i - \langle N \rangle)^2 \qquad \ldots (5.4)$$

Then, as $n \to \infty$ these averages tend towards a finite limit so from these averages, an estimate of the probability that N_i departs from $\langle N \rangle$ by more than $\langle \Delta N^2 \rangle^{\frac{1}{2}}$ can be made.

It is generally assumed that fluctuating quantities are normally distributed about their mean value based on theoretical arguments of the central limits theorem. In any case, it is exceedingly unlikely that any single observation will depart from $\langle N \rangle$ by more than a few times $\langle \Delta N^2 \rangle^{\frac{1}{2}}$. Therefore an rms criterian of probable error is adopted and any N_i is said to give $\langle N \rangle \pm \langle \Delta N^2 \rangle^{\frac{1}{2}}$. If there

Figure(5.3)

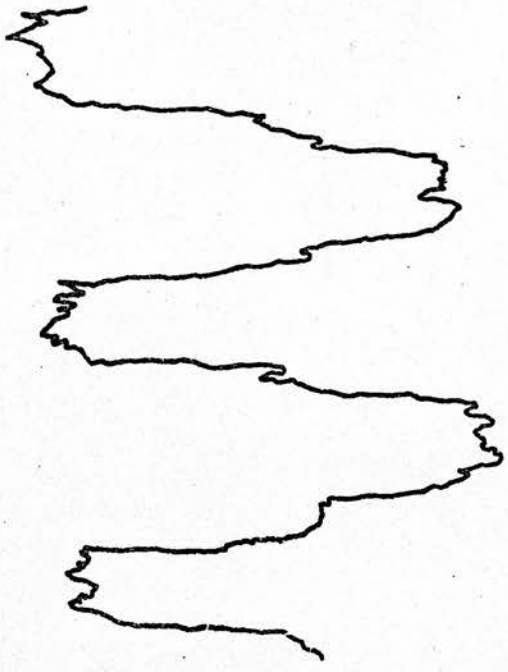

Figure(5.4)

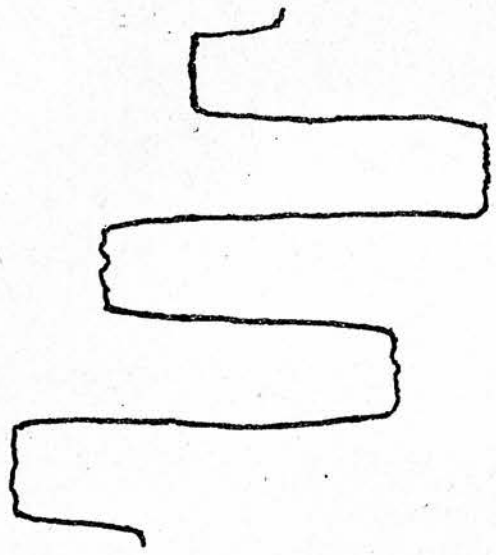

Figure (5.5)

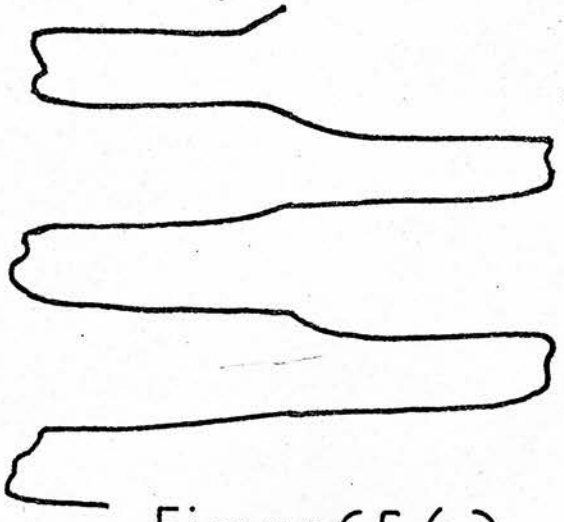

Figure (5.6)

Figure (5.7)

are m observations, the sum of the squares of the errors increases as m while the square of the sum of the readings increases as m^2. This the fractional error over m readings decreases and,

$$\langle N \rangle_m = \langle N \rangle \pm \left\langle \frac{\Delta^{N_2}}{m} \right\rangle^{\frac{1}{2}} \qquad \ldots (5.5)$$

Thus a set of 11 observations, 5 pairs, gives an average <N> say and an rms deviation such that the probability that all the N_i lie within three times the rms deviation is 0·99. This is normally the case when observing a star and, is the assumed case all through, namely that the sources emit a constant flux. Then, from the 5 pairs, a mean and standard error of the mean are assumed.

This data is now converted to a flux in the following way. Let the flux from α Lyr at some wavelength λ be given by $F_\lambda{}^{\alpha Lyr}$ and

$$F_\lambda{}^{\alpha Lyr} = S F_\lambda{}^{\alpha Lyr} \qquad \ldots (5.6)$$

where $F_\lambda{}^{\alpha Lyr}$ is the result of the observation and S is a function of zenith distance and the detector/telescope system. Then for any star, *, a relationship of the form of (5.6) can be used assuming that $F_\lambda{}^{\alpha Lyr}$ is known, which it is. Thus

$$F_\lambda{}^* = F_\lambda{}^{\alpha Lyr} \frac{S F_\lambda{}^*}{S F_\lambda{}^{\alpha Lyr}} \qquad \ldots (5.7)$$

assigns a flux at wavelength λ to the observation F_λ*. Then, a set of n observations give an average flux F_λ*(mag) given by

$$F_\lambda^*(\text{mag}) = \frac{1}{n} F_\lambda^{\alpha\text{Lyr}} \sum_n SF_\lambda^*/SF_\lambda^{\alpha\text{Lyr}} \quad \ldots (5.8)$$

F_λ*(mag) is the flux used to assign a magnitude. This method was used to set up the system of standard stars Table (5.2). A flux can then be assigned to any object provided that F_λ^{obj} is known to a sufficient accuracy and a standard or comparison star has been observed immediately before and after. It was the practice to observe a standard as part of the instrument checks, then find the faint object and finally observe a comparison star.

The calculation of fluxes was performed on the ICL 4130 computer at the Royal Observatory, Edinburgh. The flow diagram for the programme is given in figure (5.8). Note that each observation is marked as a standard, a comparison star or a galaxy. The programme is terminated by a marker. The programme calculates the air mass number for each object and, in conjunction with presumed extinction coefficients, calculates the flux received for each filter.

The internal consistency of the observation is mirrored by the mean and the standard error of the mean. This is normally very high, but as in any photometric system this is not paramount. Repeatability is the important factor. All of the standard stars in table (5.2) were measured on more than one occasion. Some were measured many times. In one observing trip where a set of stars

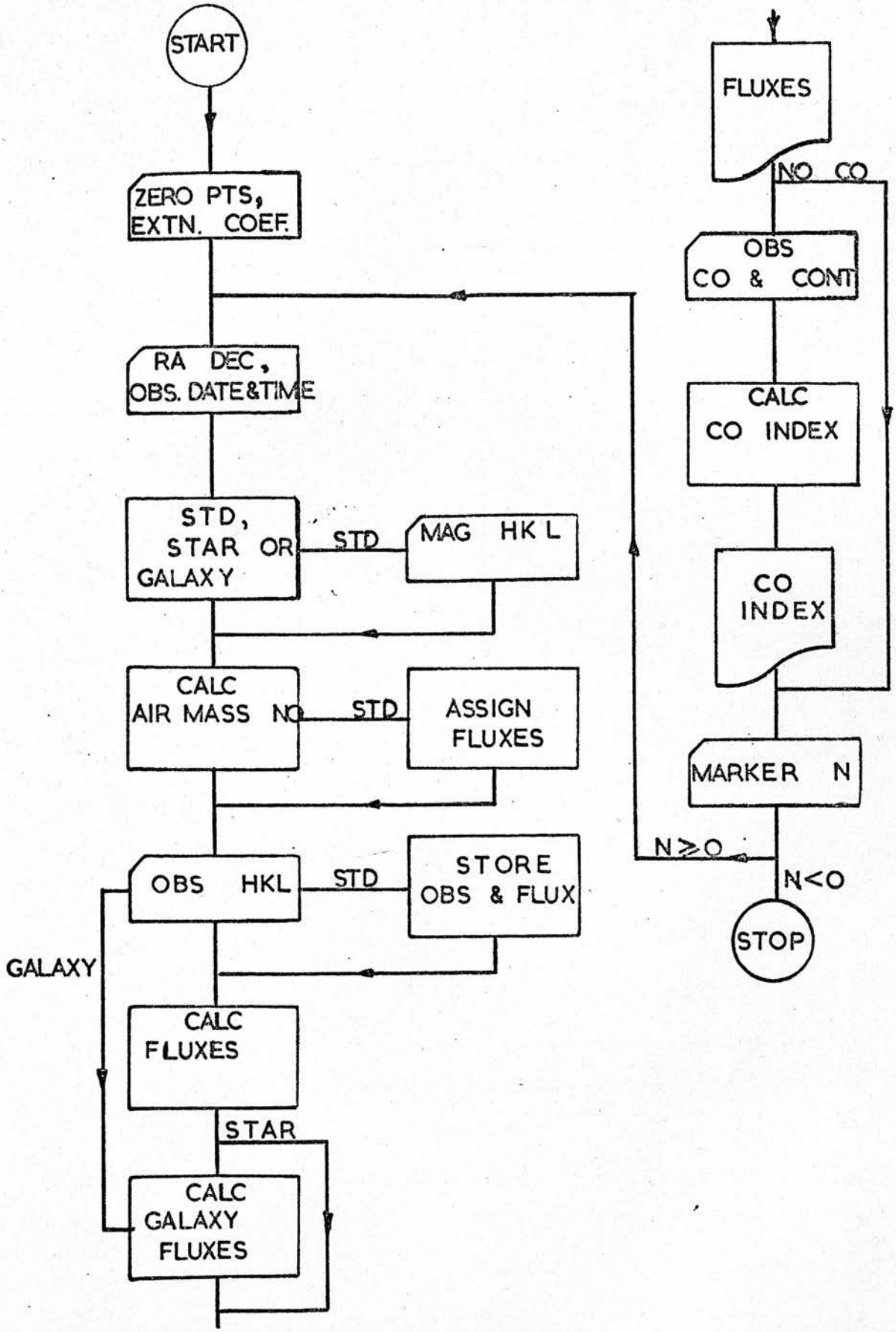
START
ZERO PTS, EXTN. COEF.
RA DEC, OBS. DATE&TIME
STD, STAR OR GALAXY
STD
MAG HK L
CALC AIR MASS NO
STD
ASSIGN FLUXES
OBS HKL
STD
STORE OBS & FLUX
GALAXY
CALC FLUXES
STAR
CALC GALAXY FLUXES
FLUXES
NO CO
OBS CO & CONT
CALC CO INDEX
CO INDEX
MARKER N
N≥O
N<O
STOP

Figure (5.8)

were observed, e.g. July 1974 when γ Sgr was used as the comparison star for the galactic centre and was observed on nine different nights the typical errors were ± 0·08 mag. In general, when comparing magnitudes from night to night and indeed from observing trip to observing trip, the errors are of this magnitude in all of H K and L - just less than 0·1 magnitudes.

5.4 H, K AND L MAGNITUDES

Table (5.3) lists the magnitudes of the stars observed. The column headings are self explanatory. Observations of β Per are given elsewhere (Smyth et al. 1975). It is of interest to compare the magnitudes listed here with those of Johnson et al. (1966). This is given as a function of V-K in figure (5.9). From this figure it can be seen that there is a certain amount of scatter distributed about zero magnitude difference.

Though the magnitudes may not correspond exactly to those of Johnson et al. (1966) the majority lie within ± 0·1 magnitudes the typical errors of this work.

Table (5.4) lists the galaxies observed, their magnitudes and types (de Vaucouleurs & de Vaucouleurs 1964). The column headings are self explanatory. The galaxies were chosen from de Vaucouleurs & de Vaucouleurs (1964) and Sérsic (1973). Most were chosen because they possessed bright nuclei. All but one of the galaxies are spiral.

The observations were made with the photometer

TABLE 5.3 - STARS

BS	NAME	H	K	L
617	α Ari	-0·54	-0·53	-0·53
936	β Per	2·11	2·21	3·30
941	K Per	1·76	1·76	1·97
1708	α Aur	-1·61	-1·60	-1·51
2216	η Gem		-1·42	
2286	μ Gem		-1·96	
2491	α CMa		-1·31	
2990	β Gem		-1·35	
3773	λ Leo	1·20	0·62	0·47
4057	γ^1Leo	-0·47	-0·70	-0·93
5984	β^1Sco	2·85	2·93	3·06
5997	ω^2Sco		2·39	
6056	δ Oph		-1·20	
6134	α Sco	-3·71	-3·79	-4·28
6406	α Her	-3·09	-3·37	-3·85
6418	π Her		-0·07	
6526	λ Her		1·11	
6603	β Oph		0·22	
6695	Θ Her		1·07	
6752	70 Oph		1·99	
7009	XY Lyr	-0·24	-0·30	-0·56
7139	δ^2Lyr	-1·13	-1·47	-1·81
8162	α Cep	1·68	1·96	1·85
8308	ε Peg	-0·72	-0·84	-1·11
8316	μ Cep	-1·39	-1·63	-2·20
8383	VV Cep	0·45	0·24	-0·10
8465	ζ Cep		0·20	
8572	5 Lac		0·16	
	HD 183143		3·10	
	RW Cep	2·20	2·45	1·71
	RW Cyg	1·01	0·74	0·08
	R Leo		-3·20	

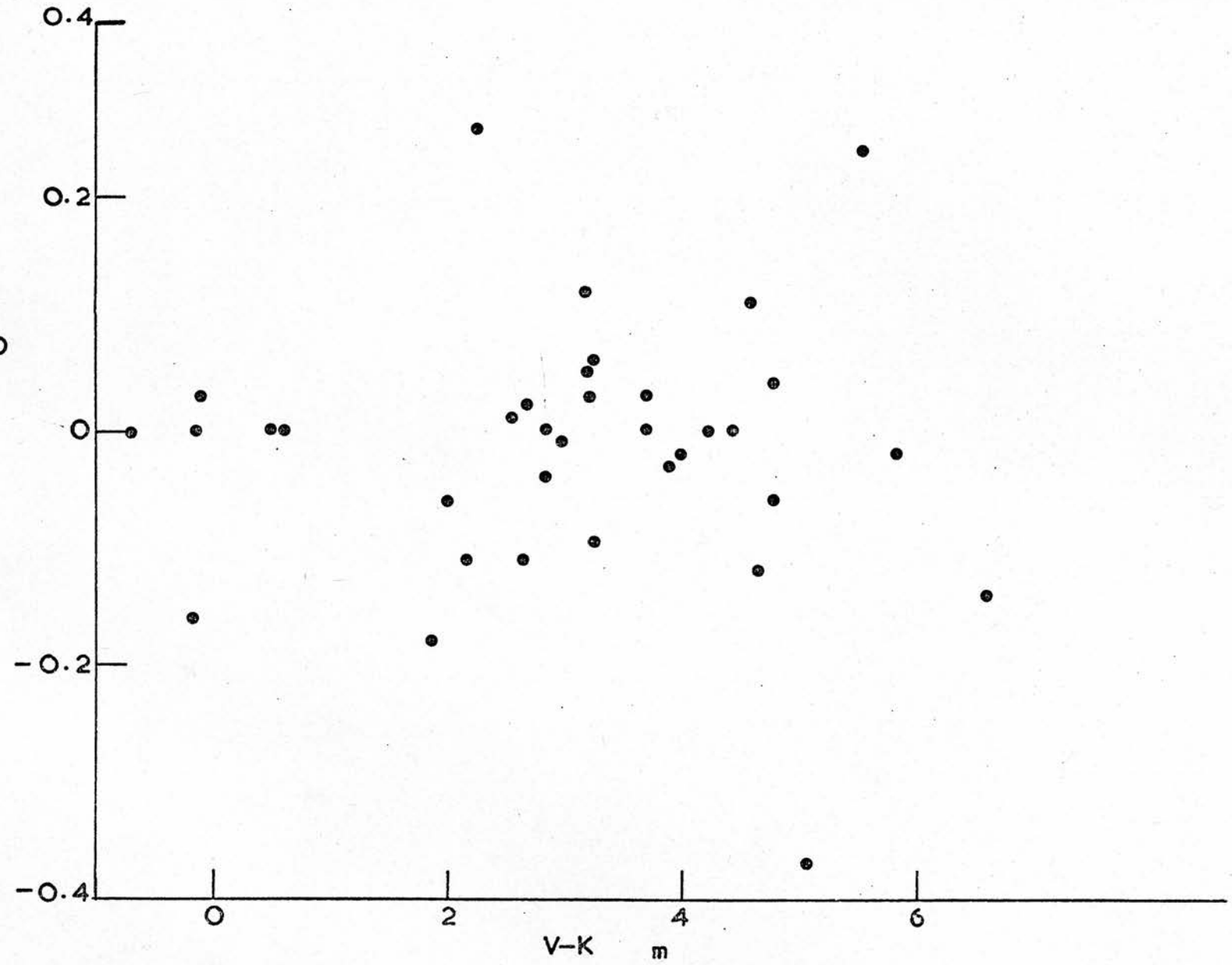

Figure(5.9)

TABLE 5.4 - GALAXIES

DATE	NGC	TYPE	H	K	L	APER-TURE
July 1974	205	E^+5p	>6·76	>6·54	>4·84	22
			>7·89	>7·43	>3·34	22
Oct. 1973	224	SA(s)b	7·18	6·53		22
			7·87	>5·86		22
			>6·62	>5·76		22
			>6·96	>6·61		22
			>7·11	7·61		22
			7·33	6·87		22
			8·39	6·59		22
July 1974			7·06	7·10	5·05	22
			7·29	7·15	>4·68	22
			>6·00	>6·56	>3·64	22
			6·99	>5·83	>2·51	22
Oct. 1973	1068	(R)SA(rs)b	7·49	7·35		22
Mar. 1974	2903	SAB(rs)bc	6·42	5·99	4·54	22
Mar. 1973	3227	SAB(s)aP		>4·10		22
Mar. 1974			>5·13	6·66	4·71	22
Mar. 1974	4594	SA(s)asp	8·20	7·01		22
			8·07	7·50		22
July 1974	6951	SAB(rs)bc	9·25	>7·87	>6·40	22

attached to the 60 inch Flux collector in Tenerife. The telescope was used with a focal ratio of f/12·8 giving a scale of 10·6 arc sec/mm.. A 2mm diameter focal plane aperture was used. The separation of the two quasi-apertures, except where intimated, was 22 arc sec in declination. Where the objects observed were extended on this scale, no correction for the flux in the 'sky' beam is allowed for in the data reduction. Since it is assumed to be small and, as yet, no satisfactory method for its compensation exists.

The infrared magnitudes given in table (5.4) were obtained by comparison with the standard and comparison stars of table (5.2). Systematic errors are expected to be relatively small. No correction for reddening has been included in the data reduction as it too is expected to be relatively small.

Table (5.5) gives the colours of the objects where it can be seen that H-K and K-L colours tend to be rather high. This is in agreement with the observations of Seyferts by Rieke & Low (1972a), Pacholczyk & Weymann 1968 and peculiar nuclei galaxies by Glass (1973b). It seems now well established that Seyfert galaxies have large K-L colours. The reason for the Sérsic (1973) peculiar nuclei galaxies having large K-L colours is not quite so evident. However there is evidence of dust or dust lanes in the nuclei of some of these and the infrared excess in L could be indicative of thermal radiation and an associated 10μ excess.

TABLE 5.5 - THE COLOURS

NGC	H-K	K-L
224	0·65	
	0·46	
	1·80	
	-0·04	2·05
	0·14	<2·47
	<1·16	
1068	0·14	
2903	0·43	1·45
3227		1·95
4594	1·19	
	0·57	
6951	<1·38	

TABLE 5.6 - GALACTIC CENTRE

Date	Position	H	K	L	Aperture
July 1974	1	>8·23	>7·11	>4·23	22
	1	>8·58	>7·19	>3·34	22
	1*	>7·18	>5·61	>3·60	22
	1*	>7·23	>6·17		22
	1*	>7·41	>7·30		22
	2*	7·04	4·83	2·33	22
	2*	>7·08	6·20		22

1 Spinrad et al. (1971a)
2 BN point source
* 52 arc sec chop.

All of the objects except NGC 205,2903 and 6951 have been observed before and appear in Appendix 2. NGC 2903 is included in a set of scanner observations of luminosity sensitive TiO bands between 0·8μ and 0·9μ by O'Connell (1974) in which he comments, 'NGC 2903 has both ultraviolet and 0·7μ to 1·1μ excess relative to normal Sc's'. There is also a report of an unresolved radio source in the nucleus (van der Kruit 1973). Rieke & Low (1972a) assign a 10μ flux of 0·22 ± 0·04 f.u. and a 21μ flux of 0·2 ± 0·1 f.u. to NGC 2903 and designate it a 'lower-luminosity' galaxy. Care must be taken in interpreting the individual colours of galaxies as they are often derived from highly uncertain observations, but the H-K and K-L colours of NGC 2903 are typical of this type of galaxy being higher than the mean values of spirals of Johnson (1966) and of the same order as those of the Seyfert type of galaxy.

NGC 205 is a peculiar elliptical companion of NGC 224. It has two conspicuous absorption patches due to dust near its centre. Its proximity to NGC 224 is such that tidal distortions are caused in its outer parts which could be the cause of the peculiarity. The upper limits of table (5.4) show that this galaxy is fainter than NGC 224 at all wavelengths.

NGC 6951 has the same morphological type as NGC 2903 and appears to be very much fainter, by about two magnitudes in each wavelength. The magnitudes of table (5.4) again suggest large H-K and K-L colours. The H-K colour would be < 1·38 again typical of the high value found for spiral

galaxies.

The two Seyfert galaxies observed NGC 1068 and NGC 3227 are well observed objects. Indeed, NGC 1068 is one of the best observed galaxies in the infrared. The observations given here compare well with those previously made (Appendix 2). The H-K colour given in table (5.5) is small compared with the others. The H-K colours of NGC 1068 and NGC 3227 show no marked peculiarities although the value of 1·95 for K-L for NGC 3227 is rather higher than the Rieke & Low (1972a) mean of 1·5 for Seyferts. These two galaxies are typical of Seyferts with infrared excess.

NGC 4594 is a remarkable object with a strong dark lane across the centre and a large nuclear bulge. It is the most luminous galaxy in the Virgo cluster. An observation of NGC 4594 is reported by Kleinmann & Low (1970b) but they also designate this galaxy as M101. M101 is, in fact, NGC 5457. Therefore the observation reported by Kleinmann & Low (1970b) as the first of its kind of that galaxy may be spurious. However, the observations reported here are of NGC 4594 and may very well be the first of this galaxy. The H-K colours are again typical of other galaxies. No observations at 3·5μ are available. The 10μ observation of Rieke & Low (1970b) is surprising if it is of NGC 4594 since the dust lane, clearly visible in any photograph, would tend to introduce a long wavelength infrared excess.

NGC 224 is a well observed galaxy. The observations

given in table (5.4) can be combined with the CO indices of Chapter 5 for a detailed study of the central 22 arc sec of this galaxy. It is assumed that the distance of NGC 224 is 708 kpc (Sandage et al. 1969) so that, for a 22 arc sec diameter region centred on the nucleus, an absolute K magnitude Mk can be estimated. Using a K magnitude of 6·98 the mean of the observations in table (5.4) Mk = -17·27 if no correction for absorption is included. The CO indices of NGC 224 indicate an integrated stellar population in the range K_5 to M_3III. A typical star in this range has Mv = -0·4 and V-K = 4·01 (Johnson 1966b). These values give for a typical star at the distance of NGC 224 Mv = 23·85, K = 19.84 and Mk = -4·41. Thus, this requires $1·39\times10^5$ typical stars which give a luminosity of $5·14\times10^7 L_\odot$ for the region and gives a stellar density of $2·41\times10^{-1}pc^{-3}$. The colours of the central region of NGC 224 are H-K = 0·14 and K-L = 0·28 (Sandage et al. 1969) while those of table (5.5) seem to be larger especially in K-L. If the large K-L colour is real then it would be necessary to include a very red object like NML Cyg or a non-thermal source in the nucleus. Since the intensity distribution across the central regions of this galaxy are very similar in the visible and the infrared (Sandage et al. 1969) the non-thermal excess seems to be ruled out.

The estimates of the number density of stars made here are reasonable enough to take the inclusion of a few O stars in the nucleus. These stars could well be embedded in dust which in turn could be the source of the longwave

infrared radiation observed.

This model is based solely on radiation observed coming from the central 22 arc sec of the galaxy and on the assumption that the CO indices measured confirm the assumed stellar population based on the observations of Sandage et al. (1969), which assign the radiation shortward of $\lambda \simeq 0{\cdot}9\mu$ to stars. The CO indices then extend this by assuming that a major portion of the radiation observed in the 2μ spectral region comes from stars.

This kind of coarse radiation model can be applied to the observations of the galactic centre assuming that the stellar population is the same as that of NGC 224. In the case of the galactic centre interstellar extinction must be taken into account. Becklin & Neugebauer (1968) assumed the interstellar extinction law to be the same as the solar neighbourhood (Johnson 1965) and from the H-K colour assigned a visual extinction of 27 magnitudes. Spinrad et al. (1971a) reduced observations at $1{\cdot}06\mu$ and $1{\cdot}18\mu$ and Borgman (1974a) when $1{\cdot}06\mu$ and $1{\cdot}16\mu$, the energy distribution of α Boo as typical of late-type stars and the extinction curve No.15 of van de Hulst (1949) gave values of the visual extinction in the direction of the galactic centre of 28 magnitudes. If this value, 28 magnitudes, is assumed then Av = 2·7 magnitudes at $\lambda = 2{\cdot}2\mu$.

For an aperture of 22 arc sec centered on the BN point source table (5.4) gives a K magnitude of 4·83. If the contribution for the BN point source, which has a K magnitude of 6·7, is taken out then the galactic centre

has an absolute K magnitude Mk = -12·66. There are several other sources in the 22 arc sec region (Becklin & Neugebauer 1975). If these are also taken into account, the general 2μ background radiation in the 22 arc sec circular diaphram which is assumed to be entirely stellar in origin has an absolute K magnitude Mk = -12·45. A typical star in the range K_5 to M_3 III has Mv = -0·4 and V-K = 4·01 (Johnson 1966b) would have Mk ≅ -4·41. Thus this model requires $1{\cdot}6\times10^3$ such stars in the 22 arc sec diameter region of the galactic centre. This result compares with those of Becklin & Neugebauer (1968 and 1969), Spinrad et al. (1971b) Borgman (1974a and 1974b) but gives a rather smaller number of stars due to the fact that the individual sources in this region of the galactic centre have been taken out.

This is also the region which emits most of the 10μ and 20μ radiation, the dominant source being the ridge of emission found by Becklin & Neugebauer (1975) which is probably heated dust. Sources at 2·2μ are seen also in this ridge which would suggest that the obscuration by the dust is low. The ridge may be a collection of individual sources which themselves could be independent sources of ionizing radiation possibly O stars. Indeed, the population of late-type stars is very likely the origin of the total luminosity in the galactic centre. Nearly all of this luminosity is absorbed and reradiated by low temperature dust in the far infrared.

APPENDICES

APPENDIX 1

The procedure described here for aligning the photometer arose from the need to carry out all the optical adjustments on the telescope.

The photometer is mounted on the telescope and a Metrologic Laser is mounted on the field stop above the primary mirror. The laser is attached to a flat plate to allow the beam to be moved horizontally. The mounting arrangement of the laser to the plate (3 sets of push-pull screws set at 120°) allowing tilting of the beam.

The centre of the top plate of the photometer main body is marked with a set of improvised cross-wires. The laser is then moved horizontally until the forward-beam falls on the cross-wires. The laser is then adjusted using the push-pull screws until the back beam falls on the centre of the secondary mirror. This process is repeated until both beams simultaneously fall on their respective targets. It is generally found that this procedure converges rapidly.

The chopping mirror is now adjusted until the laser beam passes centrally through the Dewar mounting aperture. The Dewar mounting aperture is now covered with a plane mirror and the chopping mirror tilt screws adjusted until the reflected laser beam from the plane mirror falls on the incident beam on the chopping mirror. This gives rise to a further reflection namely, from the face of the laser

tube. It now takes the finest adjustment of the chopping mirror tilt screws to bring this reflection into alignment.

This procedure having been successfully accomplished, the optical axis of the telescope defined by the laser beam now falls centrally on the Dewar mounting aperture and leaves the photometer perpendicular to the Dewar mounting plate.

The 'flick-in' mirror is now adjusted to pass the laser beam centrally through the photometer guiding eyepiece.

In the photometer there is another axis defined by the detector, Fabry lens and aperture inside the Dewar. Having so defined the optical axis, the final alignment procedure is designed to bring these two axes into concurrence. This adjustment is made 'cold', i.e. with a cold detector.

The Dewar is mounted on the photometer and the electronics connected up. A hand held Grubb Parsons chopper with a small light source attached is held in front of the secondary mirror. The laser and plate having been removed. The detector is connected via some gain to an oscilliscope.

The optical arrangements in the Dewar are such that an in focus image of the detector is projected onto the secondary. Indeed, the square detector image should be inscribed on the circular secondary. A search with the source will now reveal the position of the projected detector image. The Dewar is adjusted on its mounting

plate using the push-pull screws and, if necessary, the chopping mirror until the projected detector image falls correctly on the secondary mirror.

It is at this stage that the detector surface can be scanned for any non-uniformity of response. Indeed it became all too apparent that the detector used contained a 'hot-spot' where the response was very much higher than anywhere else.

At this stage a check can also be made on the focus of the Fabry Lens. If the Lens has been correctly focussed - normally done by calculation - the detector response should drop sharply to zero as the source moves off the secondary mirror.

The final stage of aligning is done using an Astronomical source, usually a bright standard star. The object is acquired in telescope in the usual way and steered into the view of the photometer guiding eyepiece. This position is now marked using the telescope off-set guiding facility. The telescope is now coarsely focussed since the distance of the focal plane aperture in the Dewar from the telescope mounting flange is known and the photometer guiding eyepiece may be preset to the required focus. The orientation of the crosswires in the photometer guiding eyepiece is now adjusted to correspond with R.A. and Dec.

The problem now is to find an infrared signal. If the initial stages of aligning are conscientiously carried out this final step should pose no problems. With the

star set centrally in the photometer guiding eyepiece, the detector connected via some gain to an oscilliscope and the 'flick-in' mirror out, an ever increasing raster scan will eventually reveal the positions of the infrared signals. Having found one such position it is marked with the telescope off-set system.

The adjustable 'flick-in' mirror is altered to bring the star image onto the cross-wires. The star image should then be moved using the telescope fast and slow motions to find the position of the maximum signal and further adjustments made to the 'flick-in' mirror.

The PSD is now connected. Set a short time constant, 100ms say, a reasonable gain and adjust the phase shift for a maximum signal. One consequence of a reasonably stable square chop is that there will be a wide region of maximum response possibly as much as 30° to 40°. Now insert a phase shift of 90° and check for zero output from the PSD. Increase the gain and adjust the phase shift until zero output is obtained. Remove the 90° phase shift. This should set the phase shift.

A final adjustment to the telescope focus is now made. The PSD is set as sensitive as possible with as short a time constant as possible. The telescope focus is carefully adjusted for a maximum signal.

By convention, the signal that causes a negative output from the PSD is placed on the left hand cross-wire and is called Left; similarly Right is defined.

The final adjustment to the photometer is now made to

set the positions of Left and Right. With a suitable gain and a short time constant the left hand signal is found. The star is then moved using the telescope slow motions in positive and negative R.A. and Dec to the 3dB points. The 'flick-in' mirror is then adjusted in such a way as to symmetrically place these points about the left hand cross-wire in the photometer guiding eye-piece. This process sets the position of Left. A similar process sets the position of Right.

APPENDIX 2

NAME	J	H	K	L	APER-TURE	REF
NGC 150	10.7	9.95	9.45	>5.58	37.8	6
NGC 185			11.2		NO	9
NGC 221			6.9	6.9	NO	9
		7.64	7.39	7.08	9.6	18
		7.47	7.23		10.6	
		7.47	6.90		15	
		7.29	7.06	7.16	20	
		6.98	6.75		28	
		6.57	6.35		32	
			8.1	7.7	6	21
NGC 224	7.4		6.4	6.4	NO	9
		8.80	8.57		5	22
		8.22	8.05		7.5	
		6.96	6.82	6.54	15	
			6.93		15	
		5.85	5.69	5.30	30	
			4.69		47	
			8.5		5	23
			8.0		6.6	
			6.8		14.2	
			5.7		30.5	
			5.3		35.1	
			5.0		46.4	
			4.5		70.1	
			4.0		75.7	
NGC 253		9.7	8.9	7.7	4.8	2
		9.3	8.3	7.1	6.7	
				6.8	8.8	
			7.8	6.8	9.4	
		8.6	7.9	6.9	10	
		8.2	7.4		13.5	
			7.4	6.5	15.3	
		7.7	7.1	6.3	19.3	
		7.4	6.8		26.5	
		7.6	7.1		27.7	
		7.7	7.1		29.6	
NGC 253		7.3	6.8		33.8	2
		7.4	6.8		44.8	
		7.2	6.7		58	
	8.6	7.59	6.9	6.07	25.2	6
NGC 474			10.0		NO	9
NGC 520			>11.0		12	6
NGC 598			10.8		NO	9
		11.44	11.06		9.6	18
		11.18	10.89		28	
			10.40		32	
NGC 613	9.91	8.99	8.77	7.21	25.2	6
NGC 986	10.04	9.58	9.25		25.2	6
NGC 1068			9.5		NO	8
			8.2	5.1	NO	9

NGC	1068		9.5	8.1		2.9	12
			9.2	7.9		4.2	
			8.9	7.8		5.3	
				7.9		6.3	
			8.5	7.6		7.9	
				7.4		10	
			7.9	7.2		14.5	
				7.1		20	
			7.5	6.9		22.9	
				6.89-8.78		15	14
		8.7		7.2	5.3	NO	16
		8.77	7.87	7.22	5.30	15	17
				9.7		2	20
			9.54	8.12		2.5	
			9.22	7.97		3.8	
				7.49		5	
			8.94	7.85		5	
			8.59	7.65		7.5	
			8.58	7.68	5.49	7.5	
			8.34	7.66		7.9	
			9.01	7.90		7.9	
				7.6	5.4	8	
NGC	1068		8.33	7.56	5.48	9.5	20
			8.65	7.82	5.68	9.5	
			8.34	7.56	5.29	9.5	
			8.31	7.55	5.3	9.8	
				7.49		10	
			8.49	7.71		10	
				7.54	5.38	10	
					5.48	10	
			7.96	7.30	5.41	13.5	
			8.06	7.37	5.29	13.5	
			7.93	7.30	5.43	13.5	
			7.92	7.23		15	
				7.28		15	
			7.95	7.42		15	
			7.73	7.17		15	
					5.49	15	
			7.84	7.07	5.05	15	
					>5.71	15	
				7.13		20	
				7.04	5.31	20	
			7.55	7.05	5.23	22	
			7.54	6.94		25	
			7.27	6.69		28	
			7.44	6.90		28	
			7.33	6.84		28	
				6.85		28	
			7.49	6.96		32	
			7.21	6.66		32	
			7.83	7.32		32	
					5.27	32	
				8.1	5.7	6	21
NGC	1097		8.27	7.90		25.2	6
		8.96	8.14	7.90	7.42	25.2	
				7.87	6.98	25.2	
				7.57		38	

NGC	1275	10.7		10.8-8.9	8.2-7.3	NO	9
			>10.6	9.8		6.2	20
			>10.4	9.8		7.9	
			10.49	9.63	>8.10	9.5	
			10.40	9.59		10	
			>10.1	9.56		10.5	
			10.03	9.37	8.05	13.5	
			10.0	9.29		15	
			10.0	9.32		15.3	
			10.0	9.4		15.3	
			9.9	9.2		15.3	
			9.82	9.20		19	
			10.05	9.27		19	
			9.66	9.04		28	
			9.4	9.1		32	
			9.2	8.86		32	
			8.9	7.7		6	21
NGC	1291	9.18	8.49	8.30	7.65	12	6
		8.45	7.67	7.46	7.10	25.2	
		8.50	7.68	7.47	6.89	25.2	
NGC	1313			≥9.54		25.2	6
NGC	1316	9.18	8.64	8.29	8.18	12	6
				8.07		12.6	
				7.77		18	
		8.54	7.68	7.50	6.79	25.2	
		8.27	7.51	7.34	6.87	25.2	
		8.08	7.32	6.98	6.94	37.8	
				7.00		37.8	
				6.81		50.4	
NGC	1365	10.59	9.59	8.88	7.46	12	6
		9.22	8.21	7.81	6.75	37.8	
		8.95	8.22	7.71	6.23	37.8	
NGC	1487			>11.15		12	6
NGC	1566	10.63	9.76	9.45	8.82	12	6
		9.92	9.09	8.69	8.08	25.2	
		9.70	8.91	8.64	>7.23	25.2	
		9.35	8.49	8.34		37.8	
NGC	1672	10.09	9.22	8.86	7.85	12	6
				8.83	>6.88	25.2	
NGC	1808	9.16	8.45	7.94	6.67	25.2	6
NGC	2562			9.89		30	7
NGC	2563			9.70		30	7
NGC	2782			10.0		NO	9
				>10.0		15	20
			10.1	9.57		32	
				10.1		6	21
NGC	2831			11.04		30	7
NGC	2832			10.02		30	7
NGC	2833			11.76		24	6
NGC	3031			6.6		NO	10
NGC	3034	7.6		6.0	5.0	NO	9
NE HII region		8.9		8.0	7.0	NO	
				6.2		35	10
				6.1		35	
				5.9		35	
				6.0		35	21
NGC	3115			7.9		NO	10

NGC	3158			10.08		30	7
NGC	3159			10.87		30	7
NGC	3190			8.86		30	7
NGC	3193			9.12		30	7
NGC	3227			9.1	7.8	NO	9
				7.0		NO	10
		10.5		9.2	7.3	NO	16
			10.09	9.78		9.6	20
			9.7	9.4		15.4	
			9.82	9.39		19.3	
			9.3	8.93		32	
				9.1	7.8	6	21
NGC	3256	10.26	9.81	8.78	8.24	25.2	6
NGC	3320			10.8		NO	9
NGC	3368			8.27		30	7
NGC	3379			7.89		30	7
NGC	3516		9.7	9.6		7.9	20
			9.8	9.6		7.9	
			9.9	9.23		15.4	
			9.37	9.11		15.4	
			9.2	8.85		32	
			9.27	8.87		32	
NGC	3623			8.72		30	7
NGC	3627			8.22		30	7
NGC	3675			8.7	10.0	NO	9
				9.9		NO	10
				8.7		6	21
NGC	3783	10.79	10.32	9.87	>7.91	12	6
		11.02	10.43	9.88	>8.74	12	
			9.81	9.61		25.2	
			9.90	9.43		25.2	
NGC	4051	10.5		9.6		NO	16
			10.5	9.9	8.7	7.5	20
			10.0	9.62		15.4	
			10.4	9.6		15.4	
			10.1	9.5		32	
					9.0	6	21
NGC	4151			8.4		15	4
				9.4		15	
				10.2		15	
				8.7		15	
				8.5		15	
				8.5		15	
		10.0		8.7	6.9	NO	9
				9.5-7.8		15	15
		10.0		8.7	6.9	NO	16
			10.02	9.03	7.64	3.3	19
			9.96	8.97	7.12	4.9	
				8.61		5	
			9.54	8.99	7.51	5.3	
			9.60	8.77	7.30	6.9	
			9.70	8.93	7.75	7.5	
NGC	4151		9.10	8.42		7.9	19
			9.58	9.00		7.9	
			9.66	8.95	7.63	9.6	
			9.61	8.91	7.36	9.6	
			9.22	8.45		9.6	

NGC	4151	9.46	8.70	6.78	9.8	
		9.44	8.66	7.25	9.8	
		9.55	8.75	7.42	10.1	
		9.65	8.86	7.07	10.1	
		9.96	8.88		10.6	
		9.35	8.64		12.7	
		9.13	8.41		13.6	
		9.36	8.78	7.83	15	
		9.18	8.38		15.3	
		9.81	8.99		15.4	
		8.98	8.62		15.4	
		9.23	8.07	7.26	16.5	
		9.19	8.70		20	
		9.05	8.59		20	
		8.83	8.19		20	
		8.72	8.15		23	
		8.74	8.30		32	
		8.91	8.22		32	
		8.75	8.50		33	
		8.78	8.26		40	
		9.60	8.70	7.28	5	20
			8.88		5	
			8.72		5	
		9.47	8.62		5	
		9.53	8.62	7.13	5	
		10.10	9.11		5	
		9.2	8.42		7.9	
		9.26	8.37		7.9	
		9.6	8.60		7.9	
		9.41	8.62		7.9	
				7.11	9.2	
NGC	4151	9.23	8.43	7.19	9.5	20
		9.33	8.53	7.16	9.5	
		9.37	8.55		9.6	
		9.60	8.87	6.76	9.6	
		9.33	8.59		9.8	
		9.17	8.45	6.97	10	
		9.52	8.72		10	
		9.21	8.48		10.5	
		9.11	8.41	7.20	13.5	
		9.40	8.66	6.08	13.6	
		9.00	8.29	6.96	15	
		9.11	8.47	6.93	15	
		9.11	8.40	7.16	15	
		9.10	8.46		15	
		8.84	8.27		15.3	
		8.94	8.40		15.3	
		9.18	8.39		15.3	
		8.93	8.37		15.3	
		8.89	8.23		19.5	
		9.01	8.39		19.5	
		9.01	8.31		19.5	
		8.88	8.26		19.5	
		9.03	8.39		20	
		9.10	8.50		28	
		8.51	7.97		32	
		8.88	8.14		32	

NGC	4145		8.82	8.18		32	
			8.71	8.09		32	
				9.4	7.7	6	21
NGC	4168			9.51		30	7
NGC	4374			8.03		30	7
NGC	4406			8.28		30	7
NGC	4435			8.65		30	7
NGC	4438			8.55		30	7
NGC	4458			10.66		30	7
NGC	4461			9.06		30	7
NGC	4472			7.70		30	7
NGC	4476			10.57		30	7
NGC	4478			9.20		30	7
NGC	4486			8.05		30	7
NGC	4507	11.68	10.64	10.07	>8.86	12	6
NGC	4594			7.6		NO	10
NGC	4736			8.1		NO	10
NGC	4826			6.8		NO	10
NGC	5055			8.9		NO	10
NGC	5128		8.65	8.06	6.76	7.5	1
				7.7		9.5	
			7.71	7.20	6.25	15	
				8.0		16	
				7.4	6.7	16	
			8.15	7.46	6.73	18	
			7.5	6.96	6.31	27	
			6.89	6.37		30	
			7.07	6.53	6.11	33	
			6.41	5.92	5.42	49	
			6.06	6.69	5.47	58	
			6.05	5.74	5.58	58	
			6.08	5.51	5.11	67	
			5.24	5.08		100	
					3.3	160	
NGC	5194			7.1		NO	10
			9.86	9.53	>8.80	10.1	18
			9.14	8.64		15	
			9.16	8.69		15.4	
			8.41	8.23		32	
			8.39	7.96		32	
			8.10	8.05		32	
			7.83	7.68		48	
NGC	5195		9.00	8.80		7.9	18
			9.12	8.77	8.23	9.6	
			8.82	8.40	7.91	10.1	
			8.48	8.00		15.4	
NGC	5195		8.36	8.05		15.4	18
			8.27	8.04		19.3	
			7.93	7.65		32	
			7.96	7.60		32	
			7.84	7.50		40	
NGC	5236			7.70		18	6
				7.44		24	
NGC	5253		11.38	10.55	>8.78	12	6
			11.44	10.72	8.78	12	
NGC	5350			10.44		30	7

NGC	5353			8.65		30	7
NGC	5354			9.54		30	7
NGC	5371			10.24		30	7
NGC	5457		12.32	12.09		5	18
			11.74	10.97		9.6	
			11.53	11.24		10	
			10.79	11.10		13.6	
			10.05	10.46		15	
			10.10	10.62		15	
			9.91	9.72		24	
			10.27	10.27		28	
			10.40	10.08		32	
			>10.10	9.29		32	
			9.82	9.69		40	
			9.73	9.34		58	
NGC	5548	11.9		10.1		NO	16
			11.24	10.49		9.6	20
			>10.2	10.0		15.4	
			10.68	10.18		28	
			10.1	>9.9		33	
			>10.4	9.6		33	
NGC	6753		9.76	8.35		12	6
NGC	6796			>10.4		25.2	6
NGC	6814			10.0	9.7	NO	9
			10.8	10.51	>7.94	9.5	20
			9.6	10.1		15	
NGC	6814		10.17	9.72		28	20
			9.7	9.9		32	
NGC	7469			9.1-8.5	9.7-7.2	NO	9
		10.8		9.1	8.0	NO	16
			>10.3	9.6		6.4	20
			>10.6	9.6		7.9	
			10.10	9.32	8.25	8.5	
			9.91	9.30	8.7	9.5	
			9.80	9.11	7.7	9.5	
			9.8	9.36		10.5	
			9.73	9.15		15	
				9.31		15.3	
			>9.17	9.4		15.3	
			10.2	9.3		15.3	
			10.0	9.23		15.3	
			9.82	9.27		20	
			9.7	9.11		28	
			9.68	9.01		28	
			9.4	8.9		32	
			9.9	9.27		32	
			10.0	8.80		32	
				8.8	8.8	6	21
NGC	7496			>11.0		12	6
NGC	7552	10.12	9.3	8.95	7.63	12	5,6
NGC	7582	10.45	9.65	8.92	8.19	12	5,6
			9.55	8.90	7.85	12	
NGC	7590	>11.94	>11.29	>11.27		12	5,6
NGC	7714	13.1		11.9-10.4		NO	9
				11.1		6	21
NGC	7793	12.4	11.7	10.8	>8.44	12	6
Maffei	1			9.1		3.7	23

Maffei	1		8.7		5	
			8.3		7.3	
			8.1		9.3	
			7.8		10	
Maffei	1		7.3		17.5	23
			6.9		25.7	
			6.5		35.1	
			6.7		37.7	
			6.0		59.3	
			5.7		78.3	
Markarian	9		8.7-8.0		NO	9
			10.9		6	21
Markarian	231		8.9	7.4	6	21
3C	9	16.0	14.2		7.5	11,13
3C	48	13.6	12.7		7.5	11,13
3C	57		13.2		7.5	13
3C	120		10.2-9.9	9.1	NO	9
			9.95		7.5	20
			9.87		7.5	
		10.97	9.79		7.5	
		11.2	9.96	8.39	7.5	
			10.12		9.8	
			9.86		9.8	
			9.98		9.8	
		10.92	9.94		9.8	
		11.10	10.07		10	
			10.04		10	
		10.91	9.82		10	
		10.09	10.12		15	
			9.91	7.9	15	
		11.03	10.02	8.3	20	
			9.86		24	
			10.1	9.1	6	21
3C	175		14.0		7.5	13
3C	249.1	14.0	13.0		7.5	13
3C	277.1	15.9				13
3C	273		9.5		NO	8
			9.6		NO	9
			8.7		NO	10
		11.4			NO	11
3C	273		9.6	8.0	6	21
3C	279	15.5	12.0-12.6		7.5	13
3C	286		14.2		7.5	13
3C	287		14.9		7.5	13
3C	298	15.1	14.3		7.5	11,13
3C	309.1	15.1	15.9		7.5	11,13
3C	323.1	14.1	13.1		7.5	11,13
3C	334	14.7	13.4		7.5	11,13
3C	336		16.0		7.5	13
3C	345	12.7	13.2		7.5	11,13
3C	351	13.7	12.2		7.5	11,13
3C	371	12.1			NO	11
3C	380	15.1	14.1		7.5	11,13
3C	403G	14.1			NO	11
3C	403S	11.5			NO	11
3C	432	16.0	16.0		7.5	11,13
3C	446	13.9	13.1		7.5	11,13

3C	454	16.4			NO	11
3C	455.3	15.4	11.6		7.5	11,13
4C	4.8		>14.5		7.5	13
4C	29.68	15.2	14.7		7.5	13
BL	LAC		9.5		NO	3
CTA	102	15.0	14.3		7.5	11,13
MSH	03-19		13.2		7.5	13
MSH	14-121		14.1		7.5	13
OJ	287	10.3-10.1	9.3	8.5-7.4	NO	3
			9.64-9.83	8.53-7.47	NO	24
PHL	658	14.2	14.1		7.5	11,13
PHL	938	15.7	14.2		7.5	11,13
PHL	1070		14.0		7.5	13
PHL	1377		14.7		7.5	13
PKS	0122-00		14.0		7.5	13
PKS	0237-23	14.9	13.3		7.5	13
PKS	0405-12	13.8	12.6		7.5	11,13
PKS	0859-14	≥14.1			NO	11
PKS	1327-21		13.4		7.5	13
PKS	1354+19	15.3	13.6		7.5	11,13
PKS	1510-08	15.0	12.4		7.5	11,13
PKS	2115-30	15.0	13.9		7.5	11,13
PKS	2135-14	13.7	12.3		7.5	11,13
PKS	2145+06	14.8	14.6		7.5	11,13
PKS	2154-18		11.9		7.5	13
PKS	2251+11	13.8	12.4		7.5	13
PKS	2344+09		13.9		7.5	13
TON	256	13.6	12.3		7.5	11,13
TON	469	13.4			NO	11

REFERENCES FOR APPENDIX 2

1.	Becklin et al.	1971
2.	Becklin et al.	1973
3.	Epstein et al.	1972
4.	Fitch et al.	1967
5.	Glass	1973a
6.	Glass	1973b
7.	Grasdalen	1975
8.	Johnson	1964
9.	Kleinmann & Low	1970a
10.	Kleinmann & Low	1970b
11.	Low	1968
12.	Neugebauer et al.	1971
13.	Oke et al.	1970
14.	Pacholczyk	1970
15.	Pacholczyk	1971
16.	Pacholczyk & Weymann	1968
17.	Pacholczyk & Wisniewski	1967
18.	Penston	1973
19.	Penston et al.	1971
20.	Penston et al.	1974
21.	Rieke & Low	1972
22.	Sandage et al.	1969
23.	Spinrad et al.	1971
24.	Strittmatter et al.	1972

REFERENCES

Aitken, D.K., & Jones, B.,
1972, Proc. 1st European Astronomical Meeting, 2,248.
(Ed. Mavridis, Springer-Verlag).

Aitken, D.K., Jones, B., & Penman, J.M.,
1974, Mon.Not.R.astr.Soc., 169,35p.

Allen, C.W.,
1973, Astrophysical Quantities Third Edition,
The Athlone Press.

Arp, H.,
1965, Ap.J., 141,43.

Aumann, H.H., & Low, F.J.,
1970, Ap.J., 159,L159.

Baldwin, J.R., Danziger, I.J., Frogel, J.A., & Persson, S.E.,
1973b, Ap. Letters, 14,1.

Baldwin, J.R., Frogel, J.A., & Persson, S.E.,
1973a, Ap.J., 184,427.

Balick, B., & Sanders, R.H.,
1974, Ap.J., 192,325.

Becklin, E.E., Formalont, E.B., & Neugebauer, G.,
1973b, Ap.J., 181,L27.

Becklin, E.E., Frogel, J.A., Kleinmann, D.E.,
Neugebauer, G., Ney, E.D., & Strecker, D.W.,
1971, Ap.J., 170,L15.

Becklin, E.E., Mathews, K., Neugebauer, G., & Wynn-Williams, C.G.,
1973a, Ap.J., 186,L69.

Becklin, E.E., & Neugebauer, G.,
1968, Ap.J., 151,145.

Becklin, E.E., & Neugebauer, G.,
1969, Ap.J., 157,L31.

Becklin, E.E., & Neugebauer, G.,
1974, Proc. 8th ESLAB Symposium, Frascati.

Becklin, E.E., & Neugebauer, G.,
1975, In Preparation.

Beyen, W.J., & Pagel, B.R.,
1966, Infrared Physics, 6,161.

Borgman, J.,
1974a, Proc. 1st European Astronomical Meeting, 2,188,
(Ed. Mavridis, Springer-Verlag).

Borgman, J.,
1974b, Proc. I.A.U. Symp.No.60.

Borgman, J., Koorneef, J., & de Vries, M.,
1974, Proc. 8th ESLAB Symposium, Frascati.

Boyce, P.B. & Sinton, W.M.,
1965, Sky and Telescope, 29,78.

Burbidge, E.M.,
1967, Ann.Rev.Ast. and Ap.,5,399.

Burbidge, G.R., & Stein, W.A.,
1970, Ap.J., 160,753.

Conn, G.K., & Avery, D.G.,
1960, Infrared Methods Principles and Applications,
Academic Press, London.

Deutsch, A.J., Wilson, O.C., & Keenan, P.C.,
1969, Ap.J., 156,107.

Downes, D.,
1974, Proc. 8th ESLAB Symposium, Frascati.

Downes, D., & Martin, A.H.M.,
1971, Nature,233,112.

Downes, D., & Maxwell, A.,
1966, Ap.J.,146,653.

Duinen, R.J. van, Helmerhorst, TH.J., Olthof, H., Slingerland,
J., & Wijnbergen, J.J.,
1972, Mem. Soc. R. Sci. Liege, III,597.

Ekers, R.D., Goss, W.M., Schwartz, U.J., Downes, D., & Rogstad, D.,
1974, In Preparation.

Epstein, E.E., Fogarty, W.G., Hackney, K.R., Hackney, R.L.,
Leacock, R.J., Pomphrey, R.B., Scott, R.L., Smith, A.G.,
Hawkins, R.W., Roeder, R.C., Gray, B.L., Penston, M.V.,
Tritton, K.P., Bertraud, CH., Véran, M.P., Wlérick, G.,
Bernard, A., Bigay, J.H., Merlin, P., Durand, A.,
Sause, G., Becklin, E.E., Neugebauer, G., & Wynn-Williams,
C.G.,
1972, Ap.J., 178,L51.

Fahrbach, U., Haussecker, K., & Lemke, D.,
1974, Astron. and Astrophys., 33,265.

Fitch, W.S., Pacholczyk, A.G., & Weymann, R.J.,
1967, Ap.J., 150,L67.

Fogarty, W.G., & Pacholczyk, A.G.,
1972, Mem.Soc.R.Sci.Leige, III, 575.

Frogel, J.A., & Hyland, A.R.,
1972, Mem.Soc.R.Sci.Leige, III,111.

Frogel, J.A., Persson, S.E., Aaronson, M., Becklin, E.E.,
Mathews, K., & Neugebauer, G.,
1975, Ap.J., 195,L15.

Gillett, F.C., Merril, K.M., & Stein, W.A.,
1971, Ap.J., 164,83.

Gillett, F.C., & Stein, W.A.,
1970, Ap.J., 159,817.

Glass, I.S.,
1973a, Mon.Not.R.astr.Soc., 162,35p.

Glass, I.S.,
1973b, Mon.Not.R.astr.Soc., 164, 155

Glass, I.S.,
1974, M.N.A.S.S.A., 33,53.

Goldberg, L.,
1969, Sci.American, 220,92.

Goldberg, L., Parkinson, W.H., & Reeves, E.M.,
1965, Ap.J., 141,1293.

Grasdalen, G.L.,
1975, Ap.J., 195,605.

Harper, D.A., & Low, F.J.,
1971, Ap.J., 165,L9.

Harper, D.A., & Low, F.J.,
1973, In Preparation.

Harwit, M., Soifer, B.T., Houck, J.R., & Pipher, J.L.,
1972, Nature, 236,103.

Hoffman, W.F., & Frederick, C.L.,
1969, Ap.J., 155,L9.

Hoffman, W.F., Frederick, C.L., & Emery, R.J.,
1971a, Ap.J., 164,L23.

Hoffman, W.F., Frederick, C.L., & Emery, R.
1971b, Ap.J., 170,L89.

Houck, J.R., Soifer, B.T., Pipher, J.L., & Harwit, M.,
1971, Ap.J., 169,L31.

Hubble, E.,
1930, Ap.J., 71,231.

Hulst, H.C. van der,
1949, Rech.Astr.Obs.Utrecht, 11, Pt. 1.

Humphrey, J.N.,
1965, Applied Optics, 4, 665.

Jameson, R.F., Longmore, A.J. McLinn, J.A., & Woolf, N.J.,
1974, Ap.J., 187,L109.

Jaschek, C., Conde, H., & de Sierra, A.C.,
1964, Stellar Spectra on MK System.

Johnson, H.L.,
1962, Commun.Lun.Plan.Lab., 1,73.

Johnson, H.L.,
1964, Ap.J., 139,1022.

Johnson, H.L.,
1965a, Ap.J., 141,923.

Johnson, H.L.,
1965b, Commun.Lun.Plan.Lab., 3,53.

Johnson, H.L.,
1966a, Ap.J., 143,187.

Johnson, H.L.,
1966b, Ann.Rev.Ast. and Ap., 4,193.

Johnson, H.L.,
1968, Ap.J., 154,L125.

Johnson, H.L., Coleman, I., Mitchell, R.I., & Steinmetz, D.L.,
1968, Commun.Lun.Plan.Lab., 7,83.

Johnson, H.L., & Mendez, M.E.,
1970, A.J., 75,785.

Johnson, H.L., Mitchell, R.I., Iriate, B., & Wisniewski, W.Z.,
1966, Commun.Lun.Plan.Lab., 6,63.

Johnson, H.L., & Morgan, W.W.,
1965, Ap.J., 117,313.

Jones, T.W., O'Dell, S.L., & Stein, W.A.,
1974, Ap.J., 188,353.

Jones, T.W., & Stein, W.A.,
1975, Ap.J., 197,297.

Keenan, P.C.,
1963, Stars and Stellar Systems, vol.3, 78. (Ed. K.A. Strand).

Kellerman, K.I., & Pauliny-Toth, I.I.K.,
1971, Ap. Letters, 8,153.

Kennedy, P.M., & Buscome, W.,
1974, MK Spectral Classifications. Evanston.

Krishna Swamy, K.S.,
1970, Ap.J., 167,63.

Kleinmann, D.E., & Low, F.J.,
1970a, Ap.J., 159,L165.

Kleinmann, D.E., & Low, F.J.,
1970b, Ap.J., 161,L203.

Knacke, R.F., & Capps, R.W.,
1974, Ap.J., 192,L19.

Kruit, P.C. van der,
1974, Ast. and Ap., 29,231.

Kruse, P.W., McGlauchlin, L.D., & McQuistan, R.B.,
1962, Elements of Infrared Technology.

Kukarkin, B.V., Perenago, P.P., Efremov, Yu.I., & Kholopov, P.N.,
1958, General Catalogue of Variable Stars
(2nd ed., Moscow: Publishing House of the Academy of
Sciences in the U.S.S.R).

Lequeux, J.,
1970, Ap.J., 159,459.

Levinstein, H.,
1970, Semiconductors and Semimetals, vol.5,
Infrared Detectors, Academic Press.

Limperis, T.,
1965, Handbook of Military Infrared Technology,
470, Ed.Wolfe.

Long, D.,
1967, Infrared Phys., 7,169.

Low, F.J.,
1967, Highlights of Astronomy, 145, Ed. Perek (New York:
Springer-Verlag).

Low, F.J., & Aumann, H.H.,
1970, Ap.J., 162,L79.

Low, F.J., & Johnson, H.L.,
1965, Ap.J., 141,336.

Low, F.J., & Kleinmann, D.E.,
1968, A.J. 73,868.

Low, F.J., Kleinmann, D.E., Forbes, F.F., & Aumann, H.H.,
1969, Ap.J., 157,L97.

Low, F.J., & Rieke, G.H.,
1974, Methods of Experimental Physics, 12, Pt.A, Academic
Press.

Lummis, F.L., & Petriz, R.L.,
1957, Phys.ev., 105,502.

Martin, A.H.M., & Downes, D.,
1972, Ap. Letters, 11,219.

McCammon, D., Münch, G., & Neugebauer, G.,
1967, Ap.J., 147,575.

McLaughlin, D.B., & Dijke, S.E.A. van,
1943, Ap.J., 100,63.

Mendoza, V., E.E.,
1967, Bull.Obs.Ton. y Tac., 4,114.

Mendoza, V., E.E., & Johnson, H.L.,
1965, Ap.J., 141,161.

Montgomery, F.F., Connes, P., Connes, J., & Edmonds, F.N.Jr.,
1969, Ap.J., Suppl., 19,1.

Morgan, W.W., & Keenan, P.C.,
1973, Ann.Rev.Ast. and Ap., 11,29.

Moss, T.S.,
1953, Proc. I.R.E., 43,1969.

Moss, T.S.,
1955, Photoconductivity in the Elements, Academic Press.

Neugebauer, G., Garmire, G., Rieke, G.H., & Low, F.J.,
1971, Ap.J., 166,L45.

Neugebauer, G., & Leighton, R.B.,
1969, California Institute of Technology.

O'Connell, R.W.,
1974, Ap.J., 193,L49.

Oke, J.B., & Sargent, W.L.W.,
1968, Ap.J., 151,807.

Okuda, H., & Wickramasinghe, N.C.,
1970, Nature, 226,134.

Pacholczyk, A.G.,
1970, Ap.J., 161,L207.

Pacholczyk, A.G.,
1971, Ap.J., 163,449.

Pacholczyk, A.G., & Weymann, R.J.,
1968, A.J., 73,870.

Pacholczyk, A.G., & Wisniewski, W.Z.,
1967, Ap.J., 147,394.

Penston, M.V.,
1973, Mon.Not.R.astr.Soc., 162,359.

Penston, M.V., Penston, M.J., Neugebauer, G., Triton, K.P., Becklin, E.E., & Visvanath, N.,
1971, Mon.Not.R.astr.Soc., 153,29.

Penston, M.V., Penston, M.J., Selmes, R.A., Becklin, E.E., & Neugebauer, G.,
1974, Mon.Not.R.astr.Soc., 169,357.

Petriz, R.L.,
1956, Phys.Rev., 104,1508.

Petrosian, V., Bachal, J.N., & Salpeter, E.E.,
1969, Ap.J., 155,L57.

Pottasch, S.R.,
1968, Bull.Astron.Inst.Neth., 19,469.

Pottasch, S.R.,
1974, Proc. 1st European Astronomical Meeting, 2,209, (Ed. Mavridis, Springer-Verlag).

Rees, M.J., Silk, J.I., Werner, M.W., & Wickramasinghe, N.C.,
1969, Nature, 223,788.

Reynolds, M.M., & Burley, R.M.,
1963, American Institute of Physics Handbook, Second Edition.

Ridgway, S.T.,
1974, Ap.J., 190,591.

Rieke, G.H., Harper, D.A., Low, F.J., & Armstrong, K.R.,
1973, Ap.J., 183,L67.

Rieke, G.H., & Low, F.J.,
1972a, Ap.J., 176,L95.

Rieke, G.H., & Low, F.J.,
1972b, Ap.J., 177,L115.

Rieke, G.H., & Low, F.J.,
1973, Ap.J., 184,415.

Rieke, G.H., & Low, F.J.,
1975, Ap.J., 199,L13.

Roman, N.G.,
1973, Proc. I.A.U. Symposium No. 50.

Rose, W.K., & Tinsley, B.M.,
1974, Ap.J., 190,243.

Russell, H.N.,
1934, Ap.J., 79,317.

Sandage, A.,
1973, Ap.J., 183,711.

Sanders, R.H., & Lowinger, T.,
1972, A.J., 77,292.

Scanlon, W.W.,
1956, Proc. of a Conference on semiconductors,
Garmisch Partenkirchen, Germany.

Schild, R.E., Peterson, D.M., & Oke, J.B.,
1971, Ap.J., 166,95.

Sérsic, J.L.,
1973, Pub.Astr.Soc.Pacific, 85,103.

Sérsic, J.L., & Pastoriza, M.,
1965, Pub.Astr.Soc.Pacific, 77,287.

Slater, J.C.,
1956, Phys.Rev. 103,1631.

Smith, W.J.,
1965, Handbook of Military Infrared Technology, Ed. Woolfe.

Smyth, M.J., Dow, M.J., & Napier, W.McD.,
1975, Mon.Not.R.astr.Soc., 172,235.

Spinrad, H., Liebert, J., Smith, H.E., Shweizer, F.,
& Kuhi, L.V.,
1971a, Ap.J., 165,17.

Spinrad, H., Sargent, W.L.W., Oke, J.B., Neugebauer, G.,
Landau, R., King, I.R., Gunn, J.E., Garmire, G., &
Dieter, N.H.,
1971b, Ap.J., 163,L25.

Spinrad, H., & Taylor, B.J.,
1971, Ap.J.Suppl., 22,193.

Spinrad, H., & Wing, R.F.,
1969, Ann.Rev.Ast. and Ap., 7,249.

Stein, W.A.,
1966, A.J. 144,318.

Stein, W.A.,
1975, Pub.Astr.Soc.Pacific, 87,5.

Stein, W.A., Gillett, F.C., & Merrill, K.M.,
1974, Ap.J., 187,213.

Strittmatter, P.A., Serkowski, K., Carswell, R., Stein, W.A.,
Merrill, K.M., & Burbidge, E.M.,
1972, Ap.J., 175,L7.

Sutton, E., Becklin, E.E., & Neugebauer, G.,
1974, Ap.J., 190,L69.

Thomas, J.A., Hyland, A.R., & Robinson, G.,
1973, Mon.Not.R.astr.Soc., 165,201.

Tinsley, B.M.,
1973, Ap.J., 184,L41.

Vaucouleurs, G. de, & Vaucouleurs, A. de,
1964, Reference Catalogue of Bright Galaxies.
Austin, Texas.

Vaughan, A.H., & Zirin, H.,
1968, Ap.J., 162,123.

Vleit, K.M. van,
1958, Proc. I.R.E., 46,1004.

Wickramasinghe, N.C.,
1970, Nature, 225,145.

Wickramasinghe, N.C.,
1971, Nature Phys.Sci., 230,166.

Williams, P.M.,
1975, Private Communication.

Wilman, H.,
1948, Proc.Phys.Soc.London, A60,117.

Wolfe, A.M.,
1974, Ap.J., 188,243.

Woolf, N.J.,
1973a, Proc. I.A.U. Symposium No.52,485.

Woolf, N.J.,
1973b, Ap.J., 185,237.

Wynn-Williams, C.G., & Becklin, E.E.,
1974, Pub.Astr.Soc.Pacific, 86,5.

Wynn-Williams, C.G., Becklin, E.E., & Neugebauer, G.,
1972, Mon.Not.R.astr.Soc., 160,1.

Young, A.S.,
1955, J.Sci.Instr., 32,142.

ACKNOWLEDGEMENTS

It is a pleasure to acknowledge the continuing encouragement and support of my supervisors, Dr. M.J. Smyth and Dr. P.W.J.L. Brand. I am also deeply indebted to the members of the Electrical and Mechanical Workships in the Royal Observatory, Edinburgh especially, Mr. R.W. Parker, Mr. J. Clark and Mr. R.J. Beetles for advice and guidance during the designing of the photometer.

I am grateful to Dr. T.J. Lee, Dr. D.E. Emerson, Dr. P.M. Williams and Mr. D.H. Beattie for many useful conversations on various aspects of this work.

I acknowledge the support of the Science Research Council for a Student Maintainance Grant and for observing time on the 60 Inch Flux Collector, Izaña, Tenerife.